Institute of Physics PAS

Doctoral Thesis

Practical Spin-Squeezing with Ultra-Cold Atoms in Optical Lattices

Author:
M.Sc. Tanausú Hernández Yanes

Supervisor:
Dr. Hab. Emilia Witkowska

September 11, 2024

INSTYTUT FIZYKI
POLSKIEJ AKADEMII NAUK

Abstract

Developing quantum technologies aim to employ quantum phenomena in practical implementations. For instance, more robust quantum cryptography and information tasks, such as self-testing, randomness amplification and expansion, quantum key distribution, and quantum sensing and metrology. Spin squeezed states are such quantum states particularly useful for sensing. They provide improved phase sensitivity over the classical shot-noise limit $\Delta\phi \propto 1/\sqrt{N}$. Their quantum fluctuations for the collective spin operator are reduced in one direction at the expense of the fluctuations in the orthogonal direction. This allows for improvement of the phase sensitivity of the state along the reduced fluctuations direction. Spin squeezed states are advantageous over other highly entangled states for metrological applications because they have a sufficiently large mean spin value and are resilient to different types of decoherence processes. While spin squeezed states have been proposed theoretically and even realized experimentally, states entangled close to the theoretical bound $\Delta\phi \propto 1/N$ are still out of reach. In this thesis we present different setups of ultra-cold atoms in the optical lattice, designed as potentially simple experimental implementations, for dynamical spin squeezing generation from classical coherent states. We propose different additional terms over the bare two-component Fermi– and Bose–Hubbard models like long-range dipolar interactions, spin-orbit coupling, contact interactions anisotropy or inhomogeneous magnetic fields to generate effective models capable of generating maximally squeezed spin-1/2 states. We also analyze how imperfections in the different models affect entanglement generation through parameter detuning, perturbative regimes, or particle losses at the preparation stage.

Abstract (Polish)

Rozwój technologii kwantowych ma na celu wykorzystanie zjawisk kwantowych w praktycznych implementacjach, przykładowo w kryptografii kwantowej i informacji (samotestowanie, wzmocnienie i ekspansja losowości, dystrybucja klucza kwantowego) lub metrologii kwantowej. Stany ściśnięte spinowo to stany kwantowe, które są szczególnie przydatne do niezwykle precyzyjnej metrologii. Zapewniają one czułość fazową lepszą w porównaniu z klasyczną granicą szumu śrutowego $\Delta\phi \propto 1/\sqrt{N}$. Ich fluktuacje kwantowe dla kolektywnego operatora spinowego są redukowane w jednym kierunku kosztem fluktuacji w kierunku ortogonalnym. Pozwala to na poprawę czułości fazowej stanu wzdłuż kierunku zmniejszonych fluktuacji. Stany ściśnięte spinowo są korzystniejsze od innych silnie splątanych stanów w zastosowaniach metrologicznych ponieważ mają wystarczająco dużą średnią wartość spinu i są bardziej odporne na różne typy procesów dekoherencji. Podczas gdy stany ze ściśniętym spinem zostały zaproponowane teoretycznie, a nawet zrealizowane w układach ulata-zimnych atomów, to ich praktyczne zastosowanie, w szczególności blisko teoretycznej granicy $\Delta\phi \propto 1/N$, jest nadal poza zasięgiem obecnych eksperymentów. W niniejszej rozprawie rozważamy układy ultra-zimnych atomów umieszczonych w periodycznej sieci optycznej, zaprojektowane jako potencjalnie proste implementacje eksperymentalne do dynamicznej generacji stanów scisnietych spinowo. Rozważając dwuskładnikowe modele Bose– i Fermi–Hubbarda, proponujemy nowe mechanizmy w celu wygenerowania efektywnych modeli zdolnych do generowania maksymalnie ściśniętych stanów. Te mechanizmy są wytważane przez fizyczne procesy, t.j. długozasiegowe oddziaływania dipolowe, sprzężenie spin-orbita, anizotropia oddziaływań kontaktowych lub niejednorodne pola magnetyczne. Analizujemy również, w jaki sposób niedoskonałości w przygotowaniu stanów poczatkowych lub parametrów modelu wpływają na możliwość wytworzenia stanów ściśniętych spinowo oraz ich użyteczność do praktycznych zastosowań.

Authorship attribution statement

This thesis contains nine body chapters and includes a series of published articles that all fit into a cohesive scheme in the context of spin squeezing generation in the optical lattice. These chapters are self-contained and begin with a short motivation, constructing a natural progression with respect to the central topic of the thesis. Chapters may also include results and conclusions made entirely by me which were unpublished because of length or time constrains. These extensions are too short to justify a separate publication on their own, but I expect them to be useful and informative to the reader. Each chapter ends with the compilation of corresponding publications in their original published format. This statement declares my authorship contribution to each chapter of this thesis and acknowledges any editorial help I received and, where appropriate, attributes the co-authors.

All numerical calculations in the following chapters, as well as most calculations in the included published articles, were performed based on exact diagonalization methods using code developed by me. The core library I built and some example scripts can be found in:

`https://gitlab.com/tanahy/1d-hubbard-model`.

I gave detailed explanations on how to implement such calculations from scratch in the course *Lectures on Computational Physics of Cold Atoms*, imparted by Maciej Kruk and I under the supervision of Emilia Witkowska. The course took place in the winter semester of the 2022-2023 academic year at the Institute of Physics of the Polish Academy of Sciences. The course materials can be found in:

`https://gitlab.com/tanahy/cophyca`.

Chapters 1 to 4 and 9

The contents in Chapter 1 provides an introduction and motivation to the research topic of spin squeezing in the optical lattice. The contents in Chapter 2 introduce the research topic with a historical background on the core concepts and key findings of the phenomena under study, spin squeezing. The contents in Chapter 3 put the focus on the system of interest we use to produce spin squeezed states, ultra-cold atoms in the optical lattice. The contents in Chapter 4 present the necessary background to employ a precise perturbation theory method on many body systems, the Schieffer-Wolff transformation. The contents in Chapter 9 are a brief summary and outlook of the thesis. These chapters were researched and written by me.

Chapter 5

The research article included in Chapter 5 has been published as:

M. Dziurawiec, T. Hernández Yanes, M. Płodzień, M. Gajda, M. Lewenstein, and E. Witkowska, "Accelerating Many-Body Entanglement Generation by Dipolar Interactions in the Bose-Hubbard Model", Physical Review A **107**, 013311 (2023)

Contribution: I independently reproduced all the analytical and numerical results. At the time, Marlena Dziurawiec was a Master student doing an internship in our group and we maintained weekly discussions about the project under the supervision and direction of Emilia Witkowska. I supervised Marlena Dziurawiec to help her write her own programs for simulations using exact diagonalization. Once the project advanced, we also started to receive the input of Marcin Płodzień and Mariusz Gajda during our weekly meetings. Marlena Dziurawiec and I prepared the first draft of the publication. We received editorial contributions from the other authors for the final version of the manuscript for publication.

Chapter 6

The research articles included in Chapter 6 have been published as:

T. Hernández Yanes, M. Płodzień, M. Mackoit Sinkevičienė, G. Žlabys, G. Juzeliūnas, and E. Witkowska, "One- and Two-Axis Squeezing via Laser Coupling in an Atomic Fermi-Hubbard Model", Physical Review Letters **129**, 090403 (2022)

T. Hernández Yanes, G. Žlabys, M. Płodzień, D. Burba, M. M. Sinkevičienė, E. Witkowska, and G. Juzeliūnas, "Spin Squeezing in Open Heisenberg Spin Chains", Physical Review B **108**, 104301 (2023)

Contribution: I am the first author of both publications and was responsible for the numerical simulations. I also contributed to the analytical calculations, in particular to the derivation of the effective models using the Schieffer-Wolff transformation. I produced all the figures, except for Fig. 1 of the second publication. Emilia Witkowska and I wrote the first drafts of the publications. This work was the result of a close collaboration between the two theory groups led by Emilia Witkowska and Gediminas Juzeliūnas, respectively. Emilia Witkowska made the initial proposal of the project, which organically evolved through the collaboration thanks to the collective efforts of the members involved. The analytical framework was developed during our regular meetings with propositions and cross-checking among Emilia Witkowska, Gediminas Juzeliūnas, Giedrius Žlabys and me. Marcin Płodzień provided DMRG calculations for results with large number of particles for the first publication. Domantas Burba contributed in the appendix E in the second publication. All of the authors made editorial contributions for the final versions of the publications.

Chapter 7

The research article included in Chapter 7 has been published as:

T. Hernández Yanes, A. Niezgoda, and E. Witkowska, "Exploring spin squeezing in the Mott insulating regime: Role of anisotropy, inhomogeneity, and hole doping", Physical Review B **109**, 214310 (2024)

Contribution: I am the first author of this publication and performed all numerical simulations, except for calculations regarding temperature effects; which were done by Artur Niezgoda. Emilia Witkowska led the research direction and defined the structure of the publication. Emilia Witkowska and I wrote the text of the publication, with minor editorial contributions from Artur Niezgoda. I produced all the figures of the publication.

Chapter 8

The contents in Chapter 8 are yet to be published, but are the result of a collaboration with the group led by Alice Sinatra. We expect to publish our results in a scientific article soon. The pre-print of the research article can be found as:

T. H. Yanes, Y. Bamaara, A. Sinatra, and E. Witkowska, *Bounds on detection of Bell correlations with entangled ultra-cold atoms in optical lattices under occupation defects*, (Sept. 4, 2024) `http://arxiv.org/abs/2409.02873` (visited on 09/08/2024), pre-published

Contribution: I performed all numerical and analytical calculations presented in section V of the attached manuscript. The research direction was the result of a collaboration between Youcef Baamara, Alice Sinatra, Emilia Witkowska and I. The main theoretical model, which we refer to as toy model, was developed through discussions involving all the previously mentioned authors.

In addition to the statements above, in cases where I am not the corresponding author of a published item, permission to include the published material has been granted by the corresponding author.

Tanausú Hernández Yanes, September 11, 2024

As supervisor for the candidature upon which this thesis is based, I can confirm that the authorship attribution statements above are correct.

Emilia Witkowska, September 11, 2024

Acknowledgements

I deeply thank my supervisor Dr. Hab. Emilia Witkowska for giving me the opportunity to work together over these four years in a healthy and highly-driven environment. While the path was never straight, she always managed to guide me in positive and productive directions. Thanks to her guidance I have learned how to be organized, effective, and confident in a research environment in general and in the field of ultra-cold atoms in particular.

I learned a lot from the expertise and astonishing intuition of Prof. Dr. Hab. Gediminas Juzeliūnas. My experience with him, Dr. Giedrius Žlabys, and Dr. Mažena Mackoit Sinkevičienė was invaluable and I remember fondly my short stays in Vilnius. Collaborating with Dr. Youcef Baamara and Prof. Alice Sinatra was a pleasure and our discussions were always eye-opening to me. I also thank M.Sc. Marlena Dziurawiec, Dr. Marcin Płodzień, Dr. Artur Niezgoda, Prof. Dr. Hab. Mariusz Gajda, and Prof. Dr. Maciej Lewenstein. Working with them was an enriching experience and I also owe them the success of our joint research.

I thank Univ. Prof. Dr. Francesca Ferlaino and Dr. Manfred Mark for giving me the opportunity to join their experimental group in Innsbruck and learn more about ultra-cold atoms and dipolar interactions. I particularly thank Dr. Luca Barbiero and my colleagues at the theory sub-group Dr. Thomas Bland, Dr. Pramodh Senarath Yapa, M.Sc. Leonardo Bellinato Giacomelli, and M.Sc. Elena Poli for the scientific discussions, their support, and their warmth.

Prof. Jan Mostowski allowed me to inhabit his office for a good while and gave me nuggets of wisdom which I treasure. For all the coffee breaks, chats and support through my stay at the Institute of Physics, I must thank my colleagues Mgr. Soheil Arbabi, Mgr. Luís Carnevale da Cunha, Mgr. Pamela Smardz, Mgr. Hubert Dunikowki, Dr. King Lun Ng, Dr. Quyen V. Vu, Dr. Paolo Comaron, and Dr. Hab. Piotr Deuar.

On a more personal note, the support of my family and friends, even from afar, immensely helped me push through the doctorate. The visits of my mother Carmen Rosa, my sister Atasara, my brother-in-law David, my nephew Quebehi, and my friends Alejandro, Jennifer and Itahisa always gave me energy and confidence. But the person I owe the most in this regard is my partner Águeda for her love, care, and unlimited amounts of healthy food for the curious mind. Thank you.

This work was supported by the Polish National Science Center DEC-2019/35/O/ST2/01873. I acknowledge support from the Polish National Agency for Academic Exchange through the Foreign Doctoral Internship Grant NAWA Preludium BIS 1 No. PPN/STA/2021/1/00080. A part of the computations included in this thesis was done at the Centre of Informatics Tricity Academic Supercomputer & Network.

Contents

Contents **vii**

List of Figures **ix**

1 Introduction **1**

2 Spin Squeezing **5**
2.1 Bosonic coherent states 5
2.2 Squeezed coherent states 6
2.3 Pseudo-spin and collective operators 7
2.4 Spin coherent states 9
2.5 Spin-squeezing parameter 11
2.6 Paradigmatic models 18

3 Ultra-cold Atoms in the Optical Lattice **25**
3.1 Hubbard model 25
3.2 Two-mode model 28
3.3 Heisenberg model 29

4 Perturbation Theory **39**
4.1 Schieffer–Wolff Transformation 39

5 Spin Squeezing through Dipolar Interactions in the Superfluid Phase **43**
5.1 Dipolar interactions for arbitrary geometry in second quantisation form 44
5.2 Effective model under Periodic and Open Boundary Conditions 47
5.3 Limitations of the model 50

6 Spin Squeezing through Spin Orbit Coupling in the Mott Insulating Phase **61**
6.1 Perturbation theory for the Mott Insulating Phase 61
6.2 Squeezing via Spin Orbit Coupling in the Mott Insulating Phase 64

7 Spin Squeezing under Imperfections and Holes **89**

7.1 Squeezing via Contact Interactions in the Mott Insulating Phase 89
7.2 Squeezing via Inhomogeneous Magnetic Field in the Mott Insulating Phase . . . 91
7.3 Effect of hole doping . . . 92
7.4 Movement of holes . . . 93

8 Entanglement of squeezed states under occupation defects 113
8.1 Two-body Bell Correlator . . . 114
8.2 Occupation defects and toy model . . . 116
8.3 Realistic implementations . . . 117

9 Conclusions 133

Bibliography 135

List of Figures

2.1 Bloch sphere representation of the spin directions of interest for a given squeezed state. 13
2.2 Evolution of the one-axis twisting model (2.55) with $N = 100$ particles for an arbitrary χ. 21
2.3 Evolution of the twist and turn model (2.64) with $N = 100$ particles and $\Omega = N\chi/2$ for an arbitrary χ. 22
2.4 Evolution of the two-axis counter twisting model (2.68) with $N = 100$ particles for an arbitrary χ. 24

5.1 Comparison of the spin-squeezing parameter ξ^2 and condensate fraction f_c dynamics between periodic and open boundary conditions for the Hubbard model with dipolar interactions in the Superfluid regime. 51

6.1 Sketch of energy manifolds and couplings among a selected number of possible states in the Fermi–Hubbard Hamiltonian for a lattice of three sites and two particles of opposite spin. 62
6.2 Similar sketch as in fig. 6.1, but including the spin-orbit coupling term for a two-site lattice at half-filling. 64
6.3 Illustrative example of transition from TACT dynamics to OAT dynamics through a linear term. 67

7.1 Spin squeezing dynamics induced by anisotropy of the contact interactions in the presence of a hole in the system. 94
7.2 Spin squeezing dynamics induced by an inhomogeneous magnetic field in the presence of a hole in the system. 95
7.3 Evolution of spin squeezing parameter induced by anisotropy and inhomogeneous magnetic field for different values of the tunnelling rate and filling factor. 97

Chapter 1

Introduction

We define the state of a quantum system by a combination of configurations in a given Hilbert space, which yields a certain probability distribution. Such space of configurations can be probed using certain observables that can be measured. For instance a wave-packet of light moving across space can be characterized by the observables $\hat{x}, \hat{p}$. These observables are conjugate if their commutator $[\hat{x}, \hat{p}] \equiv \hat{x}\hat{p} - \hat{p}\hat{x} \neq 0$. Their uncertainties obey the inequality $\Delta\hat{x}\Delta\hat{p} \geq \hbar/2$. We certify a minimal variance state when the inequality saturates to an equality, as no quantum state can violate this restriction. Moreover, we can find states were the variance of one observable is reduced with respect to the corresponding conjugate, while saturating the previous inequality. These kind of states yield a sub-binomial distribution, which is tighter in a given direction than a binomial distribution. These states are usually referred to as *squeezed* states, as a reference to the deformation of the probability distribution with respect to the state where the variance is isotropic in the phase space of interest.

In this work, we refer to spin as the quantum number associated with the intrinsic angular momentum of an atom. While this has implications on the statistics of the atoms, as bosons are characterised by integer valued spin and fermions are characterised by half-integer valued spin, we will take the approach of isolating a number of internal energy levels of the atoms to construct a pseudo-spin manifold. This allows us to, for instance, describe spin-1/2 dynamics while using two-level bosons.

The change in statistics allows us to construct different dynamics that are advantageous for squeezing the probability distributions of a state in the pseudo-spin phase space. We refer to this concept as spin squeezing. As we explain later on, defining spin squeezing can be challenging due to the inherent symmetries of the spin phase space. We can nevertheless find satisfactory and compact definitions for metrological purposes [6–8].

Spin squeezed states offer improved sensitivity on spectroscopic measurements in contrast with other classes of highly entangled states [9]. In fact, spin squeezing itself can be used as a relevant entanglement witness in many scenarios, as it only requires collective measurements and is quite robust to different decoherence channels [10–12]. Because of its collective measurement nature, spin squeezing is also useful in the study of quantum phase transitions [13, 14] and quantum chaos [15, 16]. It is no surprise that spin squeezing is regarded as one of the main quantum resources to probe fundamental physics questions like the electric dipole moment or dark matter [17].

Squeezing generation has been proposed through various methods like feedback loops in quantum non-demolition measurements [18–20] or tweezer arrays [21], quantum state transfer from light to atoms [22, 23], cavity feedback [24], or interactions in magnetic microchip traps (atom chips) for neutral atoms [25]. However, we will focus on dynamical generation of spin squeezing from an uncorrelated state as proposed in the pioneering work of Kitawaga and Ueda in 1993 [6].

To certify spin squeezing, we must first find an adequate definition of it. While bosonic squeezing is well constrained to a given complex plane in which squeezing is easy to represent and derive, spin squeezing happens in the phase space corresponding to the SU(2) symmetry of the spin components. This requires more careful analysis and generalization to arbitrary spin lengths becomes non-trivial [26]. We will review some of the main definitions of spin squeezing, but we will focus on the well-known definition focused on spectroscopic phase sensitivity for spin-1/2 atoms [7]. This definition is very compact and makes intuitive sense of the main features of spin squeezing, while also having a well defined lower bound to compare our results with [27].

We pay special attention to ultra-cold atoms in the optical lattice as our implementation platform of reference, since it provides high tunability and control while allowing the inclusion of many modifications that make it an ideal quantum simulator for other platforms [28, 29]. In fact, spin squeezing in the optical lattice has received special attention in recent years for its direct application to quantum clocks and quantum sensors [30–32]. Moreover, this platform offers enticing spatial resolution and constrains at the single particle level. Such advantages allow us to study fundamental aspects of correlations under short and long range interactions in ranges of parameters inaccessible to other setups [32, 33]. The optical lattice is also attractive as a platform in which to certify correlations by local measurements. These are not included in the typical definitions of spin squeezing, but can help in probing entanglement more exhaustively.

While some of the results derived in this work are applicable to higher dimensional systems, we mainly concern ourselves with one-dimensional systems. Low dimensional systems are simpler to describe, analyse and engineer.They also have an advantage in constraining the degrees of freedom such that we may find different behaviour with respect to higher dimensional systems.

States composed of particles with spin $j > 1/2$ are also subject to spin squeezing [34, 35] and are experimentally relevant [36]. In fact, spin squeezing definitions have been generalised to large spin in the past and are the main subject of current works [26, 37, 38]. Nevertheless, we limit our analysis to spin-1/2 particles to obtain a solid understanding of the phenomena and serve as a stepping stone for richer studies in higher spin manifolds in the future.

We employ different kinds of external fields and couplings among atoms in the optical lattice to generate the required correlations during dynamics and obtain highly squeezed states. In the first chapters of this work we introduce the main concepts and tools to perform the required approximations and obtain effective models which describe squeezing dynamics in the rest of the work. In the following chapters we explore long-range dipolar interactions in the superfluid phase of the Bose–Hubbard model, spin-orbit coupling in the Mott-insulating phase of the Fermi–Hubbard model, and anisotropic contact interactions as well as inhomogeneous magnetic fields in the Mott-insulating phase of the Bose–Hubbard model in search of these effective models.

Throughout this work, we set $\hbar = 1$ to ease the notation and define M as the system size, N as the number of particles and S as the spin quantum number.

Chapter 2

Spin Squeezing

2.1 Bosonic coherent states

The origin of spin squeezing can be traced back all the way to the conception of coherent states by Glauber in 1963 [39]. Coherent states were develop to study the correlation properties of the electromagnetic field [40, 41], but they rapidly became powerful tools to tackle other problems after being constructed for arbitrary Lie groups [42, 43]. Over the years, coherent states found applications in calculations involving path integrals [44], thermodynamics [45], decoherence [46, 47], the quantum-classical correspondence problem [48, 49], and many more areas [50, 51]. A fantastic overview of coherent states and their applications can be found in [52].

The inception of coherent states spur from the insight that part of the electromagnetic field operator can be decomposed in the eigenstates of the bosonic (since we are taking about light) annihilation operator. We may think this was a simple assumption, but at the time it was very innovative since the scientific community was focused on Hermitian operators, as they are experimentally observable.

We have defined the coherent states $|\alpha\rangle$ as eigenstates of the bosonic annihilation operator $\hat{a}$ such that

$$\hat{a}\,|\alpha\rangle = \alpha\,|\alpha\rangle\,. \tag{2.1}$$

We can also define them as the displaced form of the ground state

$$|\alpha\rangle = \hat{D}(\alpha)\,|0\rangle\,, \tag{2.2}$$

where $\hat{D}(\alpha)$ is a unitary operator acting on the annihilation operator $\hat{a}$, such that

$$\hat{D}^{-1}(\alpha)\hat{a}\hat{D}(\alpha) = \hat{a} + \alpha. \tag{2.3}$$

By wisely applying $\hat{D}^{-1}(\alpha)$ in eq. (2.3) and eq. (2.2) we can recover the definition in eq. (2.1). Continuing with the derivation, we choose a global phase for the coherent states by setting $\hat{D}(0) = 1$. By expanding eq. (2.3) with an infinitesimal displacement $d\alpha$ wet get

$$\hat{D}(d\alpha) = 1 + \hat{a}^\dagger d\alpha - \hat{a} d\alpha^*. \tag{2.4}$$

We can then calculate the finite displacement as

$$\hat{D}(\alpha) = e^{\alpha\hat{a}^\dagger - \alpha^*\hat{a}} = e^{-\frac{1}{2}|\alpha|^2} e^{\alpha\hat{a}^\dagger} e^{-\alpha^*\hat{a}}. \tag{2.5}$$

With this result and using the definition of the n-th excited state $|n\rangle = (\hat{a}^\dagger)^n |0\rangle / \sqrt{n!}$, we can derive [52]

$$|\alpha\rangle = e^{-\frac{1}{2}|\alpha|^2} \sum_n \frac{(\alpha)^n}{\sqrt{n!}} |n\rangle . \tag{2.6}$$

Bosonic coherent states construct an over-complete basis, meaning they are not guaranteed to be orthogonal but describe the full Hilbert space of the system [53]. Moreover, they are all minimum uncertainty states which satisfy the uncertainty relation $\Delta x \Delta p = \hbar/2$. This last property is useful for metrological applications, as they provide the highest accuracy for which $\Delta x = \Delta p$. Nevertheless, we can obtain states of increased metrological advantage by deforming the quadrature in phase space of a coherent state. As we described before, the resulted states are *squeezed*.

2.2 Squeezed coherent states

Bosonic coherent states show minimal uncertainty, but they have in principle equal quantum fluctuations for two conjugate variables like position and momentum. While already useful, we can still increase the precision of a measurement by reducing the quantum fluctuations or variance of one variable by sacrificing the other. This idea of reducing the quantum fluctuations to provide an enhancement in precision is traditionally referred to as *squeezing*, since we squeeze the probability distribution in the direction of interest in phase space.

These states of light have received much attention with their key role in the detection of gravitational waves by the LIGO [54] and Virgo interferometers [55], as sub-atomic size measurements are needed to detect such phenomena [56].

To squeeze the coherent states, we define the squeeze operator as

$$\hat{S}(\xi) = \exp\left\{ \frac{1}{2} \left(\xi^* \hat{a}^2 - \xi \hat{a}^{\dagger 2} \right) \right\}, \tag{2.7}$$

where $\xi = re^{i\theta}$ is an arbitrary complex number. Notice a certain resemblance with the displacement operator in eq. (2.5), but we create or annihilate two bosons. In fact, the squeeze operator was first conceived for the radiation states of idealised two-photon lasers [57].

We then define a squeezed coherent states as the application of the squeeze operator on a bosonic coherent state $|\alpha\rangle$

$$|\alpha, \xi\rangle = \hat{S}(\xi)|\alpha\rangle = \hat{S}(\xi)\hat{D}(\alpha)|0\rangle . \tag{2.8}$$

It is convenient to obtain an operator for which these are eigenstates, much like coherent states are eigenstates of the annihilation operator. Since we are also working with the coherent states, a transformation of the annihilation operator using the squeeze operator becomes ideal, since $\hat{S}(\xi)\hat{a}\hat{S}^{\dagger}(\xi)|\alpha, \xi\rangle = \hat{S}(\xi)\hat{a}|\alpha\rangle = \alpha|\alpha, \xi\rangle$. Thus, by expansion of the exponential operator $\hat{S}(\xi)$ we obtain the canonical transformation

$$\hat{A} = \hat{S}(\xi)\hat{a}\hat{S}^{\dagger}(\xi) = \mu\hat{a} + \nu\hat{a}^{\dagger}, \tag{2.9}$$

where $\mu = \cosh r$ and $\nu = \sinh r e^{i\theta}$.

From the creation and annihilation operators we can recover the position and momentum operators as $\hat{q} = (\hat{a} + \hat{a}^{\dagger})/\sqrt{2}$ and $\hat{p} = (\hat{a} - \hat{a}^{\dagger})/(\sqrt{2}i)$. Then, we can calculate the variances of this operators using eq. (2.9) to obtain

$$(\Delta\hat{q})^2_{\alpha,\xi}(\Delta\hat{p})^2_{\alpha,\xi} = \frac{1}{4}\left(1 + \sinh^2 2r \sin^2\theta\right)^2 \geq \frac{1}{4}. \tag{2.10}$$

The squeezed coherent states will show minimum uncertainty when $r = 0$ or $\theta = 0$ or π. The case $r = 0$ is trivial, as we simply recover the coherent states. On the former case, we either obtain

$$\Delta\hat{q} = \frac{e^{-r}}{\sqrt{2}}, \ \Delta\hat{p} = \frac{e^{r}}{\sqrt{2}}, \tag{2.11}$$

for $\xi = re^{i0} = r$, or

$$\Delta\hat{q} = \frac{e^{r}}{\sqrt{2}}, \ \Delta\hat{p} = \frac{e^{-r}}{\sqrt{2}}, \tag{2.12}$$

for $\xi = re^{i\pi} = -r$. For the results $\xi = \pm r$, we obtain the desired squeezing of the probability distribution, as the quantum fluctuations in one variable are reduced with e^{-r} at the expense of the increase in the conjugate variable. In the context of bosonic coherent states, r is naturally referred to as the *squeeze parameter*.

2.3 Pseudo-spin and collective operators

It becomes natural to wonder if coherent and squeezed states can be found in other Lie algebras. This is indeed the case, and we will now explore the scenario of the spin 1/2, which can be mapped from a two-level atom. Moving forward we will use atoms as our particles of interest in the rest of this work, so we will refer to them as such. But first, we must define the operators defining such an algebra to describe said states in the spin phase space.

We define the pseudo-spin of our atoms from a well defined subspace coming from the internal degrees of freedom of the atoms. Throughout this work, we will only consider atoms with two isolated internal states labelled as $|\uparrow\rangle, |\downarrow\rangle$. Any superposition of such states belongs to the SU(2) Lie group, so we can describe their generator operators using the Pauli matrices $\sigma_\alpha, \alpha \in x, y, z$. The Pauli matrices obey the commutation relations $[\sigma_\alpha, \sigma_\beta] = 2i\varepsilon_{\alpha\beta\gamma}\sigma_\gamma$, where $\varepsilon_{\alpha\beta\gamma}$ is the Levi-Civita symbol. This is because the single-atom operator must obey the usual angular momentum commutation relations, respecting the SU(2) algebra. We then define the spin-1/2 operators as

$$\hat{S}_j^\alpha = \frac{1}{2}\sigma_j^\alpha, \tag{2.13}$$

where α indicates one of the three generators of the algebra $\{x, y, z\}$ and j is the label for an atom. This still holds when multiple atoms occupy the same position and internal state, as the corresponding Hilbert space is a direct sum for individual atoms.

It is practical to represent the spin operators in terms of the creation and annihilation operators

$$\hat{S}_j^x = \frac{1}{2}\left(\hat{S}_j^+ + \hat{S}_j^-\right), \tag{2.14}$$

$$\hat{S}_j^y = \frac{1}{2i}\left(\hat{S}_j^+ - \hat{S}_j^-\right), \tag{2.15}$$

$$\hat{S}_j^z = \frac{1}{2}\left(\hat{u}_j^\dagger\hat{u}_j + \hat{d}_j^\dagger\hat{d}_j\right), \tag{2.16}$$

where $\hat{u}_j$ ($\hat{d}_j$) corresponds to the atom annihilation operator of state $|\uparrow\rangle$ ($|\downarrow\rangle$) at site j and $\hat{S}_j^+ = \hat{u}_j^\dagger\hat{d}_j$, $\hat{S}_j^- = \hat{d}_j^\dagger\hat{u}_j$. Since this operators are constructed by a pair of creation-annihilation operators, they not only conserve atom number but parity. Thus, there is no need to distinguish between fermionic or bosonic systems at this stage.

It follows that the collective spin of the system can be equally described as a direct sum of the Hilbert space of a collection of spins, obtaining

$$\hat{S}_\alpha = \sum_{j=1}^{N}\hat{S}_j^\alpha. \tag{2.17}$$

The collective spin operator thus describes the spin quantum number of maximal value $S = N/2$, where N is the number of spins in the system. The collective state can be easily visualised if we assume the state is separable, but it becomes harder to picture when quantum correlations appear. In such case, we can rely on a quasi-probability distribution like the Husimi function $Q(\theta, \phi)$ to portray the correlations of the system over the Bloch Sphere with radius equal to the expectation value of the mean spin direction operator.

2.4 Spin coherent states

We have defined the bosonic coherent states as a result of the diagonalization of the boson annihilation operator. Naturally, we may ask ourselves if we can define similar coherent states for atomic particles defined by their spin [58, 59]. The initial construction of the spin coherent states in quantum optics relied on the application of a classical electromagnetic field onto the spin particles of interest. The goal here was to see if we could retrieve the coherent states by identical principles of their bosonic counterpart, since the electromagnetic field could be the indirect generator of such states.

We can express the Hamiltonian of an assembly of N two-level atoms interacting with a classical electromagnetic field using the collective operators as

$$\hat{H} = \Omega\hat{S}_z + \lambda(t)\hat{S}_+ + \lambda^*(t)\hat{S}_-. \tag{2.18}$$

When the driving field $\lambda(t)$ is turned off, the Hamiltonian reduces to

$$\hat{H}_0 = \Omega\hat{S}_z, \tag{2.19}$$

which is, by construction, diagonal with respect to the angular momentum eigenstates $|S,m\rangle$ where $m \in [-S,S]$, such that $\hat{H}_0 |S,m\rangle = m\Omega |S,m\rangle$. We also refer to these eigenstates as Dicke states.

We can then express the original Hamiltonian in the interaction picture as

$$\hat{H}_I = e^{i\hat{H}_0 t}\left(\lambda(t)\hat{S}_+ + \lambda^*(t)\hat{S}_-\right)e^{-i\hat{H}_0 t}, \tag{2.20}$$

$$= i\left(\zeta(t)\hat{S}_+ - \zeta^*(t)\hat{S}_-\right), \tag{2.21}$$

with $i\zeta(t) = \lambda(t)e^{i\Omega t}$. If we then initialise the evolution of the system with the natural choice of the lowest energy state $|S,-S\rangle$, we obtain

$$|\Psi_I(t)\rangle = e^{\zeta(t)\hat{S}_+ - \zeta^*(t)\hat{S}_-}|S,-S\rangle, \tag{2.22}$$

up to a given phase factor.

If we compare this result with the displacement operator in eq. (2.5) which generates the bosonic coherent states, we can see a clear path to compute the spin coherent states. The first step is to identify $\zeta(t) \to \zeta$ as our parameter to generate the coherent states and split the unitary operator $e^{\zeta\hat{S}_+ - \zeta^*\hat{S}_-}$ using the Baker–Campbell–Hausdorff formula to obtain

$$e^{\zeta\hat{S}_+ - \zeta^*\hat{S}_-} = e^{\tau\hat{S}_+}e^{\ln\left(1+|\tau|^2\right)\hat{S}_z}e^{-\tau^*\hat{S}_-}. \tag{2.23}$$

with $\tau = \tan|\zeta|e^{i\arg\zeta}$. The action of the lowering operator $\hat{S}_-$ on the state $|S,-S\rangle$ vanishes, so the computation reduces to expanding the spin coherent state in terms of the angular momentum eigenstates $|S, m\rangle$ using the ladder operator such that

$$|S, m\rangle = \sqrt{\frac{(S-m)!}{(2S)!(S+m)!}} \left(\hat{S}_+\right)^{S+m} |S, -S\rangle . \tag{2.24}$$

Then, we obtain

$$\begin{aligned} |S, -S\rangle_\zeta &= e^{\zeta \hat{S}_+ - \zeta^* \hat{S}_-} |S, -S\rangle , \\ &= e^{\tau \hat{S}_+} e^{\ln\left(1+|\tau|^2\right)\hat{S}_z} e^{-\tau^* \hat{S}_-} |S, -S\rangle , \\ &= (1+|\tau|^2)^{-S} e^{\tau \hat{S}_+} |S, -S\rangle , \\ &= (1+|\tau|^2)^{-S} \sum_{m=-S}^{S} \frac{(\tau \hat{S}_+)^{S+m}}{(S+m)!} |S, -S\rangle , \\ &= (1+|\tau|^2)^{-S} \sum_{m=-S}^{S} \sqrt{\binom{2S}{S+m}} \tau^{S+m} |S, m\rangle . \end{aligned} \tag{2.25}$$

If we inspect the unitary operator again, we can see it as a rotation around a given axis in the $x-y$ plane since $\hat{S}_\pm = \hat{S}_x \pm i\hat{S}_y$. We can parameterise the operator as

$$\hat{R}(\theta, \phi) = e^{-i\theta\left(\sin\phi \hat{S}_x - \cos\phi \hat{S}_y\right)}, \tag{2.26}$$

for $\zeta = 1/2\theta e^{-i\phi}$. This means spin coherent states are but rotations of the angular momentum state $|S, -S\rangle$, so they will be eigenstates of the corresponding rotated $\hat{S}_z$ operator. We can illustrate more clearly the angles of rotation by performing this rotation on the quantisation axis such that

$$\begin{aligned} \hat{R}(\theta, \phi)\hat{S}_z |S, -S\rangle &= -S |S, -S\rangle_\zeta , \\ &= \hat{R}(\theta, \phi)\hat{S}_z \hat{R}^{-1}(\theta, \phi)\hat{R}(\theta, \phi) |S, -S\rangle , \\ &= \left(-\sin\theta \left(\cos\phi \hat{S}_x - \sin\phi \hat{S}_y\right) + \cos\theta \hat{S}_z\right) |S, -S\rangle_\zeta , \end{aligned} \tag{2.27}$$

which illustrates that the spin coherent state $|S, -S\rangle \zeta$ is an eigenstate of the spin operator $\hat{R}(\theta, \phi)\hat{S}_z \hat{R}^{-1}(\theta, \phi)$ along the direction of the vector $(S, \theta + \pi, \phi)$ in spherical coordinates. Notice that here we have shown that the spin coherent state is an eigenstate of the rotated quantisation axis z, not of the ladder operator $\hat{S}_-$, as we could in principle expect from the derivation of the bosonic coherent states. In any case, we will find more convenient and intuitive to express the spin coherent states with these angles, so we can rewrite eq. (2.25) with $\tau = \tan(\theta/2)\, e^{-i\phi}$ to obtain

$$
\begin{aligned}
|\theta, \phi\rangle &\equiv |S, -S\rangle\, \zeta, \\
&= \sum_{m=-S}^{S} \sqrt{\binom{2S}{S+m}} \left(\cos\frac{\theta}{2}\right)^{S-m} \left(\sin\frac{\theta}{2} e^{-i\phi}\right)^{S+m} |S, m\rangle\,.
\end{aligned} \tag{2.28}
$$

We can further decompose the coherent states to picture them more easily as a product state of individual spins polarised in the same direction. To do so, we can use two key ingredients: First, the lowest angular momentum state of an ensemble of N spins is uniquely defined as $|S = N/2, -S\rangle = \otimes_j^N |{\downarrow_j}\rangle$. Second, collective rotations act identically on the subspace of each spin. Thus, the spin coherent states can also be written as

$$
|\theta, \phi\rangle = \hat{R}(\theta, \phi) \bigotimes_j^N |{\downarrow_j}\rangle = \bigotimes_j^N \left(\cos\frac{\theta}{2} |{\downarrow_j}\rangle + e^{i\phi} \sin\frac{\theta}{2} |{\uparrow_j}\rangle \right). \tag{2.29}
$$

Since the spin coherent states are constructed in a very similar fashion to the bosonic coherent states, we may expect similar properties like the formation of a complete basis or the fulfilment of minimum variance in Heisenberg's uncertainty. While it can be shown that the former is true, the later is more subtle since the quadrature changes from a complex plane to an spherical surface. The uncertainty relation in spin space may be written as $(\Delta\hat{S}_x)^2(\Delta\hat{S}_y)^2 \geq |\langle\hat{S}_z\rangle|^2/4$. From the previous definitions of the coherent states as rotations we can find that, for a spin coherent state $|\theta, \phi\rangle$,

$$
\left(\Delta\hat{S}_x\right)^2 \left(\Delta\hat{S}_y\right)^2 - \frac{1}{4} \left|\left\langle \hat{S}_z \right\rangle\right|^2 = \frac{1}{4} S^2 \sin^4\theta \cos^2\phi \sin^2\phi. \tag{2.30}
$$

This result only vanishes when $\theta = 0, \pi$ or $\phi = n\pi/2; \forall n \in \mathbb{Z}$. Thus, the uncertainty in the quadrature $x - y$ is minimised only when the state is polarised along z or projects onto the x or y directions. In contrast with the bosonic coherent states, we do not minimise the uncertainty in all directions, but must choose wisely to take advantage of a particular coherent state. This issue is immediately solved when we remember that the spin coherent states are a result of the rotation of the state polarised along $\hat{S}_z$ for the spherical coordinates (θ, ϕ). Thus, for each coherent state, we find minimum product uncertainty in the plane perpendicular to it's polarisation direction, given by said angles.

2.5 Spin-squeezing parameter

Squeezed states are, broadly speaking, those which reduce the measurement uncertainty of the observable of interest due to entanglement with respect to an uncorrelated state, up to the limit set by Heisenberg's uncertainty principle. In the case of the bosonic coherent states, the squeeze operator in eq. (2.7) acting on a coherent state generates an arbitrarily squeezed state when $\xi = \pm r; r \in \mathbb{R}$, where r is the bosonic squeezing parameter. The bosonic squeezed state is then obtained as in eq. (2.8). This, however, is not so trivially found on spin systems, as the quadrature depends on the polarisation direction of a given state and other relevant variables like the spin length may vary during the squeezing process.

There are different definitions of spin-squeezing depending on their utility and we will give a brief overview of some of them.

We mainly aim to use spin squeezed states to improve measurement precision brought by this reduction in uncertainty. Thus, spin squeezing has immediate applications in Ramsey spectroscopy [9], gravitational-wave interferometry [55] or atomic clocks [60].

However, we will also acknowledge definitions focused on detection of quantum entanglement in the form of Bell violations, as spin squeezed states are more resilient to different decoherence channels than highly entangled states like the GHZ state [10, 61].

To simplify notation, we refer to the mean spin direction, which can be calculated from three orthogonal directions, as n; as it is normal to the plane of interest. We refer to the direction of minimal variance orthogonal to n as min. Finally, we refer to to the orthogonal direction to these previous two as $\perp$. In the next subsections we will write the set of three orthogonal spin operators in this frame of reference as $\hat{S}_n, \hat{S}_{\min}, \hat{S}_\perp$. We illustrate this coordinate system in fig. 2.1.

Minimal Variance of Spin

The minimal variance is the main value to measure squeezing and obtain a metrological advantage. However, depending on the evolution of the system, the direction in which this variance is found can change in time. While it is possible to find the direction of minimal variance of the spin components numerically, this task can be tackled analytically by finding the minimal eigenvalue of the corresponding covariance matrix [62]. Moreover, with this direction we can obtain theoretical results of the squeezing parameter for models where the expectation values are known. While this calculation can become a bit tedious [62, 63], we will simplify it by working on a rotated reference frame to reduce the optimisation problem to a single variable.

For convenience, let us rotate our reference frame such that the z-direction coincides with the mean spin direction n,

$$\hat{S}_{x'} = \cos\theta(\cos\phi\hat{S}_x + \sin\phi\hat{S}_y) - \sin\theta\hat{S}_z, \tag{2.31}$$

$$\hat{S}_{y'} = -\sin\phi\hat{S}_x + \cos\phi\hat{S}_y, \tag{2.32}$$

$$\hat{S}_{z'} = \hat{S}_n = \sin\theta(\cos\phi\hat{S}_x + \sin\phi\hat{S}_y) + \cos\theta\hat{S}_z, \tag{2.33}$$

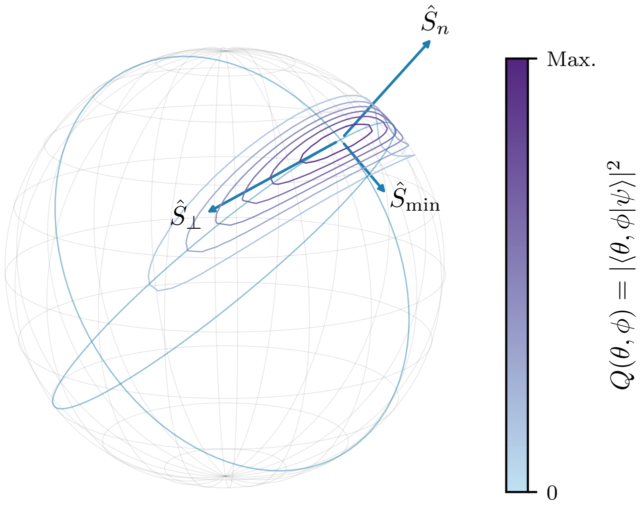

Figure 2.1: Bloch sphere representation of the spin directions of interest for a given squeezed state.

where

$$
\begin{aligned}
\theta =& \arccos \frac{\langle \hat{S}_z \rangle}{\sqrt{\langle \hat{S}_x \rangle^2 + \langle \hat{S}_y \rangle^2 + \langle \hat{S}_z \rangle^2}}, \\
\phi =& \operatorname{sgn} \langle \hat{S}_y \rangle \arccos \frac{\langle \hat{S}_x \rangle}{\sqrt{\langle \hat{S}_x \rangle^2 + \langle \hat{S}_y \rangle^2}}.
\end{aligned}
$$

The variance of interest is then calculated in the $(\hat{S}_{x'}, \hat{S}_{y'})$ plane, so we can define the minimal variance direction as a vector characterised by the angle α. The spin operator along the minimal variance direction is then

$$\hat{S}_{\text{min}} = \vec{n}_{\text{min}} \cdot \left(\hat{S}_{x'}, \hat{S}_{y'}, \hat{S}_{z'} \right) = \cos\alpha \hat{S}_{x'} + \sin\alpha \hat{S}_{y'}. \tag{2.34}$$

with corresponding variance

$$
\begin{aligned}
\left(\Delta \hat{S}_{\text{min}} \right)^2 =& \left\langle \hat{S}^2_{\text{min}} \right\rangle - \left\langle \hat{S}_{\text{min}} \right\rangle^2, \\
=& \frac{1+\cos 2\alpha}{2} \left(\Delta \hat{S}_{x'} \right)^2 + \frac{1-\cos 2\alpha}{2} \left(\Delta \hat{S}_{y'} \right)^2 + \frac{\sin 2\alpha}{2} \left(\Delta \hat{S}_{x'} \hat{S}_{y'} \right),
\end{aligned}
$$

where the variance along the direction $\vec{n}$ is $(\Delta \hat{S}_{\vec{n}})^2 = \langle \hat{S}^2_{\vec{n}} \rangle - \langle \hat{S}_{\vec{n}} \rangle^2$ and $\left(\Delta \hat{S}_{\vec{n}} \hat{S}_{\vec{m}} \right) = \langle \hat{S}_{\vec{n}} \hat{S}_{\vec{m}} + \hat{S}_{\vec{m}} \hat{S}_{\vec{n}} \rangle - 2 \langle \hat{S}_{\vec{n}} \rangle \langle \hat{S}_{\vec{m}} \rangle$.

By minimising $\left(\Delta\hat{S}_{\min}\right)^2$ with respect to α we obtain

$$2\left(\Delta\hat{S}_{\min}\right)^2 = \left(\Delta\hat{S}_{x'}\right)^2 + \left(\Delta\hat{S}_{y'}\right)^2 + \sqrt{\left(\left(\Delta\hat{S}_{x'}\right)^2 - \left(\Delta\hat{S}_{y'}\right)^2\right)^2 + \left(\Delta\hat{S}_{x'}\hat{S}_{y'}\right)^2}, \tag{2.35}$$

for

$$\cos 2\alpha = -\frac{\left(\Delta\hat{S}_{x'}\right)^2 - \left(\Delta\hat{S}_{y'}\right)^2}{\sqrt{\left(\left(\Delta\hat{S}_{x'}\right)^2 - \left(\Delta\hat{S}_{y'}\right)^2\right)^2 + \left(\Delta\hat{S}_{x'}\hat{S}_{y'}\right)^2}}. \tag{2.36}$$

In eq. (2.36) α is undefined with a phase $n\pi; \forall n \in \mathbb{Z}$. This is irrelevant, as the variance only depends on the direction of the resulting vector, which is identical in all cases. While this result is expressed in the rotated frame, it is simple to write in the original frame by expanding the variances and co-variances using eqs. (2.31) and (2.32).

The result implies that as long as we have the expectation values of the first and second moments of the collective spin in three arbitrary orthogonal directions, we can find the minimal variance and its direction immediately at each instance in time. On the other hand, it allows us to predict the minimal variance direction and require fewer measurements in an experiment. This minimal variance can be used to calculate the spin squeezing parameter definitions given in the following subsections.

Definition by Kitagawa and Ueda

The first definition of spin squeezing was given by Kitagawa and Ueda in 1993 with their seminal work "Squeezed spin states" [6]. Borrowing the results of bosonic squeezed states, they adapted the concept for to two-level atoms instead of photons. With the spin coherent states being well understood and defined [58, 59], the next step was to define under which conditions squeezing can happen. Due to the SU(2) algebra, the quadrature of the spin components to minimise the variance product is not uniquely defined. As we have seen in section 2.4, we can pick the plane perpendicular to the initial coherent state to guarantee the Heisenberg's uncertainty is minimal. Without loss of generality, we can assume the mean spin direction is preserved and we only need to pay attention to the initially defined quadrature. In the original paper [6], the authors only looked at the changes in the variances by means of different unitary transformations that we will see in detail in section 2.6. Still, we can extract a normalised spin-squeezing parameter from their results by normalising the minimal variance perpendicular to the mean spin ($(\Delta\hat{S}_{\min})^2$) as

$$\xi_S^2 = \frac{\left(\Delta\hat{S}_{\min}\right)^2}{S/2} = \frac{4\left(\Delta\hat{S}_{\min}\right)^2}{N}, \tag{2.37}$$

since the spin length for a spin coherent state is given by $S = N/2$, where N is the number of spins in the system. It is easy to see that $\xi_S^2 = 1$ for a spin coherent state, as in such case $(\Delta\hat{S}_{\min})^2 = (\Delta\hat{S}_\perp)^2 = N/4$. As the coherent states lack quantum correlations, we may expect certain correlated states to yield $\xi_S^2 < 1$. In fact, it has been shown that ξ_S^2 is related to negative correlations [9] and concurrence [64].

Definition by Wineland et al.

Around the same time, Wineland et al. constructed a squeezing parameter to measure accuracy enhancement in Ramsey spectroscopy [7, 8]. In this framework the spin coherent states act as a noise reference. This parameter is derived through the definition of phase sensitivity, rather than the quadrature approach of bosonic squeezing that ξ_S^2 relies on.

Let us suppose we want to measure a phase ϕ which characterises a rotation of a given state on a perpendicular axis.Without loss of generality, we assume the state is originally located along the z direction ($\langle\hat{S}_x\rangle = \langle\hat{S}_y\rangle = 0$) and we rotate it by phase ϕ around the x direction such that

$$\hat{S}_{y'} = \hat{R}_x(\phi)\hat{S}_y\hat{R}_x^{-1}(\phi) = \cos\phi\hat{S}_y - \sin\phi\hat{S}_z, \tag{2.38}$$

is the new axis y in the rotated frame. It follows that

$$\begin{aligned}\left\langle\hat{S}_{y'}\right\rangle &= \cos\phi\left\langle\hat{S}_y\right\rangle - \sin\phi\left\langle\hat{S}_z\right\rangle = -\sin\phi\left\langle\hat{S}_z\right\rangle, \\ \left(\Delta\hat{S}_{y'}\right)^2 &= \cos^2\phi\left(\Delta\hat{S}_y\right)^2 + \sin^2\phi\left(\Delta\hat{S}_z\right)^2 - \frac{1}{2}\sin 2\phi\left\langle\hat{S}_y\hat{S}_z + \hat{S}_z\hat{S}_y\right\rangle.\end{aligned}$$

Then, phase sensitivity can be accounted for through error propagation as

$$\Delta\phi = \frac{\Delta\hat{S}_{y'}}{\left|\partial\langle\hat{S}_{y'}\rangle/\partial\phi\right|} = \frac{\Delta\hat{S}_{y'}}{\left|\cos\phi\langle\hat{S}_z\rangle\right|}. \tag{2.39}$$

If ϕ is sufficiently small, we can approximate $\cos\phi \sim 1$ and $(\Delta\hat{S}_{y'})^2 \sim (\Delta\hat{S}_y)^2$. Then

$$\Delta\phi = \frac{\Delta\hat{S}_y}{\left|\langle\hat{S}_z\rangle\right|}. \tag{2.40}$$

We can write this result for the phase sensitivity achievable along the direction of minimal variance as

$$\Delta\phi = \frac{\Delta\hat{S}_{\min}}{\langle\hat{S}_n\rangle}, \tag{2.41}$$

where $\langle\hat{S}_n\rangle = \sqrt{\langle\hat{S}_x\rangle^2 + \langle\hat{S}_y\rangle^2 + \langle\hat{S}_z\rangle^2}$.

For instance, for a spin coherent state we obtain

$$(\Delta\phi)_{\mathrm{SCS}} = \frac{1}{\sqrt{N}}. \tag{2.42}$$

which is generally referred to as the shot-noise limit or standard quantum limit.

The spin squeezing parameter proposed by Wineland et al. is constructed as

$$\xi_R^2 = \frac{(\Delta\phi)^2}{(\Delta\phi)_{\mathrm{SCS}}^2} = \frac{N\left(\Delta\hat{S}_{\mathrm{min}}\right)^2}{\langle\hat{S}_n\rangle^2}. \tag{2.43}$$

In this framework the spin squeezing parameter is established as a sensitivity ratio between an arbitrary state and the spin coherent states. If the state is highly correlated, the sensitivity increases and $\xi_R^2 < 1$. In such case, the state provides a phase sensitivity advantage over the shot-noise limit.

Moreover, we can compare it with the previously defined spin squeezing parameter ξ_S^2

$$\frac{\xi_R^2}{\xi_S^2} = \left(\frac{N/2}{\langle\hat{S}_n\rangle}\right)^2 \geq 1, \tag{2.44}$$

since $N/2 = S \geq \langle\hat{S}_n\rangle$, to deduce the spin squeezing parameter proposed by Wineland et al. is strictly more restrictive.

Lastly, ξ_R^2 has a lower bound due to the uncertainty relation

$$\left(\Delta\hat{S}_{\mathrm{min}}\right)^2\left(\Delta\hat{S}_{\perp}\right)^2 \geq \frac{1}{4}|\langle\hat{S}_n\rangle|^2, \tag{2.45}$$

which can be written as

$$\xi_R^2 \geq \frac{N}{4\left(\Delta\hat{S}_{\perp}\right)^2}. \tag{2.46}$$

We can show the eigenstates with the largest eigenvalue of $(\Delta\hat{S}_{\perp})^2$ are of the form [8]

$$|\psi_{\perp}\rangle = \frac{1}{\sqrt{2}}\left(|S,S\rangle_{\perp} + e^{i\phi}|S,-S\rangle_{\perp}\right), \tag{2.47}$$

and yield $(\Delta\hat{S}_{\perp})^2 = S^2$. So in general, $(\Delta\hat{S}_{\perp})^2 \leq S^2 = (N/2)^2$ and we obtain

$$\xi_R^2 \geq \frac{1}{N}. \tag{2.48}$$

If we saturate this inequality, we have reached the so-called Heisenberg limit [27], which is the ideal scenario where the state is maximally squeezed.

Through the rest of this work, we refer to ξ_R^2 as simply the spin squeezing parameter ξ^2.

Spin squeezing as an entanglement witness

Spin squeezing is attractive to detect entanglement, as it constitutes an experimentally more accessible quantity than other observables like concurrence of entanglement entropy. In some systems the individual spins are, in fact, not accessible. This makes spin squeezing a relevant quantity, which also has the advantage of requiring few measurements.

However, particular definitions of spin squeezing might be able to show different kinds of entanglement. In other words, spin squeezing definitions can construct different entanglement criteria. For instance, it has been shown that $\xi_S^2 < 1$ implies negative pairwise correlations [9]. This is clear to picture if we recall that, to generate spin squeezing, we require quantum correlations to surpass the shot-noise limit offered by the spin coherent states.

As the state becomes more non-separable in this scheme, entanglement is built up [65], which can be shown by introducing a Lagrange multiplier in results for ξ_R^2. This can also be represented in the following spin squeezing criteria [66]

$$\frac{(\Delta \hat{S}_{\min})^2}{\langle \hat{S}_n \rangle^2 + \langle \hat{S}_\perp \rangle^2} \geq \frac{1}{N}, \tag{2.49}$$

which certifies many-body entanglement as the state becomes non-separable. It can be found that symmetric states that violate eq. (2.49) are two-qubit entangled [64], which is not the case in general [67].

This pattern of spin squeezing criteria tailored towards a specific type of entanglement, but fails to detect entanglement in general, is repeated for criteria for many-body singlet states [68, 69], entangled Dicke states [69] and three-qubit entanglement [70, 71].

An alternative path to singular criteria that can only separate certain entangled states from others is to accumulate a number of inequalities such that their combined results give us more information about entanglement of spin squeezed states [70, 71]. Thus, it is possible to combine several generalised spin squeezing inequalities for different criteria to determine if a given arbitrary spin squeezed state of spin-1/2 is entangled [67, 72]:

$$\left\langle \hat{S}_x^2 \right\rangle + \left\langle \hat{S}_y^2 \right\rangle + \left\langle \hat{S}_z^2 \right\rangle \leq \frac{N(N+2)}{4}, \tag{2.50}$$

$$(\Delta \hat{S}_x)^2 + (\Delta \hat{S}_y)^2 + (\Delta \hat{S}_z)^2 \geq \frac{N}{2}, \tag{2.51}$$

$$\left\langle \hat{S}_\alpha^2 \right\rangle + \left\langle \hat{S}_\beta^2 \right\rangle - \frac{N}{2} \leq (N-1)(\Delta \hat{S}_\gamma)^2, \tag{2.52}$$

$$(N-1)\left[(\Delta \hat{S}_\alpha)^2 + (\Delta \hat{S}_\beta)^2\right] \geq \left\langle \hat{S}_\gamma^2 \right\rangle + \frac{N(N-2)}{4}, \tag{2.53}$$

where α, β, γ take all the possible permutations of x, y, z. While not as compact as the spin squeezing parameters, this set of simple inequalities is complete in the sense of unequivocally detecting entanglement when information about the state is limited to the first and second moments of the collective spin components. No other inequality based on these observables will be able to detect more entangled states. Interestingly, this set of criteria can also detect separable two-body entanglement despite not including correlations among multiple parties.

It is possible to map this set of criteria to the case of particles with spin $j > 1/2$ [26] through the use of modified second moments of spin components. These criteria can be recovered from a generalized entanglement witness for local observables when the local spin components are chosen as the observables of interest [38]. This witness is constructed on the violation of separability in a data-driven approach, it provides a more compact, while less explicit, criteria to study entanglement detection.

It is also possible to use this data-driven perspective to construct Bell inequalities that detect separability which depend only on first and second collective moments [37]. They can be adapted to spin squeezed states to detect entanglement in a wider variety of scenarios, since they can include any number of outcomes and settings in the measurements. We will explore these advantages in Chapter 8 to detect entanglement for spin-1/2 systems in the presence of occupancy defects.

2.6 Paradigmatic models

Kitawaga and Ueda [6] took the idea of dynamical generation of squeezed light and applied it to a system of atoms with total spin S. While they admit squeezing generation can happen with higher order terms, they defined the simplest non-linear Hamiltonians which could generate squeezing in a spin system, One-Axis Twisting (OAT) and Two-Axis Counter Twisting (TACT). These models are clearly based on the Kerr medium dynamics [73] and squeeze operator (2.7), found in quantum optics. The success of these models rely on the conservation of total spin, while forcing the probability distribution to change non-linearly over the surface of the Bloch sphere. Any linear term would introduce a rotation of the state, without incurring in deformations of the probability distribution by itself. Thus, the simplest form of non-linearity we can introduce are second moment operators. These models allow us to breach the standard quantum limit, obtaining much higher correlations than an ensemble of N uncorrelated measurements.

One-Axis Twisting

To obtain the desired squeezing of the probability distribution, we may look for a unitary transformation over the coherent state that changes relative phases of the state components but not its mean direction. That way, the centre of the distribution stays in the same place but correlations can build up entanglement, and thus squeezing. Since spin coherent states can be expanded in angular momentum states, we might look for a unitary operator $\hat{U}(t) = e^{i\hat{H}t} = e^{itF(\hat{S}_z)}$, as they are eigenstates of $\hat{S}_z$. If we work in the Heisenberg picture to see the evolution of the ladder operators, we obtain

$$\hat{S}_+(t) = \left(\hat{S}_-(t)\right)^\dagger = \hat{U}(t)\hat{S}_+(0)\hat{U}^\dagger(t) = \hat{S}_+(0)e^{itf(\hat{S}_z)}, \tag{2.54}$$

where $f(\hat{S}_z) = F(\hat{S}_z + 1) - F(\hat{S}_z)$. If we plug $F(\hat{S}_z) = \chi\hat{S}_z$, the phase shift is global and no correlations can build up over time. If instead we pick $F(\hat{S}_z) = \chi\hat{S}_z^2$, $f(\hat{S}_z) = 2\chi(\hat{S}_z + 1/2)$ so we can obtain phase correlations among the total angular momentum components of the state.

Thus, we define the one-axis twisting model as

$$\hat{H}_{\text{OAT}} = \chi\hat{S}_z^2. \tag{2.55}$$

This model is in fact analogous to the dynamics found for coherent light in an optical Kerr non-linear medium, which is characterised by [73].

$$\hat{H} = \kappa(\hat{a}^\dagger\hat{a})^2, \tag{2.56}$$

where $\hat{a}$ is the photon annihilation operator.

In order to maximise the correlations, we want our initial spin coherent state to be perpendicular to the twisted axis [6], for instance along the x direction.

Equation (2.55) is a convenient Hamiltonian, as expectation values can be calculated analytically, so the minimum variance (2.35) is well defined in this case. We can approximate the minimal value of the squeezing parameter (2.43) generated by eq. (2.55) for $N \gg 1, |2\chi t| \ll 1$ as [74]

$$\xi^2_{\text{best,OAT}} \simeq \frac{3^{2/3}}{2}\frac{1}{N^{2/3}}. \tag{2.57}$$

It is relevant to point out the direction of minimal variance changes over time and at the optimal time it goes like $\alpha \sim \arctan\left(N^{-1/3}\right)/2$ [6]. The corresponding best squeezing time is found to be [74]

$$\chi t_{\text{best,OAT}} \simeq 3^{1/6}\frac{1}{N^{2/3}}. \tag{2.58}$$

A semi-classical approach might help us understand the dynamics of the one-axis twisting Hamiltonian. One precise method could be the mapping of operators in Hilbert space to differential operators on the classical phase space. This representation is widely successful and relies on the over-completeness of the coherent states as a basis [50, 75]. In our particular case we can rely on a simpler mean-field approximation, since we want a quick description of the coherent states trajectories for a given energy functional [76]. This approximation assumes the coherent state is not distorted during evolution, but should be sufficient to understand the dynamics of the probability distribution at short times. For this mean-field approximation, we replace the creation-annihilation operators by complex numbers such that

$$S_x \to S \sin\theta \cos\phi, \tag{2.59}$$
$$S_y \to S \sin\theta \sin\phi, \tag{2.60}$$
$$S_z \to S \cos\theta, \tag{2.61}$$

represent the mean-field spin operators parameterised for conjugate variables θ, ϕ.

The mean-field Hamiltonian for $\hat{H} = \chi \hat{S}_z^2$ would be $H = \chi S^2 \cos^2\theta$, so the corresponding equations of motion are

$$\frac{\mathrm{d}\phi}{\mathrm{d}t} = \frac{1}{S}\frac{\partial H}{\partial \theta} = -\chi S \sin 2\theta, \tag{2.62}$$
$$\frac{\mathrm{d}\theta}{\mathrm{d}t} = -\frac{1}{S}\frac{\partial H}{\partial \phi} = 0. \tag{2.63}$$

With $\theta \in (0, \pi]$, the energy fluctuations change sign at $\theta = \pi/2$, so upper hemisphere coherent states move in one direction while lower half ones move in the opposite direction. Not only that, but the magnitude of this displacement varies with the latitude. We can expect the probability distribution to nearly follow these rules too in a fashion similar to a shear force applied to the initially coherent state.

This thesis in printed form allows the reader to see an animation of the one-axis twisting model dynamics by flipping the right corners of the document pages from end to beginning. The Husimi distribution corresponding to the best squeezing time from eq. (2.58) is drawn in a different color to easily identify the time at which spin squeezing is optimized. While later distributions might look more squeezed, the mean spin length is reduced in time and at some point the Gaussian character of the state is also lost. However, cat states or a revival of the initial coherent state can be obtained at later times [77]. The animation is computed for $N = 100$ particles and $t \leq 4t_{\mathrm{best,OAT}}$.

The one-axis twisting model has been widely studied due to its simplicity and ubiquity in many systems and scenarios. In fact, its application has been proposed in many platforms like Bose-Einstein condensates [66, 78], optical cavities [79], lattice clocks [80, 81], or bulk molecular gases [32, 82].

Twist And Turn

Interestingly, it has been found that the addition of a linear term orthogonal to the twisting axis in eq. (2.55), aptly named as the twist and turn (TAT) Hamiltonian

$$\hat{H}_{\mathrm{TAT}} = \chi \hat{S}_z^2 + \Omega \hat{S}_x, \tag{2.64}$$

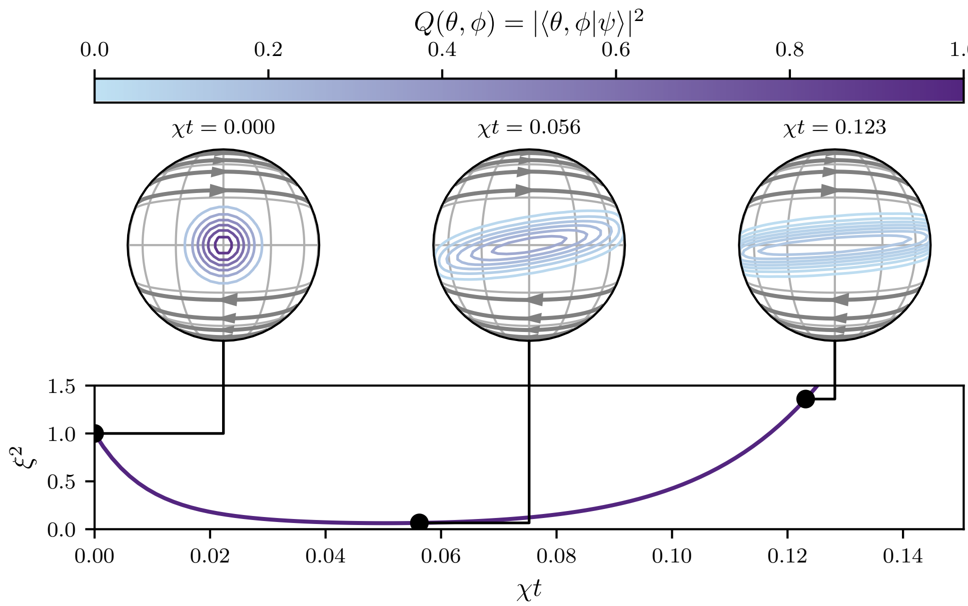

Figure 2.2: Evolution of the one-axis twisting model (2.55) with $N = 100$ particles for an arbitrary χ. Bloch spheres in Hammer projection show the quasi-probability Husimi distribution $Q(\theta, \phi) = |\langle \theta, \phi|\psi(t)\rangle|^2$, for certain points in time. Grey quiver lines in the Bloch spheres portray the mean-field results from eqs. (2.62) and (2.63). The lower panel shows the evolution of the squeezing parameter ξ^2.

can provide squeezing acceleration over eq. (2.55) [83, 84]. While the twisting provides a shear on the probability distribution, the linear term allows a faster spread of the distribution as it realigns the already squeezed distribution with the twisting axis. We can again obtain an understanding of the dynamics under this model at short times through a semi-classical picture.

$$\frac{\mathrm{d}\phi}{\mathrm{d}t} = -\chi S \sin 2\theta + \Omega \cos\theta \cos\phi, \tag{2.65}$$
$$\frac{\mathrm{d}\theta}{\mathrm{d}t} = \Omega \sin\theta \sin\phi. \tag{2.66}$$

While with one-axis twisting we find instability along the equator, the solutions on this case gives us an unstable fixed point along the axis of rotation $\hat{S}_x$. We can see an example of these dynamics in fig. 2.3.

States that maximise Ramsey spectroscopy sensitivity are eigenstates of eq. (2.64) [85]. Moreover, control over the linear term can lead to longer coherence times of the squeezed states with the simple implementation of an external field [86]. The twist and turn Hamiltonian can generate more entanglement than eq. (2.55) [84], but its detection requires high-order non-linear

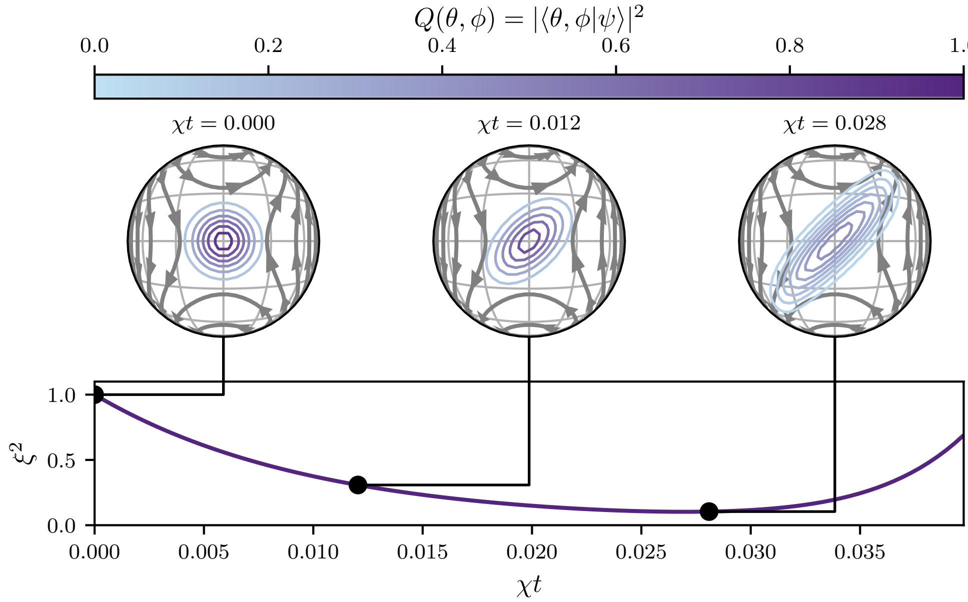

Figure 2.3: Evolution of the twist and turn model (2.64) with $N = 100$ particles and $\Omega = N\chi/2$ for an arbitrary χ. Bloch spheres in Hammer projection show the quasi-probability Husimi distribution $Q(\theta, \phi) = |\langle \theta, \phi|\psi(t)\rangle|^2$, for certain points in time. Grey quiver lines in the Bloch spheres portray the mean-field results from eqs. (2.65) and (2.66). The lower panel shows the evolution of the squeezing parameter ξ^2.

definitions of the squeezing parameter or measuring quantum Fisher information [87].

Two-Axis Counter Twisting (TACT)

While the one-axis twisting model appears in many contexts naturally, it is unable to reach the lower bound of the spin squeezing parameter $\xi_R^2 \sim N^{-2/3} > N^{-1}$. There are, potentially, better options to generate squeezing and reach the Heisenberg limit, rivalling the entanglement of the GHZ states [88]. Moreover, the optimal squeezing angle changes with time and number of particles, which can be problematic for direct experimental measurements. We may imagine that if we compensate the *twisting* of the probability distribution with an action at an orthogonal direction, we might find not only a fixed squeezing angle but even more squeezing.

Similarly to the one-axis twisting model, we can take inspiration from another result of quantum optics like the squeeze operator (2.7) to obtain the Hamiltonian

$$\hat{H}_{\mathrm{TACT}} = \chi \left(\hat{S}_z^2 - \hat{S}_y^2 \right). \tag{2.67}$$

This is the two-axis counter twisting model (TACT), also simply known as the two-axis twisting model (TAT). Notice this last naming convention can be confusing when taking into account the twist and turn model (TAT). The negative sign in eq. (2.68) is important, as

$$\hat{S}^2 = \hat{S}_x^2 + \hat{S}_y^2 + \hat{S}_z^2. \tag{2.68}$$

is conserved unless our Hamiltonian breaks the SU(2) symmetry. Such scenario is explicitly detrimental for eq. (2.43), as it would inevitably reduce the spin length $\langle \hat{S}_n \rangle$. Otherwise, $\hat{S}_z^2 + \hat{S}_y^2 = \hat{S}^2 - \hat{S}_x^2$ simply recovers the one-axis twisting result with a global phase factor.

As with the one-axis twisting model, the choice of twisting axes is arbitrary as long as they are orthogonal to each other, so it might be more natural to define it as

$$\hat{H}_{\mathrm{TACT}} = \chi \left(\hat{S}_+^2 - \hat{S}_-^2 \right), \tag{2.69}$$

since the evolution of a spin coherent state expanded in the angular momentum basis $|S, m\rangle$ is more explicit in this form and directly mimics eq. (2.7).

The model can be solved analytically on short times and $N \gg 1$, showing its maximally squeezed state can almost reach the Heisenberg limit sensitivity [76] as

$$\xi^2_{\mathrm{best,TACT}} = \frac{e}{2}\frac{1}{N}, \tag{2.70}$$

at time

$$\chi t_{\mathrm{best,TACT}} = \frac{\ln 2N}{2N}. \tag{2.71}$$

To optimise squeezing, the initial spin coherent state has to be orthogonal to the twisting axes. We can get an intuition about this fact by employing the mean-field approximation [76] on eq. (2.69). In this case $H = -2i\chi \sin^2\theta \sin 2\phi$ and the equations of motion are

$$\frac{\mathrm{d}\phi}{\mathrm{d}t} = -2iS\chi \sin 2\theta \sin 2\phi, \tag{2.72}$$

$$\frac{\mathrm{d}\theta}{\mathrm{d}t} = 4iS\chi \sin^2\theta \cos 2\phi. \tag{2.73}$$

These derivatives represent a velocity field in the phase space, which we can use to calculate unstable fixed points where the mean spin will not drift but will have competing pulls to generate squeezing. The stability of the fixed points $\frac{\mathrm{d}\phi}{\mathrm{d}t} = \frac{\mathrm{d}\theta}{\mathrm{d}t} = 0$ can be extracted from the stability matrix [1]. In this case, we obtain that the unstable fixed points are located at $\theta = 0, \pi, \forall\phi$. Our optimal initial coherent states should be located at the poles of the Bloch sphere.

The energy fluctuations also show us how the squeezing evolves approximately in fig. 2.4, and numerical simulations show the dynamics are faster than for one-axis twisting.

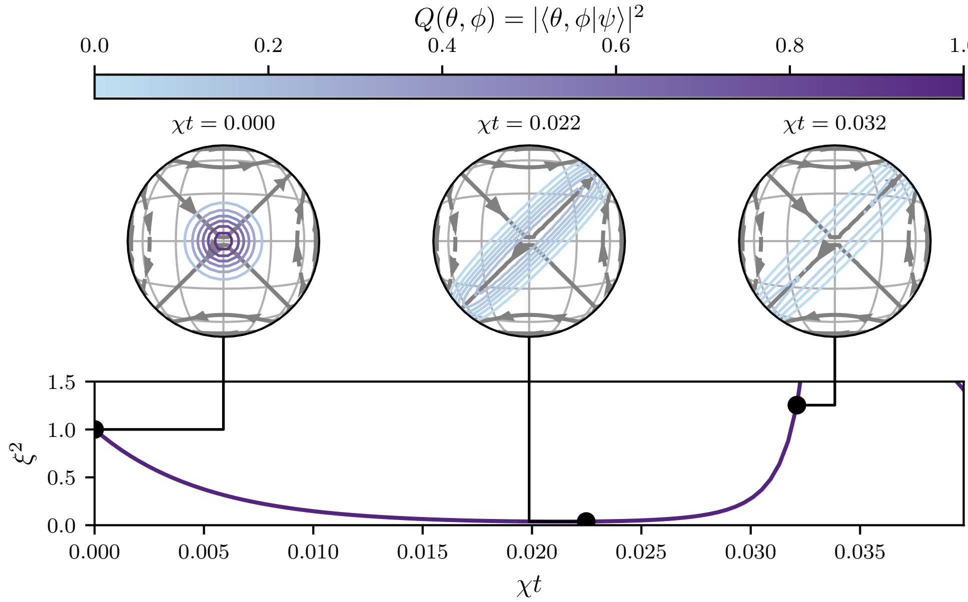

Figure 2.4: Evolution of the two-axis counter twisting model (2.68) with $N = 100$ particles for an arbitrary χ. Bloch spheres in Hammer projection show the quasi-probability Husimi distribution $Q(\theta, \phi) = |\langle\theta, \phi|\psi(t)\rangle|^2$ for certain points in time. Grey quiver lines in the Bloch spheres portray the mean-field results from eqs. (2.72) and (2.73). The line width is fixed in this case to better visualize the direction of the energy fluctuations. The lower panel shows the evolution of the squeezing parameter ξ^2.

Heisenberg limited squeezing is still difficult to reach with two-axis counter twisting models, due to different decoherence channels in experimental setups [89]. But it is predicted to generate highly entangled states much more resilient to decoherence than other proposals if implemented, for instance, using interactions mediated by photon exchange [90]. Very recently, some experiments claimed to have observed the two-axis counter twisting model through polar molecules and Floquet engineering [91], and optical cavities [92].

Chapter 3

Ultra-cold Atoms in the Optical Lattice

In the past, many experimental platforms have been explored to realise spin squeezing, as seen in Chapter 1. We choose ultra-cold atoms in the optical lattice since its a novel platform which describes theoretical models found in statistical and condensed matter physics [28], with a remarkable level of control and tunability. In fact, optical lattices are seen as very flexible and currently one of the best platforms for quantum simulations [29]. This is not only because of the degree of control and reliability they posses, but for the sheer variety of models that can be achieved, even at the level of the Hubbard model [93, 94].

While the wide range of reproducible models can be overwhelming, we focus on the simplest implementations of the Hubbard model for two component systems where slight modifications may give rise to effective models that induce spin squeezing. We hope the exploration contained in this work can serve as a stepping stone to predict spin squeezing phenomena in more complex models. In this chapter, we sketch the derivation of our main models of interest in the optical lattice, the two-component Hubbard model and the Heisenberg model.

3.1 Hubbard model

We may describe the Hamiltonian of a periodic atomic system in second quantisation form as

$$\begin{aligned}\hat{H} &= \int d\boldsymbol{r}\boldsymbol{\Psi}^{\dagger}(\boldsymbol{r})H(\boldsymbol{r})\boldsymbol{\Psi}(\boldsymbol{r}) \\ &+ \frac{1}{2}\int d\boldsymbol{r}\int d\boldsymbol{r'}\boldsymbol{\Psi}^{\dagger}(\boldsymbol{r})\boldsymbol{\Psi}^{\dagger}(\boldsymbol{r'})V(\boldsymbol{r},\boldsymbol{r'})\boldsymbol{\Psi}^{\dagger}(\boldsymbol{r})\boldsymbol{\Psi}^{\dagger}(\boldsymbol{r'}),\end{aligned} \tag{3.1}$$

where $H(\boldsymbol{r}) = \frac{\hbar\nabla^2}{2m} + V_{\text{lattice}}(\boldsymbol{r})$ is the single particle Hamiltonian and $\boldsymbol{\Psi}(\boldsymbol{r}) = \sum_i \phi_i(\boldsymbol{r})\hat{c}_i$ is the field operator written as a sum over the complete set of single particle quantum numbers with $\hat{c}_i$ being the annihilation operator and $\phi_i(\boldsymbol{r})$ the spatial component of the wave-function of quantum numbers determined by i. Depending on the particle statistics being a bosonic or fermionic, the operator shall respect commutation or anti-commutation relations, respectively. Notice the second term in 3.1 accounts for two-body interactions through the potential $V(\boldsymbol{r}, \boldsymbol{r}')$.

For now, let us focus on the first part of the right-hand side of eq. (3.1). The single particle Hamiltonian $H(\boldsymbol{r})$ describes the movement of a particle in a periodic potential $V_{\text{lattice}}(\boldsymbol{r}) = V_{\text{lattice}}(\boldsymbol{r} + \boldsymbol{R}_i)$, where the vector $\boldsymbol{R}_i$ characterizes its periodicity. The solutions of the corresponding Schrodinger equation along $\boldsymbol{R}_i$ are the so-called Bloch functions [95]

$$\Phi^{(n)}_{\boldsymbol{q},\sigma}(\boldsymbol{r}) = e^{i\boldsymbol{q}\boldsymbol{r}} u^{(n)}_{\boldsymbol{q},\sigma}(\boldsymbol{r}), \tag{3.2}$$

for a periodic function

$$u^{(n)}_{\boldsymbol{q},\sigma}(\boldsymbol{r} + \boldsymbol{R}_i) = u^{(n)}_{\boldsymbol{q},\sigma}(\boldsymbol{r}), \tag{3.3}$$

where $\boldsymbol{q}$ is the quasi-momentum which comes from the translational symmetry of the potential, σ is a given internal state of the particle and n enumerates the possible solutions for a given $\boldsymbol{q}$. These solutions are usually referred to as bands, since they form a band structure in the first Brillouin zone. Throughout the text we will refer to the internal states σ as *spin components*, as we can reconstruct the SU(2) algebra required for the spin from a superposition of such internal states. This does not necessarily mean these internal states are actual spin degrees of freedom, as they can be treated as a pseudo-pin without any loss of generality in our current framework.

We can apply a discrete Fourier transformation to the Bloch functions to obtain the Wannier functions

$$w_{\sigma,n}(\boldsymbol{r} - \boldsymbol{R}_i) = w_{i,\sigma,n}(\boldsymbol{r}) = \frac{1}{\sqrt{M}} \sum_{\boldsymbol{q}} e^{-i\boldsymbol{q}\cdot\boldsymbol{R}_i} \Phi^{(n)}_{\boldsymbol{q},\sigma}(\boldsymbol{r}). \tag{3.4}$$

As they are a linear combination of the Bloch functions, they are solutions to the single particle Hamiltonian $H(\boldsymbol{r})$.

If the depth of the periodic potential is large enough, the lowest band, $n = 0$, is well separated from the higher energy bands. In such case, we can expect the particles to not leave the lowest band at sufficiently low temperatures. It is then safe to expand the field operator in the Wannier function basis for $n = 0$, such that

$$\boldsymbol{\Psi}(\boldsymbol{r}) = \sum_{i,\sigma} w_i(\boldsymbol{r})\hat{c}_{i,\sigma}, \tag{3.5}$$

where we have assumed $w_i(\boldsymbol{r}) = w_{i,\sigma}(\boldsymbol{r})$; $\forall\sigma$ and omitted the band structure index n. This assumption about the isolation of the lowest Bloch band is called the *tight-binding* approximation. The Hamiltonian can then be expressed as

$$\begin{aligned}\hat{H} =&\sum_{i,j}\sum_{\sigma_i,\sigma_j}\hat{c}^{\dagger}_{i,\sigma_i}\left(H_{ij}\right)\hat{c}_{j,\sigma_j}\\&+\frac{1}{2}\sum_{i,j,k,l}\sum_{\sigma_i,\sigma_j,\sigma_k,\sigma_l}\hat{c}^{\dagger}_{i,\sigma_i}\hat{c}^{\dagger}_{j,\sigma_j}\left(V_{ijkl}\right)\hat{c}_{k,\sigma_k}\hat{c}_{l,\sigma_k},\end{aligned}\tag{3.6}$$

where

$$H_{ij} = \int d\boldsymbol{r} w_i^*(\boldsymbol{r})H(\boldsymbol{r})w_j(\boldsymbol{r}),\tag{3.7}$$

$$V_{ijkl} = \int d\boldsymbol{r}\int d\boldsymbol{r'} w_i^*(\boldsymbol{r})w_j^*(\boldsymbol{r'})V(\boldsymbol{r},\boldsymbol{r'})w_k(\boldsymbol{r})w_l(\boldsymbol{r'}),\tag{3.8}$$

are the matrix (tensor) elements that can construct associated operators based on the values of the integrals.

Wannier functions are highly localized around $\boldsymbol{r}-\boldsymbol{R}_i$, which allows us to perform certain approximations. For instance, we may only consider tunnelling of the particles among nearest-neighbour sites of the lattice. This is not the case when the periodic potential is very shallow, as the tight-binding approximation stops being valid. On the other hand, if two-body interactions are well described by a contact potential $V(\boldsymbol{r},\boldsymbol{r'}) = g\delta(\boldsymbol{r}-\boldsymbol{r'})$, the dominating contribution will be on-site.

If our system is composed of spin-1/2 fermions, the previous approximations yield the Fermi–Hubbard model

$$\hat{H}_{\mathrm{FH}} = -J\sum_{\sigma=\uparrow,\downarrow}\sum_{\langle i,j\rangle}\left(\hat{c}^{\dagger}_{i,\sigma}\hat{c}_{j,\sigma}+\mathrm{h.c.}\right)+U\sum_i\hat{n}_{i,\uparrow}\hat{n}_{i,\downarrow},\tag{3.9}$$

where $\langle i,j\rangle$ indicates nearest neighbours, $\left\{\hat{c}^{\dagger}_{i,\sigma},\hat{c}_{j,\sigma'}\right\} = \delta_{i,j}\delta_{\sigma,\sigma'}$, $\hat{n}_{i,\sigma} = \hat{c}^{\dagger}_{i,\sigma}\hat{c}_{i,\sigma}$ and

$$J = -\int d\boldsymbol{r} w_i^*(\boldsymbol{r})H(\boldsymbol{r})w_j(\boldsymbol{r})\Big|_{\langle i,j\rangle},\tag{3.10}$$

$$U = g\int d\boldsymbol{r}|w_i(\boldsymbol{r})|^4,\tag{3.11}$$

for arbitrary i,j if the lattice potential is isotropic. We may also find the tunnelling coefficient J marked as t in the literature.

Similarly, if our system is composed of bosons with two internal states, we obtain the two-component Bose–Hubbard model

$$\begin{aligned}\hat{H}_{\mathrm{BH}} =& -J\sum_{\sigma=\uparrow,\downarrow}\sum_{\langle i,j\rangle}\left(\hat{b}^{\dagger}_{i,\sigma}\hat{b}_{j,\sigma}+\mathrm{h.c.}\right)+U_{\uparrow\downarrow}\sum_i\hat{n}_{i,\uparrow}\hat{n}_{i,\downarrow}\\&+\frac{U_{\uparrow\uparrow}}{2}\sum_i\hat{n}_{i,\uparrow}\left(\hat{n}_{i,\uparrow}-1\right)+\frac{U_{\downarrow\downarrow}}{2}\sum_i\hat{n}_{i,\downarrow}\left(\hat{n}_{i,\downarrow}-1\right),\end{aligned}\tag{3.12}$$

where $\left[\hat{b}^\dagger_{i,\sigma}, \hat{b}_{j,\sigma'}\right] = \delta_{i,j}\delta_{\sigma,\sigma'}$, $\hat{n}_{i,\sigma} = \hat{b}^\dagger_{i,\sigma}\hat{b}_{i,\sigma}$ and

$$U_{\sigma,\sigma'} = g_{\sigma,\sigma'} \int d\boldsymbol{r} |w_i(\boldsymbol{r})|^4. \tag{3.13}$$

While sophisticated methods to calculate this coefficients exists [96], approximating the Wannier functions yields reasonable results on certain lattice depths. Let us assume the periodic potential of the lattice is sufficiently deep. The three-dimensional lattice potential obtained from counter-propagating light beams can be expressed as

$$V_{\text{lattice}}(\boldsymbol{r}) = \sum_{l=x,y,z} V_{0,l} \sin^2(\boldsymbol{k}_l \cdot \boldsymbol{r}), \tag{3.14}$$

where $V_{0,l}$ is the potential depth and $\boldsymbol{k}_l = 2\pi/\boldsymbol{\lambda}_l$ with $\boldsymbol{\lambda}_l$ the potential wavelength along a given direction. If the potential depth is sufficiently large, each potential minima can be replaced by a harmonic well. In turn, this allows to approximate the Wannier functions as Gaussian's, such that

$$w_i(\boldsymbol{r}) \approx \prod_{l=x,y,z} \phi_l(\boldsymbol{r} - \boldsymbol{R}_i), \tag{3.15}$$

where

$$\phi_l(\boldsymbol{r} - \boldsymbol{R}_i) = \frac{e^{-((\boldsymbol{r}-\boldsymbol{R}_i)\cdot\hat{\boldsymbol{l}})^2/2\sigma_l^2}}{\pi^{1/4}\sqrt{\sigma_l}}, \tag{3.16}$$

with σ_l being the harmonic oscillator length along unitary direction $\hat{\boldsymbol{l}}$.

As the Hubbard models contain only particle creation-annihilation terms and are particle number conserving, it is natural to describe them in an occupation basis, also referred to as Fock states. This basis makes computations intuitive, as it simplifies the picture of the system to particles allocated to different lattice sites. The construction of the Fock basis depends on the particle statistics, as the order in which the creation-annihilation operators act on a given Fock state is relevant for the sign of the resulting state in the case of fermions [97].

While we can obtain a rich phase diagram for both two-component Hubbard models [98, 99], we focus our attention on the two regimes found for their single-component counterparts, the superfluid regime ($J \gg U$) and the Mott insulating regime ($U \gg J$). We will find relevant models for these two scenarios in the next sections.

3.2 Two-mode model

If the tunnelling parameter J is much larger than the contact interactions $U_{\sigma,\sigma'}$, the particles delocalize over the whole lattice such that the occupation per site flattens and the system behaves as a condensate. We can assume this is the case if the condensate fraction $f_c = \sum_{i,j} \sum_\sigma \langle \hat{c}^\dagger_{i,\sigma} \hat{c}_{j,\sigma} \rangle / (NM)$ approximately equals one at unit-filling ($M = N$). Under this scenario we can severely reduce our Hilbert space if we go to quasi-momentum representation of the operators via a discrete Fourier transform. That is,

$$\hat{c}_{j,\sigma} = \frac{1}{\sqrt{M}} \sum_q e^{i2\pi jq/M} \tilde{c}_{q,\sigma}, \tag{3.17}$$

where $q \in [0, M-1]$ and $\tilde{c}^\dagger_{q,\sigma} |n_{q,\sigma}\rangle = \sqrt{n_{q,\sigma}+1}\, |n_{q,\sigma}+1\rangle$. As the particles move without friction over the lattice, we may only occupy the states of different spin with $q = 0$. The states in the $q = 0$ manifold can be expressed as

$$|n, N-n\rangle = \frac{\left(\tilde{c}^\dagger_{q=0,\uparrow}\right)^n \left(\tilde{c}^\dagger_{q=0,\downarrow}\right)^{N-n}}{\sqrt{n!}\sqrt{(N-n)!}} |0, 0\rangle, \tag{3.18}$$

for $n \in [0, N]$.

This approximation fails in the case of fermions due to the Pauli exclusion principle, forcing higher momentum states to be populated. However, for bosons we do not have this limitation. By introducing eq. (3.17) in eq. (3.12) and then setting $q = 0$ [100], we obtain the following two-mode model

$$\hat{H}_{\text{TMM}} = -2J\tilde{N} + \omega \tilde{N}^2 + \phi \tilde{S}_z \tilde{N} + \chi \tilde{S}_z^2, \tag{3.19}$$

where

$$\omega = \frac{U_{\uparrow\uparrow} + U_{\downarrow\downarrow} + 4U_{\uparrow\downarrow}}{8M}, \tag{3.20}$$

$$\phi = \frac{U_{\uparrow\uparrow} - U_{\downarrow\downarrow}}{2M}, \tag{3.21}$$

$$\chi = \frac{U_{\uparrow\uparrow} + U_{\downarrow\downarrow} - 2U_{\uparrow\downarrow}}{2M}, \tag{3.22}$$

and $\tilde{N} = \tilde{n}_{q=0,\uparrow} + \tilde{n}_{q=0,\downarrow}$ with $\tilde{n}_{q,\sigma} = \tilde{b}^\dagger_{q,\sigma} \tilde{b}_{q,\sigma}$, and $\tilde{S}_z = \hat{S}_z / \sqrt{M} = \sum_j (\hat{b}^\dagger_{j,\uparrow} \hat{b}_{j,\uparrow} - \hat{b}_{j,\downarrow} \hat{b}_{j,\downarrow}) / (2\sqrt{M})$. As we expect the state to stay in the $q = 0$ manifold, we may assume $\tilde{N} \approx N$. The term $\phi \tilde{S}_z \tilde{N}$ constitutes a rotation of the state in the Bloch sphere around the z direction. The last term on the right side of eq. (3.19) matches the one-axis twisting model from Section 2.6 and is able to generate spin squeezing by itself.

3.3 Heisenberg model

If we go to the opposite regime where $U_{\sigma,\sigma'} \gg J$, the energy spectrum shows a separation between the single-occupied states and states with multiple occupied sites. This happens because the kinetic energy contribution is not sufficient to compensate for the large on-site contact interactions.

To derive an effective model under these circumstances at unit-filling ($N = M$), we may employ second order perturbation theory. To do so we have to separate the spectrum according to a perturbation term threshold. In this case, the spectrum is given by the contact interactions, which are naturally diagonalized by the Fock occupation basis. The tunnelling term acts naturally as the perturbation in this regime and allows to couple, at least, single occupied states with double occupied states. Details on how to perform this calculation can be found in Chapters 4 and 6. After appropriate derivation, we obtain the so called XXZ Heisenberg model

$$\hat{H}_{\mathrm{XXZ}} = -J_{\perp} \sum_{i=1}^{M} \left(\hat{S}_i^x \hat{S}_{i+1}^x + \hat{S}_i^y \hat{S}_{i+1}^y + \Delta \hat{S}_i^z \hat{S}_{i+1}^z \right). \tag{3.23}$$

If $\Delta = 1$, we go from the XXZ to the XXX model, also known as spin exchange model. In our case, we find that for fermions $J_{\perp} = 4J^2/U$, $\Delta = 1$; so we obtain the XXX model. However, we find that for bosons $J_{\perp} = 4J^2/U_{\uparrow\downarrow}$, $\Delta = U_{\uparrow\downarrow}/U_{\downarrow\downarrow} + U_{\uparrow\downarrow}/U_{\uparrow\uparrow} - 1$; which allows us to obtain the XXZ model.

If the system is not at unit-filling, tunnelling may happen between single occupied states directly. This yields the so-called t–J model, which is exactly like the Heisenberg model with the additional tunnelling term projected onto the single occupied states only.

The Heisenberg model was first postulated by Werner Heisenberg and Paul Dirac at the dawn of quantum mechanics, as a way to solve the long standing problem of ferromagnetism [101, 102]. Some time after this proposal, Hans Bethe obtained the eigenstates of the model under periodic boundary conditions through a well chosen *ansatz* [103, 104]. These type of solutions are now referred to as the coordinate Bethe ansatzs [105], a tool that exceeded its initial conception as an ad-hoc solution and is employed in some way or another to obtain the eigenenergies of different Hamiltonians like the Lieb-Lininger model [106]. The solutions are usually presented as quasi-particles, called magnons or spin waves depending on the sub-field, that travel through the spin chain and may interact with each other. We are interested in the eigenenergies and eigenstates of the Heisenberg model in order to perform perturbation theory appropriately. In the following subsection, we describe the spin wave solutions and their derivation in more unusual settings like open boundary conditions.

Magnons in the isotropic Heisenberg model

The reason the Bethe ansatz works in the first place, is because the model is integrable due to the symmetries it has. For instance, we can see it commutes with the operator $\hat{S}_z$, but it also commutes with $\hat{S}^2$. Thus, Dicke states are well defined eigenstates of the model.

The ansatz solutions are usually introduced following the argument that we can define a vacuum state as $|0\rangle = \otimes_j |\downarrow_j\rangle$. This state will be an eigenstate with the lowest eigenvalue possible, and the ansatz uses it as a reference to construct the excited eigenstates. The excited eigenstates are then constructed from local excitations, such that each sector is diagonalised to obtain the full spectrum.

Let us solve the one and two magnon excitations, so that we can generalise to any number of them. We may refer to the local excited states from the vacuum state as

$$|l\rangle = \hat{S}_l^+ |0\rangle = \hat{S}_l^+ \bigotimes_{j=1}^{M} |{\downarrow_j}\rangle . \tag{3.24}$$

To solve the single excitation sector, we can rely on the translational symmetry of the system, such that we can define a translator operator $U|l\rangle = |l+1\rangle$. The eigenstates of this operator are characterised by the eigenvalues $e^{-i2\pi q/M}$, where $q \in (0, M-1]$ is the quasi-momenta of the solution. We can solve the eigenvalue problem by writing the eigenstates as a superposition of the locally excited states $|l\rangle$

$$|q\rangle = \sum_{l}^{M} a(l) |l\rangle , \tag{3.25}$$

and apply the translator operator to find the recursion relation $\langle l+1|q\rangle = e^{i2\pi q/M} a(l)$ to obtain

$$|q\rangle = \frac{1}{\sqrt{M}} \sum_{l}^{M} e^{i2\pi q l/M} |l\rangle . \tag{3.26}$$

Unsurprisingly, this is equivalent to a discrete Fourier transform of the locally excited states. These states are also eigenstates of the Heisenberg Hamiltonian, with eigenvalues

$$E_q - E_0 = J(1 - \cos(2\pi q/N)). \tag{3.27}$$

Notice that when $q = 0$, the energy is the same as the vacuum state $|0\rangle$, but the state is a trivial superposition of states with a single spin flipped. It is, in fact, the Dicke state $|S, -(S+1)\rangle$. In any case, we refer to the solution (3.26) as a single magnon excitation, where the magnon is a collective spin excitation of quasi-momenta q.

While this sector is trivially solved, the sector with two spin flips is more complicated, as scattering processes among spin excitations have to be taken into account. For this reason, let us repeat this calculation with the Bethe ansatz. We want to solve the eigenvalue problem with the state in eq. (3.25), so we assume this is the case and solve $\hat{H}|q\rangle = E_q|q\rangle$ as a system of equations of the form

$$2(E_q - E_0)a(l) = J\left(2a(l) - a(l-1) - a(l+1)\right), \tag{3.28}$$

$\forall j \in [1, M]$ with $a(l+M) = a(l)$. The Bethe ansatz here is the plane wave solution $a(l) = e^{i2\pi q/M}, \forall q \in (0, M-1]$, such that we recover eq. (3.26) after renormalisation.

The relevance of the ansatz appears when we want to solve the two excitations sector. In such case, the solution will still be a superposition of states with two spin flipped $|l_1, l_2\rangle$ as

$$|q_1, q_2\rangle = \sum_{l_1<l_2} a(l_1, l_2) |l_1, l_2\rangle . \tag{3.29}$$

The insight of Bethe was that we can see the coefficients as a sum of two plane wave solutions, one accounts for two magnons travelling freely, and the other is the scattering process between them.

$$a(l_1, l_2) = A(q_1, q_2) e^{i2\pi(q_1 l_1 + q_2 l_2)/M} + A'(q_1, q_2) e^{i2\pi(q_1 l_2 + q_2 l_1)/M}. \tag{3.30}$$

The ansatz solves the system of equations for the eigenvalue problem obtained from eq. (3.29) when $|l_1 - l_2| > 1$ and the corresponding eigenvalue is

$$E_{q_1,q_2} - E_0 = J \sum_{n=1}^{2} (1 - \cos(2\pi q_n/M)). \tag{3.31}$$

This makes sense, as it is equivalent to two freely moving magnons. However, there is a set of M equations corresponding to the scenario $|l_1 - l_2| = 1$ which are unfulfilled unless

$$\frac{A}{A'} \equiv e^{i\theta} = -\frac{e^{i2\pi(q_1+q_2)/M} + 1 - 2e^{i2\pi q_1/M}}{e^{i2\pi(q_1+q_2)/M} + 1 - 2e^{i2\pi q_2/M}}. \tag{3.32}$$

Thus, we can rewrite the ansatz as

$$a(l_1, l_2) = e^{i2\pi(q_1 l_1 + q_2 l_2)/M + \theta/2} + e^{i2\pi(q_1 l_2 + q_2 l_1)/M - \theta/2}. \tag{3.33}$$

Applying periodic boundary conditions and translation invariance, we obtain

$$Mq_1 = \lambda_1 + \frac{\theta}{2\pi}, \tag{3.34}$$

$$Mq_2 = \lambda_2 - \frac{\theta}{2\pi}, \tag{3.35}$$

where $\lambda_1, \lambda_2 \in [0, M-1]$ are the so-called Bethe quantum numbers. An analysis on the eigenvalue solutions gives relevant physical interpretation to the wave-function and the resulting eigenvalues. However, we continue our discussion with the generalisation to any number of magnon excitations, as we are only interested in the form of the solution.

We can again postulate that an eigenstate of the Hamiltonian can have the form

$$|\{q_n\}\rangle = \sum_{l_1<\ldots<l_n} a(l_1, \ldots, l_n) |l_1, \ldots, l_n\rangle . \tag{3.36}$$

The solution for this case can be found from the two magnon scattering as

$$a(l_1, \dots, l_n) = \sum_{\mathcal{P} \in S_n} \exp\left(i \frac{2\pi}{M} \sum_{j=1}^{n} q_{\mathcal{P}_j} l_j + \frac{i}{2} \sum_{k<j} \theta_{\mathcal{P}_k \mathcal{P}_j} \right), \tag{3.37}$$

where $\mathcal{P}$ indicates all possible permutations of the n magnons. This solution yields the energy value

$$E_{\{q_n\}} - E_0 = J \sum_{j=1}^{n} (1 - \cos(2\pi q_j / M)). \tag{3.38}$$

Again, explicit solutions can be found, some analytically but most of them numerically. We are, however, only interested in the integrable aspect of this analysis, as well as the possibility to decompose the sectors into different subspaces.

For our purposes of separating the states into subspaces of different energy, we must collect all of these states and reformulate the different excited states sectors using operators with quasi-momenta different than zero in all cases. We accommodate the states generated with one magnon of quasi-momenta $q = 0$ as a member of the lower subspace. For example, if we have two-magnon states $|q_1, q_2\rangle$ where $q_1 = 0$, this is equivalent to a single magnon excitation and we relegate this state to the single magnon manifold. If in this same example, $q_1 = q_2 = 0$, then there are effectively no magnons, even if the magnetisation changes by two, and the state is relegated to the lowest energy manifold.

Notice that the states defined for different magnetisation with all magnons $\{q_n\} = 0$ are equivalent to the action of a collective ladder operator n times (with the corresponding normalisation factor) on the vacuum state $|0\rangle = \otimes_j |\downarrow_j\rangle = |S, -S\rangle$. Thus, we find that the lowest energy manifold is composed of the states $|S, m\rangle\,; \forall m \in [-S, S]$. We also refer to these states as Dicke states [107]. We can argue the Dicke states are eigenstates of the Heisenberg model without the Bethe ansatz, because of the SU(2) symmetry of the model. Since $[\hat{H}_{\mathrm{XXX}}, \hat{S}_\pm] = 0$, coherent states are also eigenstates of the isotropic Heisenberg model.

We can follow this logic to properly collect all the states of similar nature, independently of their magnetisation, in the different subspaces by constructing them using generators based on n number of magnons of $q_j \neq 0 \forall j \in [1, n]$.

In this framework, we can generate these magnon states $|m + n, \{q_n\}\rangle$ from an arbitrary Dicke state $|S, m\rangle$, as long as the required symmetry conditions are fulfilled. To check this, we define the generator operator

$$\tilde{S}^+_{\{q_n\}} |S, m\rangle = |m + n, \{q_n\}\rangle\,, \tag{3.39}$$

which acts on an arbitrary Dicke state and returns an state excited with a set of n magnons from the Bethe ansatz in eq. (3.37). We can check that there is a limit in the magnetisation where flipping more spins can only lead to the state vanishing. Naturally, the hermitian operator $\tilde{S}^{-}_{\{q_n\}} = (\tilde{S}^{+}_{\{q_n\}})^{\dagger}$ will also be a generator of this subspace, which allow us to see the size of the generated subspace is restricted in magnetisation by the number of spins flipped. It can be shown these are eigenstates of $\hat{S}^2, \hat{S}_z$ with eigenvalues

$$\hat{S}^2 \left|m+n, \{q_n\}\right\rangle = (S-n)(S-n+1)\left|m+n, \{q_n\}\right\rangle, \tag{3.40}$$

$$\hat{S}_z \left|m+n, \{q_n\}\right\rangle = (m+n)\left|m+n, \{q_n\}\right\rangle, \tag{3.41}$$

$\forall -(S-n) < m < S-n$.

We have not only separated the subspaces properly by number of non-zero magnons present, but we can see these magnon states have restrictions both in total spin and corresponding magnetisation. This insight is key in the search of metrologically useful states, as lowering the total spin of the state is directly detrimental to the measurement precision, since is analogous with the reduction of spin length or number of particles.

Another important realisation is that these subspaces of different number of magnons can have similar energies for at least part of their spectrum. For example, it is clear that for $E_{q_1=M-1} = J(1-\cos(2\pi(M-1)/M)) \sim 2J$ and $E_{q_1=1,q_2=1} = 2J(1-\cos(2\pi/M)) \sim 4J/M$, we have $E_{q_1=M-1} > E_{q_1=1,q_2=1}$ if $M > 2$. Since the energy increases with q_n, the energy of the two-magnon states will catch up and surpass the energy of the given single magnon state.

While this degeneracy may seem problematic since we wanted to separate the different subspaces, states of different number of magnons are orthogonal to each other and they form isolated orthonormal basis. This follows from the fact that they are eigenstates of $\hat{S}^2$ and $\hat{S}_z$ with different quantum numbers, and such states must be orthogonal. If our system does not have a term that couples states of different number of magnons, we can safely ignore this issue for the application of perturbation theory.

Single magnon solutions under open boundary conditions

In the case of open boundary conditions, the plane wave ansatz is incorrect, as the translation symmetry is broken at the boundaries. However, the solution is simple to obtain and can be instructive for similar problems.

We propose the eigenstates for single magnon excitations under open boundary conditions to be

$$\left|q\right\rangle = \sum_{l=1}^{M} a(l)\left|l\right\rangle, \tag{3.42}$$

in the same manner as with periodic boundary conditions. However, we do not solve the eigenvalue problem through a trial solution in a recurrence relation.

The eigenvalue problem can then be written as

$$\begin{cases} 2(E-E_0)a(1) = J\left[a(2)-a(1)\right], \\ 2(E-E_0)a(l) = J\left[a(l-1)-a(l))+(a(l+1)-a(l))\right], \quad \forall\, 1<l<M, \\ 2(E-E_0)a(M) = J\left[a(M-1)-a(M)\right], \end{cases} \tag{3.43}$$

Special equations for the boundary terms can be annoying to work with, so we can employ the fact that the coefficients outside the system are undefined [108]. In other words, $a(0), a(M+1)$ are free parameters that we can use to redefine the equations at the boundaries and recover the same equation for all sites.

Thus, we can have

$$2(E-E_0)a(l) = J\left[(a(l-1)-a(l))+(a(l+1)-a(l))\right];, \tag{3.44}$$

$\forall l$ if $a(0) \equiv a(1)$ and $a(M+1) \equiv a(M)$.

We can solve this equation by writing it as a recurrence relation

$$a(l-1) - 2ca(l) + a(l+1) = 0, \tag{3.45}$$

where $c = 1 + (E-E_0)/J$.

The natural trial solution is $a(l) = r^l$, so we shift indexes by one and obtain

$$a(l) - 2ca(l+1) + a(l+2) = r^l(r^2 - 2cr + 1) = 0. \tag{3.46}$$

This equation has l trivial solutions and $r_\pm = c \pm \sqrt{c^2-1}$. As we have two characteristic roots, the solution is a linear combination of both, yielding

$$a(l) = Ar_+^l + A'r_-^l. \tag{3.47}$$

We can further simplify the solution by noticing that $r_+r_- = 1$, so that $r_-^l = r_+^{-l}$. Let us relabel $r \equiv r_+$, for simplicity. Coefficients A, A' can be found by applying the boundary constraints and the normalisation condition. From the boundary constraints we find

$$r^{2(M+1)} = 1, \tag{3.48}$$

and we get

$$a(l) = Ar^{M-1/2}\left(r^{l-(M-1/2)} + r^{-(l-(M-1/2))}\right). \tag{3.49}$$

From eq. (3.48), it's clear the solution can be a complex number such that $|r| = 1$, so solving the equation with $r = e^{i\theta}$ yields

$$r = e^{i\pi q/M};\ \forall q \in [0, M-1], \tag{3.50}$$

with eigenvectors after normalisation

$$|q\rangle = \sqrt{\frac{2}{M}}\sum_{l=1}^{M}\cos\left[\frac{\pi}{M}q\left(l-\frac{1}{2}\right)\right], \tag{3.51}$$

and eigenvalues

$$E_q - E_0 = J(1-\cos(\pi q/M)). \tag{3.52}$$

Single magnon solutions for spin chains with vacancies

This possible scenario is analogous to open boundary conditions, as introducing a single vacancy in a ring is the same as creating open boundary conditions, since our Hamiltonian only acts on nearest neighbours. Thus, vacancies in between partial chains of spins will yield a system of independent magnons among partial chains.

While the final result is already quite clear, we will proceed to develop a properly derived solution from the ground up as an exercise for more complicated systems where longer range spin interactions are present.

We will refer to the set of locations of vacancies or holes for a given moment in time, or realisation if they are fixed in place, as $\{h\}$.

We propose the eigenstates for single magnon excitations to be defined as

$$|\psi\rangle = \sum_{l \notin \{h\}} a(l) |l\rangle \,, \tag{3.53}$$

where $|l\rangle$ is defined with respect of a given vacuum state with vacancies on sites $\{h\}$.

The eigenvalue problem can then be written as

$$2(E - E_0)a(l) = J\left[\delta_{l+1 \notin \{h\}}(a(l-1) - a(l)) + \delta_{l-1 \notin \{h\}}(a(l+1) - a(l))\right], \tag{3.54}$$

for the N equations where $l \notin \{h\}$. To get rid of the Kronecker deltas, the trick is identical to the one employed with open boundaries: use vacancy coefficients as free parameters. We can rewrite the set of equations as

$$2(E - E_0)a(l) = J\left[(a(l-1) - a(l)) + (a(l+1) - a(l))\right], \tag{3.55}$$

if and only if

$$\begin{cases} a(l-1) = a(l), & \text{if } l-1 \in \{h\}\,, \\ a(l+1) = a(l), & \text{if } l+1 \in \{h\}\,, \end{cases} \tag{3.56}$$

for $l \notin \{h\}$. We may be wary of the scenario where only one vacancy appears between occupied sites, creating the constraint $a(l) = a(l+1) = a(l+2)$ where the vacancy is located at site $l+1$. This constraint is artificial, since we argued that empty sites act as free parameters for the solution, so we can write in that particular scenario that $a(l+1) = a(l) + a(l+2)$, without any loss of generality.

This equation yields the same recurrence relation as per the open boundaries case, so the solution for a partial chain of occupied sites from site l_k to $l_k + L_k - 1$ is

$$a_k(l) = \begin{cases} \sqrt{\frac{2}{L_k}} \cos\left[\frac{\pi}{L_k} q_k (l - \left(l_k - \frac{1}{2}\right)\right]; & \forall l \in [l_k, l_k + L_k - 1], \\ 0; & \text{otherwise}, \end{cases} \tag{3.57}$$

with $q_k \in (0, L_n - 1]$. Each solution $a_k(l)$ is independent, so we have L_k solutions for each partial chain k. In other words, each partial chain is independent and the quasi-momenta of the single magnon solution on each one depends on its length.

Chapter 4

Perturbation Theory

The typical textbook introduction to perturbation theory frames it as a tool to implement corrections of increasing precision to the calculation of a given eigenenergy of the system of interest [109]. However, perturbation theory also allow us to reconstruct a complete effective Hamiltonian, including all matrix elements up to a given order.

Perturbation theory relies on the assumption that we can decompose the system Hamiltonian $\hat{H}$ into a dominating part which can be diagonalised in a given basis and treat the rest as a small off-diagonal contribution, $\hat{H} = \hat{H}_0 + \hat{V}$. If the perturbation is sufficiently small with respect to some energy scale, we can compute an effective Hamiltonian based on sensible approximations and project onto a given energy manifold. The resulting effective Hamiltonian will have the advantage of a reduced Hilbert space and thus simplify the analysis of the dynamics. In most cases, this effective Hamiltonian will be only an approximation of the original, but it will portray its main features.

While other methods allow us to obtain an effective Hamiltonian $\hat{H}_{\text{eff}}$ for many-body systems, like the Feynman-Dyson diagram technique or the self-energy formalism [110], we will focus on the Schieffer–Wolff transformation as our tool of trade. Other perturbative expansions might not be as reliable in their approximations, to the point of even yielding non-Hermitian Hamiltonians as an output [111]. It is important to remark that the effective Hamiltonian is only defined up to a unitary rotation of the projected energy manifold. This means different methods produce different Taylor series of $\hat{H}_{\text{eff}}$, so the cutoff greatly affects the similarity between applications of perturbation theory. A detailed comparison with alternative perturbative methods can be found in [112].

4.1 Schieffer–Wolff Transformation

This particular application of perturbation theory relies on the use of a unitary transformation on the exact Hamiltonian to decouple energetically separated state manifolds. The core idea is simple: given a large energy gap ΔE between the low and high energy manifolds given by $\hat{H}_0$, if the perturbation $\epsilon\hat{V}$ couples them but is small enough when compared with ΔE, we can obtain an effective Hamiltonian by projecting onto the target energy manifold appropriately. We define it as

$$\hat{H}_{\text{eff}} = \hat{P}_0 \hat{U} \left(\hat{H}_0 + \epsilon \hat{V} \right) \hat{U}^\dagger \hat{P}_0, \tag{4.1}$$

where $\hat{P}_0$ is the projector operator to the target energy manifold or subspace $\mathcal{P}_0$ and $\hat{U}$ is a unitary transformation that preserves $\mathcal{P}_0$. By definition, $\mathcal{P}_0$ is invariant under $\hat{H}_0$, but not under $\hat{V}$. Notice we are free to choose which energy manifold we project to, as the procedure only relies on the energy gap between manifolds.

The unitary transformation $\hat{U}$ is in fact the Schieffer–Wolff transformation. We can see $\hat{U}$ as a direct rotation between subspaces, which can be written as $\hat{U} = \exp\left(\hat{W}\right)$ where $\hat{W}$ is an anti-hermitian operator that acts off-diagonally between subspaces. This operator is uniquely defined and has the following properties:

1. $\exp\left(\hat{W}\right) \hat{P}_\perp \exp\left(-\hat{W}\right) = \hat{P}_0$,
2. $\hat{P}_0 \hat{W} \hat{P}_0 = \hat{P}_\perp \hat{W} \hat{P}_\perp = 0$,
3. $\|\hat{W}\| < \pi/2$,

as long as $\|\hat{P}_\perp - \hat{P}_0\| < 1$. In other words, we can represent the operator $\hat{W}$ as

$$\hat{W} = \begin{pmatrix} 0 & \hat{W}_{0,\perp} \\ -\hat{W}^\dagger_{0,\perp} & 0 \end{pmatrix}, \tag{4.2}$$

where the sub-indices in the matrix blocks correspond to the subspaces $\mathcal{P}_0, \mathcal{P}_\perp$. This decomposition makes clear the block-off-diagonal shape of $\hat{W}$ and will be relevant when we try to derive a practical form of the transformation. Likewise, we can decompose the perturbation in two contributions: a block-diagonal part $\hat{V}_\text{d}$ and a block-off-diagonal part $\hat{V}_\text{od}$ such that

$$\hat{V} = \hat{V}_\text{d} + \hat{V}_\text{od}. \tag{4.3}$$

We have defined the functional form of the operators concerning the transformation. Now, we perform an expansion of 4.1 through the Baker-Campbell-Haussdorf formula [113] to obtain

$$\hat{H}_{\text{eff}} = \hat{P}_0 \left(\hat{H}_0 + \epsilon\hat{V} + \left[\hat{W}, \hat{H}_0\right] + \left[\hat{W}, \epsilon\hat{V}\right] + \frac{1}{2}\left[\hat{W}, \left[\hat{W}, \hat{H}_0\right]\right] + \mathcal{O}(\hat{V}^3) \right) \hat{P}_0 \tag{4.4}$$

We can make the effective Hamiltonian block-diagonal to first order if we choose

$$\left[\hat{H}_0, \hat{W}\right] = \epsilon \hat{V}. \tag{4.5}$$

Since $\hat{W}$ is block-off-diagonal, it conveniently implies $\left[\hat{W}, \hat{V}\right] = \left[\hat{W}, \hat{V}_{\mathrm{od}}\right]$. On the other hand, 4.5 becomes ill-defined if $\hat{V}_{\mathrm{d}} \neq 0$. To fix this, we must extract the block-diagonal contribution so that

$$\left[\hat{H}_0, \hat{W}\right] = \epsilon \hat{V}_{\mathrm{od}}. \tag{4.6}$$

Then

$$\hat{H}_{\mathrm{eff}} = \hat{P}_0 \left(\hat{H}_0 + \epsilon \hat{V}_{\mathrm{d}} + \frac{1}{2} \left[\hat{W}, \epsilon \hat{V}_{\mathrm{od}}\right] + \mathcal{O}(\hat{V}^3) \right) \hat{P}_0. \tag{4.7}$$

We represent 4.6 in the eigenbasis of $\hat{H}_0$ to define $\hat{W}$. Let $\{|n\rangle\}$ be an orthonormal eigenbasis such that $\hat{H}_0 |n\rangle = E_n |n\rangle$, $\forall n$. Since $\hat{W}, \hat{V}_{\mathrm{od}}$ are block-off-diagonal, we can only solve 4.6 for two eigenvectors of different subspaces, such that $|n\rangle \in \mathcal{P}_i, |m\rangle \in \mathcal{P}_j$ but $\mathcal{P}_i \not\subset \mathcal{P}_j$. In such case,

$$E_n W_{nm} - W_{nm} E_m = \epsilon V^{\mathrm{od}}_{nm}, \tag{4.8}$$

where n, m correspond to eigenvectors of different subspaces, which guarantees $E_n \neq E_m$. We can finally define the matrix elements of the generator $\hat{W}$ as

$$W_{nm} = \begin{cases} \frac{\epsilon V^{\mathrm{od}}_{nm}}{E_n - E_m}, & \text{iif } |n\rangle \in \mathcal{P}_i, |m\rangle \in \mathcal{P}_j, \mathcal{P}_i \not\subset \mathcal{P}_j, \\ 0, & \text{else.} \end{cases} \tag{4.9}$$

The previous expansion of the unitary transformation is then justified if the generator is infinitesimal, implying $|\Delta E| \gg |\epsilon \hat{V}_{\mathrm{od}}|$. The upper bound of this constrain can be defined with high accuracy [112], but this loose condition is sufficient for our purposes.

After projecting on the subspace of interest, we obtain

$$\hat{H}^{\mathrm{eff}}_{nm} = E_{nm} \delta_{nm} + \epsilon \hat{V}^{\mathrm{d}}_{nm} + \frac{\epsilon^2}{2} \sum_l \left(\frac{V^{\mathrm{od}}_{nl} V^{\mathrm{od}}_{lm}}{E_n - E_l} + \frac{V^{\mathrm{od}}_{nl} V^{\mathrm{od}}_{lm}}{E_m - E_l} \right) + \mathcal{O}(\hat{V}^3), \tag{4.10}$$

where $|n\rangle , |m\rangle \in \mathcal{P}_0, |l\rangle \in \mathcal{P}_\perp$. It is important to remember that this projection is also applied to the eigenbasis, meaning we constrain the Hilbert space to $\mathcal{P}_0$.

While we have derived the Schieffer–Wolff transformation up to second-order contributions, the transformation can be extended to infinite terms. The price for such increase in accuracy is the use of a formalism that relies on super-operators and recursive relations [112]. Said formalism has the advantage of skipping the full spectral decomposition of $\hat{H}_0$. This will be unnecessary for us since our goal is to define quadratic Hamiltonians; higher order terms might only increase the complexity of our results unnecessarily.

Chapter 5

Spin Squeezing through Dipolar Interactions in the Superfluid Phase

Until now, we had overview on the phenomena of spin squeezing, ultra-cold atoms in the optical lattice as our physical platform of interest and perturbation theory as a tool to derive effective models. From this chapter until the end of this work, we introduce brand new results from our research about the topic of spin squeezing. In this chapter, we present a proposal for its implementation with ultra-cold atoms in the lattice using dipole interactions; published as:

M. Dziurawiec, T. Hernández Yanes, M. Płodzień, M. Gajda, M. Lewenstein, and E. Witkowska, "Accelerating Many-Body Entanglement Generation by Dipolar Interactions in the Bose-Hubbard Model", Physical Review A **107**, 013311 (2023).

A first good guess in our quest to obtain experimentally feasible spin squeezed states through dynamical protocols could be to look for systems that explicitly resemble the characteristics of the OAT and TACT models. In them we can see how the unitary evolution operator $\hat{U}(t) = e^{-i\hat{H}t}$ generates all-to-all correlations by virtue of the second moments of the collective spin operators. It is then reasonable to suspect long-range interactions might play a similar role in the generation of entanglement, as they create pairwise correlations among all particles in the system.

For instance, the dipolar interaction can be a good candidate for the required correlation generation. Dipolar interaction decays with a power law $\propto r^{-3}$ where r is the distance between them. Even so, such interactions might add up in time to generate highly entangled states. In fact, lattice models using dipolar interactions with spin dynamics as the only degree of freedom can show spin squeezing [60, 114].

Nevertheless, the self-imposed constraints of dimensionality and derivation from the Hubbard model brought us to a different hypothesis: dipolar interactions might add up to all-to-all correlations if particles travel without friction across the lattice. Under this assumption we derived the dipolar interactions for two-component bosons in second quantization form and studied the effective model in the superfluid phase of the Bose Hubbard Model ($J \gg U$).

Calculation of the dipolar interactions in the lattice is difficult to perform precisely, as in this case second quantisation formalism yields a complicated integral. But if we assume that Wannier functions heavily localise the integrand, we can take the rest as constant and integration becomes trivial. This naive approximation was already shown in [28] for the single component Bose Hubbard model, but we extended it to the case of two-components with polarisation direction of the dipoles along the quantisation axis of the spins in the lattice.

In the superfluid phase, when the condensate fraction is close to unity, the dynamics are dominated by the operators of quasi-momenta $q = 0$ in the Fourier representation. This allows us to represent the effective model as a two-mode system, since only the $q = 0$ momenta will be occupied.

If we write the model in this fashion and skip the constant terms, we arrive at

$$\hat{H}_{\text{eff}} = \chi \left(\tilde{S}_z^2 - \eta \tilde{S}_x^2 \right), \tag{5.1}$$

where the tilde stands for the $q = 0$ component of a given operator discrete Fourier transform, $\chi = (U_{\uparrow\uparrow} + U_{\downarrow\downarrow} - 2U_{\uparrow\downarrow})/2M$, and $\eta \approx 3\gamma^2\zeta(3)/\chi$. The first term in the effective model comes purely from the Bose–Hubbard model, as described in Section 3.2, while the second term comes from the dipolar interactions. As we will see, η weakly depends on the boundary conditions of the system, but it will converge when $M \to \infty$.

This means we have two main tunable parameters, the anisotropy in the two-component contact interactions ($U_{\uparrow\uparrow} + U_{\downarrow\downarrow} \neq 2U_{\uparrow\downarrow}$) and the dipolar interactions. We can use these not only to generate optimal squeezing but also to study the continuous transition between the OAT and TACT models.

Remarkably, we have found that anisotropic TACT ($0 < \eta < 1$) yields identical scaling of the spin-squeezing parameter to pure TACT ($\eta = 1$) unless $\eta \ll 1$ by orders of magnitude, where we recover the OAT model. The only discrepancy is a slight time re-scaling of the squeezing process.

To understand these results, it is important to explain with some detail the calculations we performed to arrive at them.

5.1 Dipolar interactions for arbitrary geometry in second quantisation form

In this section, we derive the dipolar interactions in second quantisation form to express said interactions at the same level as the Hubbard model, derived in section 3.1. We follow similar approximations to [93, 115], but extend the results to two-component bosons and the spin operator. To fully understand the derivation, it is helpful to describe the dipole moment in second quantisation form as well, since its construction as a form factor provides direct insight in how to express it in terms of spin operators. We adopt the notation of chapter 3 to express this formalism. For instance, we define $\hat{c}_{i,\sigma_i}$ as the annihilation operator associated with the Wannier function $w_i(\boldsymbol{r})$ under the tight-binding approximation in the optical lattice. We also adopt the tensor notation for the two-body interactions introduced in eqs. (3.6) and (3.8).

Definition of dipole moment in second quantisation form

For pedagogical reasons, let us imagine the magnetic dipole moment is part of the single particle Hamiltonian such that $H_d(\boldsymbol{r}) = f(\boldsymbol{r})\mu^\alpha(\boldsymbol{r})$, with α being a given projection direction in coordinate space. Once this concept is established for a single particle properly, we will study the dipolar interaction.

We can express the magnetic dipole moment as proportional to the spin length on a given projection as

$$\mu^\alpha(\boldsymbol{r}) = -\gamma \left\langle \hat{S}^\alpha(\boldsymbol{r}) \right\rangle. \tag{5.2}$$

As we are working in the lattice, we can define the state measuring eq. (5.2) as a combination of all Wannier functions in the system. It becomes useful to express eq. (5.2) in terms of the matrix elements among the Wannier functions. We can define the spin operators which describe the interaction of two Wannier functions $w_i^*(\boldsymbol{r}), w_k(\boldsymbol{r})$ as

$$\hat{S}^x_{ik} = \frac{1}{2}\left(\hat{S}^+_{ik} + \hat{S}^-_{ik}\right), \tag{5.3}$$

$$\hat{S}^y_{ik} = \frac{1}{2i}\left(\hat{S}^+_{ik} - \hat{S}^-_{ik}\right), \tag{5.4}$$

$$\hat{S}^z_{ik} = \frac{1}{2}\left(\hat{c}^\dagger_{i,\uparrow}\hat{c}_{k,\uparrow} + \hat{c}^\dagger_{i,\downarrow}\hat{c}_{k,\downarrow}\right), \tag{5.5}$$

where $\hat{S}^+_{ik} = \hat{c}^\dagger_{i,\uparrow}\hat{c}_{k,\downarrow}$, $\hat{S}^-_{ik} = \hat{c}^\dagger_{i,\downarrow}\hat{c}_{k,\uparrow}$. In general, we would not require such a definition of the spin operators in light of the high localisation of the Wannier functions in the lattice. But since we have separated the spatial wave-function from the corresponding operator, we must continue the analysis before integration with this concept in mind. In practice, one may see this kind of term as a scattering at the spin level.

It follows that the dipole moment projection acts as a tensor that reconstructs the corresponding spin operator when summed over with all the pairs of creation-annihilation operators required. In other words,

$$\sum_{\sigma_i,\sigma_j} \hat{c}^\dagger_{i,\sigma_i}\mu^\alpha(\boldsymbol{r})\hat{c}_{j,\sigma_j} = -\gamma\hat{S}^\alpha_{ij}. \tag{5.6}$$

If we apply this concept to the calculation of the single particle Hamiltonian given by $H_d(\boldsymbol{r})$ we obtain

$$\hat{H}_d = -\gamma \sum_{i,j} f_{ij} \hat{S}^{\alpha}_{ij}, \tag{5.7}$$

where $f_{ij} = \int d\boldsymbol{r} \omega^*_i(\boldsymbol{r}) f(\boldsymbol{r}) \omega_j(\boldsymbol{r})$. For instance, if $f(\boldsymbol{r}) = 1$, the orthogonality of the Wannier functions trivially yields the result $\hat{H}_d = -\gamma \sum_i \hat{S}^{\alpha}_i = -\gamma \hat{S}^{\alpha}$ with $\hat{S}^{\alpha}_i = \hat{S}^{\alpha}_{ii}$ being the on-site spin operator of spatial projection α and $\hat{S}^{\alpha}$ the corresponding collective spin operator.

Dipolar interactions in second quantisation form

If we express the dipole moment as a vector of orthogonal projections $\boldsymbol{\mu}(\boldsymbol{r}) = (\mu^x(\boldsymbol{r}), \mu^y(\boldsymbol{r}), \mu^z(\boldsymbol{r}))$, we can express the interaction between two dipoles as

$$V_{\mathrm{dd}}(\boldsymbol{r}, \boldsymbol{r}') = \gamma^2 \frac{\boldsymbol{\mu}(\boldsymbol{r}) \cdot \boldsymbol{\mu}(\boldsymbol{r}')}{|\boldsymbol{r} - \boldsymbol{r}'|^3} - 3\gamma^2 \frac{\boldsymbol{\mu}(\boldsymbol{r}) \cdot (\boldsymbol{r} - \boldsymbol{r}')\, \boldsymbol{\mu}(\boldsymbol{r}') \cdot (\boldsymbol{r} - \boldsymbol{r}')}{|\boldsymbol{r} - \boldsymbol{r}'|^5}. \tag{5.8}$$

In view of the derivation for a single dipole, we must take into account the spin degrees of freedom to calculate the dipolar interactions. If we include the corresponding creation-annihilation operators and sum over the spin degrees of freedom we get

$$\hat{V}_{\mathrm{dd}}(\boldsymbol{r}, \boldsymbol{r}') = \sum_{\sigma_i, \sigma_j, \sigma_k, \sigma_l} \hat{c}^{\dagger}_{i,\sigma_i} \hat{c}^{\dagger}_{j,\sigma_j} V_{\mathrm{dd}}(\boldsymbol{r}, \boldsymbol{r}') \hat{c}_{k,\sigma_k} \hat{c}_{l,\sigma_l} \tag{5.9}$$

$$= \gamma^2 \frac{\boldsymbol{S}_{ik} \cdot \boldsymbol{S}_{jl}}{|\boldsymbol{r} - \boldsymbol{r}'|^3} - 3\gamma^2 \frac{\boldsymbol{S}_{ik} \cdot (\boldsymbol{r} - \boldsymbol{r}')\, \boldsymbol{S}_{jl} \cdot (\boldsymbol{r} - \boldsymbol{r}')}{|\boldsymbol{r} - \boldsymbol{r}'|^5} \tag{5.10}$$

where $\boldsymbol{S}_{ik} = (\hat{S}^x_{ik}, \hat{S}^y_{ik}, \hat{S}^z_{ik})$ is a vector of orthogonal projections.

At this point is relevant to separate the integral calculation in two cases, when the dipoles are in the same lattice site ($|\boldsymbol{r} - \boldsymbol{r}'| < d$) and when not ($|\boldsymbol{r} - \boldsymbol{r}'| \gtrsim d$). In the former case the influence of the lattice is the same for both dipoles and calculations are to be done in momentum space. The result is simply a contribution to the contact interaction terms [28]. In the latter case the depth of the lattice potential strongly localises the dipoles and certain approximations can be taken. The Wannier functions are very well localised around the lattice sites and make other arguments in the integral almost constant. Then, we can assume the Wannier functions act as a delta function for other arguments in the integral so that

$$\begin{aligned}\hat{V}_{\mathrm{dd},ijkl}\Big|_{i\neq j} =& \int d\boldsymbol{r} \int d\boldsymbol{r}' w_i^*(\boldsymbol{r}) w_j^*(\boldsymbol{r}') \left[\hat{V}_{\mathrm{dd}}(\boldsymbol{r},\boldsymbol{r}')\right]_{|\boldsymbol{r}-\boldsymbol{r}'|\gtrsim d} w_k(\boldsymbol{r}) w_l(\boldsymbol{r}') \\ \approx& \hat{V}_{\mathrm{dd}}(\boldsymbol{R}_i,\boldsymbol{R}_j) \int d\boldsymbol{r} w_i^*(\boldsymbol{r}) w_k(\boldsymbol{r}) \int d\boldsymbol{r}' w_j^*(\boldsymbol{r}') w_l(\boldsymbol{r}') \\ \approx& \hat{V}_{\mathrm{dd}}(\boldsymbol{R}_i,\boldsymbol{R}_j)\delta(\boldsymbol{R}_i-\boldsymbol{R}_k)\delta(\boldsymbol{R}_j-\boldsymbol{R}_l).\end{aligned}$$

We now have all the ingredient to obtain the dipolar interactions in second quantization form in accordance with eq. (3.6). If we change labels and express the vector $\boldsymbol{R}_j - \boldsymbol{R}_k$ in spherical coordinates $|\boldsymbol{R}_j - \boldsymbol{R}_k|, \theta_{jk}, \phi_{jk}$ we obtain

$$\begin{aligned}\hat{V}_{\mathrm{dd}} =& \frac{1}{2}\sum_{i,j,k,l} \hat{V}_{\mathrm{dd},ijkl}\Big|_{i\neq j} \\ =& \frac{1}{2}\sum_{j,k\neq j} \frac{\gamma^2}{|\boldsymbol{R}_j-\boldsymbol{R}_k|^3}\Bigg(\left(1-3\cos^2\theta_{jk}\right)\hat{S}_j^z\hat{S}_k^z \\ &- \frac{1-3\cos^2\theta_{jk}}{4}\left(\hat{S}_j^+\hat{S}_k^- + \hat{S}_j^-\hat{S}_k^+\right) \\ &- \frac{3\sin 2\theta_{jk} e^{-i\phi_{jk}}}{4}\left(\hat{S}_j^+\hat{S}_k^z + \hat{S}_j^z\hat{S}_k^+\right) \\ &- \frac{3\sin 2\theta_{jk} e^{i\phi_{jk}}}{4}\left(\hat{S}_j^-\hat{S}_k^z + \hat{S}_j^z\hat{S}_k^-\right) \\ &- \frac{3}{4}\sin^2\theta_{jk}\left(e^{-i2\phi_{jk}}\hat{S}_j^+\hat{S}_k^+ + e^{i2\phi_{jk}}\hat{S}_j^-\hat{S}_k^-\right)\Bigg),\end{aligned} \tag{5.11}$$

where $\hat{S}_j^{\pm} = \hat{S}_j^x \pm i\hat{S}_j^y$.

For simplicity we will focus on particles in a line, where $\theta_{jk} = \frac{\pi}{2}\ \forall j,k$; $\phi_{jk} = 0\ \forall k > j$; $\phi_{jk} = \pi\ \forall k < j$ and $|\boldsymbol{R}_j - \boldsymbol{R}_k| = d\,|j-k|$ so that

$$\hat{V}_{\mathrm{dd}} = \frac{1}{2}\sum_{j,k\neq j}\frac{\gamma^2}{d^3\,|j-k|^3}\left(\hat{S}_j^z\hat{S}_k^z - 2\hat{S}_j^x\hat{S}_k^x + \hat{S}_j^y\hat{S}_k^y\right). \tag{5.12}$$

For simplicity we either assume d is absorbed into γ or $d = 1$.

5.2 Effective model under Periodic and Open Boundary Conditions

Periodic Boundary Conditions

To assume periodic boundary conditions means that, if we sit in a particular lattice site j, we interact with the k site in the same manner as with sites $k \pm M$; where M is the periodicity of the lattice. The difference between these cases is that one of them will be spatially closer than the others to site j and since the dipolar interaction inversely depends on the cube of the distance $d = |j-k| \geq 1$, we only consider the contribution from the closest site of the three. Such minimal distance can be expressed as

$$d_{\min}(j,k) = \min(|j-(k-M)|\,, |j-k|\,, |j-(k+M)|).$$

It can be found that

$$d_{\min}(j,k) = \begin{cases} |j-k|\,; & |j-k| \leq \lfloor \frac{M}{2} \rfloor, \\ M - |j-k|\,; & |j-k| > \lfloor \frac{M}{2} \rfloor. \end{cases} \tag{5.13}$$

Then the dipolar interactions under periodic boundary conditions will look like

$$\hat{V}_{\mathrm{dd}} = \frac{1}{2} \sum_{j}^{M} \sum_{k \neq j}^{M} \frac{\gamma^2}{d^3_{\min}(j,k)} \left(\hat{S}^z_j \hat{S}^z_k - 2\hat{S}^x_j \hat{S}^x_k + \hat{S}^y_j \hat{S}^y_k \right), \tag{5.14}$$

If we go to the momentum representation with the transformation

$$\tilde{S}^{\alpha}_q = \frac{1}{\sqrt{M}} \sum_q e^{i2\pi qj/M} \hat{S}^{\alpha}_j, \tag{5.15}$$

and assume that we are in the superfluid phase ($J \gg U$), we can consider the system to be at $q=0$ only. From eq. (5.15) we have $\hat{S}_\alpha = \sqrt{M}\tilde{S}_\alpha \equiv \sqrt{M}\tilde{S}^{\alpha}_{q=0}$. The $q=0$ approximation implies $\hat{S}^{\alpha}_j = \tilde{S}_\alpha/\sqrt{M}; \forall j \in [1,M]$, which simplifies calculations as now the dipolar interactions look like

$$\hat{V}_{\mathrm{dd}} = \frac{\gamma^2}{2M} \left(\sum_{j,k\neq j}^{M,M} \frac{1}{d^3_{\min}(j,k)} \right) \left(\tilde{S}^2 - 3\tilde{S}^2_x \right), \tag{5.16}$$

where $\tilde{S}^2 = \tilde{S}^2_x + \tilde{S}^2_y + \tilde{S}^2_z$, allowing us to focus on the calculation of the sum. This can be expressed in terms of the collective operators in coordinate space as

$$\hat{V}_{\mathrm{dd}} = \frac{\gamma^2}{2M^2} \left(\sum_{j,k\neq j}^{M,M} \frac{1}{d^3_{\min}(j,k)} \right) \left(\hat{S}^2 - 3\hat{S}^2_x \right). \tag{5.17}$$

However, we will maintain the two-mode notation $\tilde{S}_\alpha$, as is more explicit for the superfluid regime and the two-mode model is numerically more advantageous than its coordinate space counterpart. We can proceed with a change of variable $d = j-k$ to rewrite this sum.

$$\sum_{j,k\neq j}^{M,M} \frac{1}{d^3_{\min}(j,k)} = \sum_{j}^{M} \sum_{\substack{d=j-1 \\ d\neq 0}}^{j-M} \frac{1}{\min(|d|\,, M-|d|)^3} \tag{5.18}$$

After a change of variables $d = j - k$ and making use of 5.13, we obtain

$$\sum_{j,k\neq j}^{M,M} \frac{1}{d_{\min}^3(j,k)} = 2M \sum_{d=1}^{\lfloor \frac{M}{2} \rfloor} \frac{1}{d^3} - 2\left(\left\lfloor \frac{M}{2} \right\rfloor + 1 - \left\lceil \frac{M}{2} \right\rceil\right) \frac{1}{\lfloor \frac{M}{2} \rfloor^2}. \tag{5.19}$$

If M is odd ($\lceil \frac{M}{2} \rceil = \lfloor \frac{M}{2} \rfloor + 1$) the last term vanishes, but if M is even ($\lceil \frac{M}{2} \rceil = \lfloor \frac{M}{2} \rfloor = \frac{M}{2}$) the last term survives. However, it's still half the last term of the sum so we can safely ignore this discrepancy between even and odd cases.

The result is a very fast converging sum which at the large M limit recovers the Riemann zeta function evaluated at $s = 3$, also called Apéry's constant, $\zeta(3) = \sum_{n=1}^{\infty} \frac{1}{n^3}$.

With this result, we finally obtain

$$\hat{V}_{\text{dd}} \simeq \gamma^2 \zeta(3) \left(\tilde{S}^2 - 3\tilde{S}_x^2\right). \tag{5.20}$$

In the periodic boundary conditions case, $\eta = 3\gamma^2\zeta(3)/\chi$.

The final effective Hamiltonian, ignoring constant terms is

$$\hat{H}_{\text{eff}}^{(\text{PBC})} = \chi \left(\tilde{S}_z^2 - \eta \tilde{S}_x^2\right), \tag{5.21}$$

Open boundary conditions

The effective model under open boundary conditions looks exactly like eq. (5.21). However, the Hamiltonian written in momentum representation in the superfluid phase will be incorrect if we repeat the previous zero momentum approximation, since boundary conditions matter. However, numerical evidence shows we can still apply said approximation if we re-normalize with respect to the condensate fraction, as contributions from $q \neq 0$ terms seem to be negligible. This is possible because the condensate fraction in the open boundary conditions case, while non-unitary, remains largely constant. Then,

$$\hat{S}_j^{\alpha} \approx \frac{1}{f_c\sqrt{M}} \tilde{S}_{\alpha}, \tag{5.22}$$

which can also be expressed as

$$\tilde{S}_{\alpha} \approx \frac{f_c}{\sqrt{M}} \hat{S}_{\alpha}. \tag{5.23}$$

With this correction in mind, we obtain

$$\hat{V}_{\text{dd}} \simeq \frac{\gamma^2}{2Mf_c^2} \left(\sum_{j,k\neq j}^{M,M} \frac{1}{|j-k|^3}\right) \left(\tilde{S}^2 - 3\tilde{S}_x^2\right). \tag{5.24}$$

We can solve the double sum factor in the same manner as the previous case of periodic boundary conditions, obtaining

$$\sum_{j,k\neq j}^{M,M} \frac{1}{|j-k|^3} = 2M \sum_{d=1}^{M-1} \frac{1}{d^3} - 2 \sum_{d=1}^{M-1} \frac{1}{d^2}. \tag{5.25}$$

Both sums in the right hand side converge to the Riemann zeta function at different values of s. The final result can then be approximated to

$$\hat{V}_{\text{dd}} \simeq \frac{\gamma^2}{f_c^2} \left(\zeta(3) - \frac{\zeta(2)}{M} \right) \left(\tilde{S}^2 - 3\tilde{S}_x^2 \right). \tag{5.26}$$

In the open boundary conditions case, if we take $1/f_c^2$ as a prefactor, we obtain $\eta = 3\gamma^2(\zeta(3) - \zeta(2)/M)/\chi$. In the limit $M \to \infty$, the result converges to that of the periodic boundary conditions case since $\zeta(2)$ is a constant.

As such, the effective Hamiltonian becomes

$$\hat{H}_{\text{eff}}^{(\text{OBC})} = \frac{\chi}{f_c^2} \left(\tilde{S}_z^2 - \eta \tilde{S}_x^2 \right). \tag{5.27}$$

We compare the obtained effective models with exact numerical calculations of the extended Bose–Hubbard model including the dipolar interactions of eq. (5.12) in fig. 5.1. The condensate fraction remains mostly constant throughout the dynamics, which allows us to apply the zero-momentum approximation safely. This approximation works well even under open boundary conditions if the re-normalization over f_c is applied. Without the re-normalization, the effective model would show a slower squeezing process than the periodic boundary conditions counterpart since $\eta^{(\text{OBC})} < \eta^{(\text{PBC})}$, which is not the case.

5.3 Limitations of the model

Nevertheless, this setup has a number of issues. For instance, we assume the the geometry of the system under periodic boundary conditions is a line, not a ring. The ring geometry is feasible, but it would complicate the calculation of the dipolar interactions contribution to the effective model. The interaction can be forced to act as if in a line by applying a strong confinement trap, but this may affect the experimental feasibility. Moreover, the dipolar interactions we calculated require a strong localization approximation and might yield different results under careful scrutiny. In a realistic setting, particles experience some friction when tunnelling in the superfluid phase and we might see single, double or even triple particle losses due to collisions. This is detrimental for squeezing [63].

These disadvantages motivates us to find scalable spin squeezing in other experimentally feasible settings. For instance in the Mott insulating phase, where particle losses due to collisions are far less likely. The cost for such

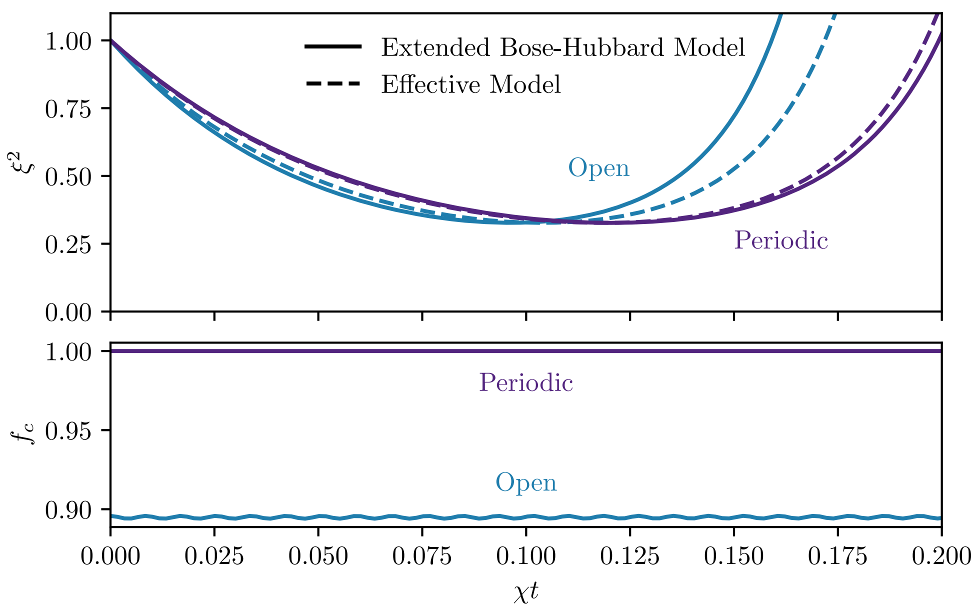

Figure 5.1: Comparison of the spin-squeezing parameter ξ^2 (left) and condensate fraction f_c (right) dynamics between periodic and open boundary conditions for the Hubbard model with dipolar interactions in the Superfluid regime. $M = N = 8, J = 100E_{\text{recoil}}, U = (1, 1, 0.05)\, E_{\text{recoil}}, \gamma = 5.13E_{\text{recoil}}$. Thus, $\chi = 0.16E_{\text{recoil}}$ and $\eta^{(\text{PBC})} = 1, \eta^{(\text{OBC})} = 0.83$.

schemes is that the recovery of OAT and TACT models require more sophisticated techniques due to the absence of the zero-momentum approximation.

Dostęp do artykułu „Accelerating many-body entanglement generation by dipolar interactions in the Bose-Hubbard model”

znajduje się tutaj: https://doi.org/10.1103/PhysRevA.107.013311

Chapter 6

Spin Squeezing through Spin Orbit Coupling in the Mott Insulating Phase

In the previous chapter we proposed a setup in the superfluid regime that achieves a continuous transition between OAT and TACT, in principle reaching the Heisenberg limit. However, this proposal has several experimental difficulties like particle losses due to collisions and changes in the dipole interactions due to more realistic geometries of the lattice. In this chapter we propose to work in the Mott insulating regime to tackle these issues. To generate squeezing, we rely on second-order perturbation theory and build an optimal perturbation through the so-called spin-orbit coupling term. Finally, we find interesting differences between working under periodic and open boundary conditions, even yielding non-vanishing discrepancies when $M \to \infty$.

The results shown in this chapter are the result of our own research and have been published as:

T. Hernández Yanes, M. Płodzień, M. Mackoit Sinkevičienė, G. Žlabys, G. Juzeliūnas, and E. Witkowska, "One- and Two-Axis Squeezing via Laser Coupling in an Atomic Fermi-Hubbard Model", Physical Review Letters **129**, 090403 (2022),

T. Hernández Yanes, G. Žlabys, M. Płodzień, D. Burba, M. M. Sinkevičienė, E. Witkowska, and G. Juzeliūnas, "Spin Squeezing in Open Heisenberg Spin Chains", Physical Review B **108**, 104301 (2023).

6.1 Perturbation theory for the Mott Insulating Phase

One way to minimise particle losses is to reduce the number of collisions possible in the system. Fermions are a natural choice for this because of the exclusion principle, which allows to have up to two particles of different spin per site. This automatically reduces the collisions with respect to bosons.

Another strategy to reduce collisions is to work in a phase of matter where they are highly unlikely. In contrast with the superfluid phase, the Mott insulating phase ($J \ll U$) keeps the system into the single occupied states manifold. Even if our initial state had double occupied sites in it, particle losses due to collisions will be more favourable due to the strong contact interactions and we will eventually reach a state of single occupied sites. Alternatively, quantum distillation [116] allow us to retrieve a state of single occupied sites and discard the double occupied sites as they move to the boundaries of the system.

As described in section 3.3, in the Mott insulating phase particles can still tunnel freely if holes are present, obtaining the so-called t–J model [117]. But if the system is at half-filling ($M = N$) the lattice is fully occupied and tunnelling processes are effectively suppressed.

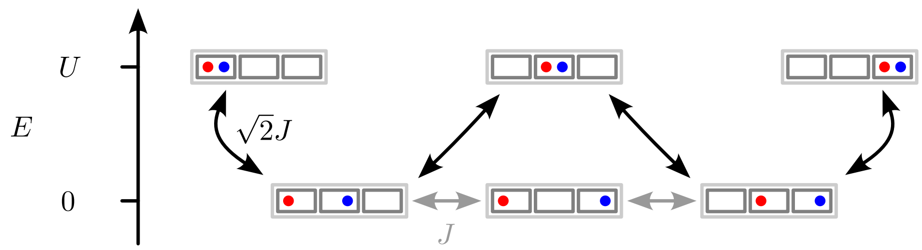

Figure 6.1: Sketch of energy manifolds and couplings among a selected number of possible states in the Fermi–Hubbard Hamiltonian for a lattice of three sites and two particles of opposite spin ($M = 3, N_\uparrow = 1, N_\downarrow = 1$). Lattice sites are represented by rectangles while particles are represented with circles of different colour for the spin. Couplings are given by $\langle\psi_i|\, \hat{H}_{\text{tun}}\, |\psi_j\rangle$ while energies are calculated with $\langle \hat{H}_{\text{int}} \rangle$. Couplings of magnitude $\sqrt{2}J, J$ are represented with black and grey arrows, respectively. If $\Delta E = U \gg \sqrt{2}J$, we may apply perturbation theory to obtain an effective Hamiltonian from second-order processes.

In such case, the Fermi–Hubbard model (introduced in section 3.1, eq. (3.9)) becomes Ising-like, which is usually referred to as a Heisenberg model [101]. In the case of the Fermi–Hubbard model, the result reduces directly to the Heisenberg XXX model, also known as the Spin Exchange Hamiltonian

$$\hat{H}_{\text{SE}} = J_{\text{SE}} \sum_j \left(\hat{S}^x_j \hat{S}^x_{j+1} + \hat{S}^y_j \hat{S}^y_{j+1} + \hat{S}^z_j \hat{S}^z_{j+1} - \frac{1}{4} \right), \tag{6.1}$$

where $J_{\mathrm{SE}} = 4J^2/U$.

While these constraints are beneficial to avoid particle losses by collisions, generating quadratic Hamiltonians under these conditions is more involved than in the superfluid regime.

One way to find them is to use the exact same tool which allows us to map to the XXX model, the Schrieffer-Wolff transformation introduced in chapter 4. If a given state belongs to a certain energy manifold given by the partial Hamiltonian $\hat{H}_0$, but another part of the full Hamiltonian $\hat{V}$ couples said state to a different manifold, we can use perturbation theory to treat this coupling as a virtual transition. If the energy gap is sufficiently large, the transition will be fast enough so that the result is an effective transition between states of the initial manifold. If such a process is second-order only, it produces an effective coupling which is quadratic, or at the very least a product of two terms that correspond to the coupling term $\hat{V}$. For more details, see section 4.1.

With this in mind, we can start thinking on the required constraints so that spin squeezing is optimal, like the energy manifold we want to isolate the excited states manifold we want to use for the required virtual processes.

By inspection of the spin squeezing parameter (2.43), it becomes clear we want a state that maximises $\langle \hat{S}_n \rangle$, so we want our initial state to have the maximal total spin possible. Naturally, we can pick a spin coherent state as our initial state so satisfy this condition. These states are also eigenstates of $\hat{H}_{\mathrm{SE}}$, since they conserve the SU(2) symmetry.

We must now look for the high energy manifold we plan to use as a stepping stone for our quadratic Hamiltonian. Since we want our perturbation to be proportional to the spin operators to obtain the result we desire, a natural proposition is to construct an eigenstate from local spin excitations. If we solve the eigenvalue problem in such a way for PBC, we will find the so called spin wave states, also known as magnons in the literature [105], which can also be obtained through the Bethe ansatzs [104], as explained in section 3.3.

$$|S = N/2 - 1, m, q\rangle = \sum_j e^{2\pi q j/M} \hat{S}_j^{\pm} |S = N/2, m \mp 1\rangle \,, \tag{6.2}$$

where $q \in [1, M-1]$.

These states belong to a lower total spin manifold and are eigenstates of $\hat{H}_{\mathrm{SE}}$ with eigenvalue $E_q = J_{\mathrm{SE}}(1 - \cos 2\pi q/M)$.

With all other pieces in place, the only elements missing are the perturbation that matches the coupling between energy manifolds and to make the magnitude of this perturbation sufficiently small with respect to the energy gap.

6.2 Squeezing via Spin Orbit Coupling in the Mott Insulating Phase

We found the historically called spin orbit coupling (SOC), more aptly referred to as atom light coupling in this context, matches the generator of the spin waves states with the form

$$\hat{H}_{\mathrm{SOC}} = \Omega \sum_j \left(e^{i\phi j} \hat{S}_j^+ + e^{-i\phi j} \hat{S}_j^- \right). \tag{6.3}$$

This term can be derived from the interaction of a classical light field with the particles in the lattice when the angle of incidence and wavelength of said light source doesn't match those of the lattice potential.

We analytically found the SOC term survives and mostly doesn't affect the Mott insulating phase mapping if $J \ll U, \Omega \ll U$. If applied as is, this term will generate on-site spin flips which will complicate the perturbation theory analysis. However, if we apply a unitary transformation so this term is diagonal, we will see virtual processes involving tunnelling and spin flipping at the same time. After application of perturbation theory, we go back to the lab frame by applying again the unitary transformation to obtain the first effective Hamiltonian. While some corrections appear like the Dzyaloshinskii–Moriya interaction, they are highly suppressed if these conditions are fulfilled.

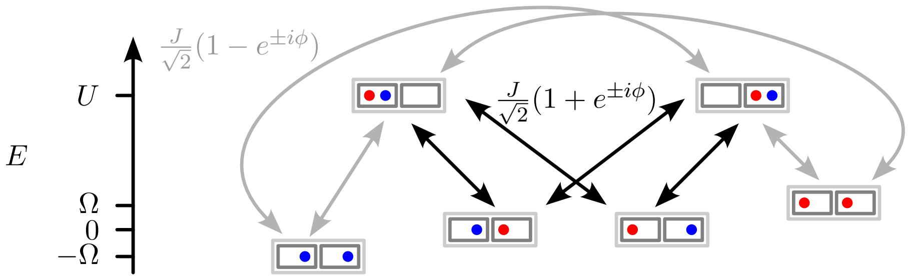

Figure 6.2: Similar sketch as in fig. 6.1, but including the spin-orbit coupling term for a two-site lattice at half-filling ($M = N = 2$). The Hamiltonian has also being transformed to diagonalise the spin-orbit coupling term. Black and grey arrows corresponds to coupling strengths $\frac{J}{\sqrt{2}}(1 + e^{\pm i\phi})$, $\frac{J}{\sqrt{2}}(1 - e^{\pm i\phi})$, respectively.

Now we can finally apply second-order perturbation theory to our already perturbed Hamiltonian to obtain an effective model with quadratic form. Under PBC, the phase ϕ must be commensurate with the lattice so that $\phi = 2\pi n/M$. Then, we obtain

$$\hat{H}_{\text{eff}}^{(2)} = \begin{cases} -2\chi_\phi \hat{S}_x^2 & \text{if} \quad \phi = \pi, \\ \chi_\phi \hat{S}_z^2 & \text{else,} \end{cases} \tag{6.4}$$

where

$$\chi_\phi = \frac{\Omega^2}{2J_{\text{SE}}\left(1 - \cos\phi\right)} \frac{1}{M-1}. \tag{6.5}$$

Interestingly, this means we can achieve not only a OAT model in different quantisation axis by tuning the phase ϕ, but also generate TACT by including different SOC terms in our Hamiltonian through the use of multiple off-axis light sources.

While this is sufficiently remarkable on it's own, we found the spin wave states change their form under OBC. This resulted in the unexpected realisation that, while our base Hamiltonian looks barely identical than under PBC, we obtain a much richer effective Hamiltonian for the same perturbation. After the appropriate phase shift, the effective Hamiltonian can be expressed as

$$\hat{H}_{\text{eff}} = \chi\left(\hat{S}^2 + \hat{S}_z^2 - \eta\hat{S}_x^2 + \eta\hat{S}_y^2 + \gamma\hat{S}_x\right), \tag{6.6}$$

where all parameters depend on ϕ.

These new terms and coefficients with respect to PBC appear because we allow the phase ϕ to be non-commensurate with the lattice, $\phi \neq 2\pi q/M;\ \forall q \in [1, M-1]$. This means we excite a number, if not all, of the spin wave states with different fidelity, tuning the parameter η accordingly. This has the disadvantage that the energy gap condition can become more restrictive on these phases. However, this effect becomes less prominent with the system size. On the other hand, η allows us to obtain more squeezing than the OAT model, as it becomes closer to a TACT model.

The largest complication from these non-commensurate phases is the appearance of a linear term with coefficient $\chi\gamma$ in eq. (6.6). This term acts as a fast rotation of the state in the Bloch sphere, suppressing the *twisting* effect of any term not aligned with its rotation axis. In any case, it will at most reduce the squeezing level to that of the OAT model if we choose an initial coherent state orthogonal to the given axis.

To better understand this effect, we may analyze the TACT-OAT transition in a simpler model, illustrated in fig. 6.3. If the Hamiltonian is given by

$$\hat{H} = \chi\left(\hat{S}_z^2 - \hat{S}_y^2\right) + v\hat{S}_z, \tag{6.7}$$

we may wonder at which point the linear term $v\hat{S}_z$ dominates the dynamics. We can estimate the magnitude of the terms from the maximal spin length of the system, which is $S = N/2$. In that case, the magnitude of the TACT term $\hat{H}_{\text{TACT}} = \chi(\hat{S}_z^2 - \hat{S}_y^2)$ may have the ceiling $\sim \chi(N/2)^2$. Likewise, the linear term $v\hat{S}_z$ will have a magnitude $\sim vN/2$. When the linear term is negligible ($v \ll \chi N/2$) the evolution is akin to the pure TACT model. However, when the linear term dominates ($v \gg \chi N/2$) the state rotates around the Bloch sphere very fast. The squeezing effect produced on one side of the sphere is cancelled by immediately turning to the opposite side, where the *twisting* is excecuted in the opposite direction. Only the twisting along the z-axis remains, since its unaffected by the linear term. This effect is obscured in the mean-field portrait, as the linear term dominates the energy. A rotated frame treatment might help to recover more accurate streamplots.

In any case, for phases $\phi \neq \pi$ but commensurate with the lattice, we do not obtain a OAT model like under PBC but an anisotropic TACT model with $\eta = 1/2$. This result does not vanish when $M \to \infty$, showing boundary conditions are critical for this system.

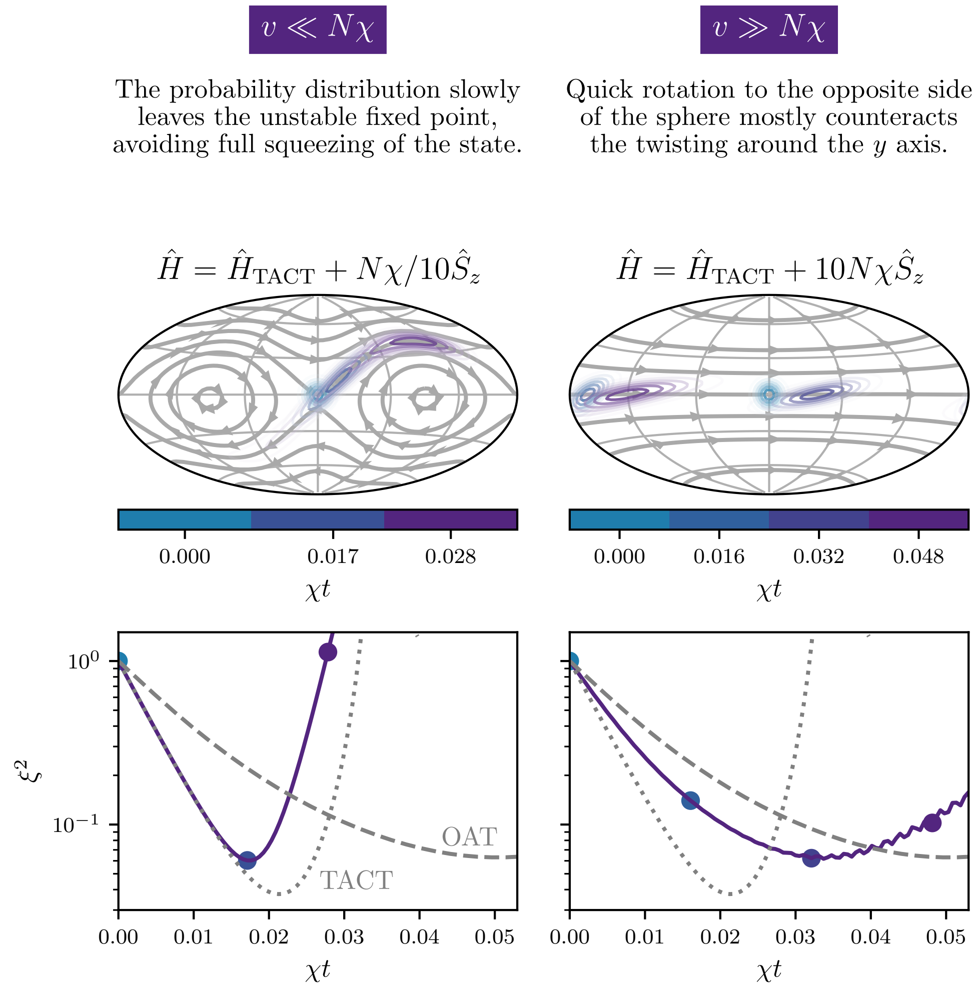

Figure 6.3: Illustrative example of transition from TACT dynamics , $\hat{H}_{\mathrm{TACT}} = \chi(\hat{S}_z^2 - \hat{S}_y^2)$, to OAT dynamics , $\hat{H}_{\mathrm{OAT}} = \chi\hat{S}_z^2$, through a linear term $v\hat{S}_z$. In the left column, we observe the effect of a linear term being smaller than the TACT model ($v = N\chi/10$). In the right column, the linear term is larger than the TACT model ($v = 10N\chi$). The top row briefly describes the corresponding effect of the linear term. The middle row shows Bloch spheres in Hammer projection where different colors identify different points in time. The bottom row compares the exact numerical results of the squeezing parameter to portray the transition from TACT-like dynamics to OAT-like dynamics. Colored points indicate the same moments in time as in the middle row panels. $N = 100$.

Dostęp do artykułu „One- and Two-Axis Squeezing via Laser Coupling in an Atomic Fermi-Hubbard Model”

znajduje się tutaj: https://doi.org/10.1103/PhysRevLett.129.090403

Dostęp do artykułu „Spin squeezing in open Heisenberg spin chains”

znajduje się tutaj: https://doi.org/10.1103/PhysRevB.108.104301

Chapter 7

Spin Squeezing under Imperfections and Holes

We have found a very successful scheme when extending the Fermi–Hubbard model with spin orbit coupling in the Mott insulating phase. We achieve OAT and TACT under both PBC and OBC while reducing the risk of particle losses. We can also obtain very similar results for bosons, for which the derivation of the effective models is almost identical. However, spin orbit coupling can be difficult to engineer in the lab when looking for a very precise value of the phase, more so for a geometry that respects PBC. In this chapter, we explore spin squeezing in the Mott insulating phase using bosons by studying two different sources of OAT models: inhomogeneous magnetic fields and anisotropic contact interactions. We work under OBC whenever possible to produce more realistic results with respect to experimental conditions. To validate the robustness of these implementations, we also consider the effects of occupation defects in the form of site vacancies or holes.

The results shown in this chapter are the result of our own research and have been published as:

T. Hernández Yanes, A. Niezgoda, and E. Witkowska, "Exploring spin squeezing in the Mott insulating regime: Role of anisotropy, inhomogeneity, and hole doping", Physical Review B **109**, 214310 (2024).

7.1 Squeezing via Contact Interactions in the Mott Insulating Phase

We already made use of anisotropic contact interactions in the superfluid regime to generate squeezing in chapter 5, but it also has a relevant effect in the Mott insulating regime. In this scenario, as explained in section 3.3, in the presence of anisotropy $\Delta \neq 1$ we obtain the Heisenberg XXZ model as an effective model of the base Bose–Hubbard model.

$$\hat{H}_{\mathrm{XXZ}} = -J_{\perp} \sum_{i=1}^{M} \left(\hat{S}_i^x \hat{S}_{i+1}^x + \hat{S}_i^y \hat{S}_{i+1}^y + \Delta \hat{S}_i^z \hat{S}_{i+1}^z \right). \tag{7.1}$$

While this is a well known fact, the key insight becomes apparent when we take into account some of our previous observations while developing our effective models:

- Local spin excitations build up the magnon states, which are excited states of the XXX model.
- If the perturbation does not match with a particular magnon excitation, it might couple to a number of them, if not all.
- These excitations can be produced along any axis, not only perpendicular to the spin quantisation axis.

Given these observations, what would happen if we have a perturbation in our Hamiltonian that excites two spins instead of a single one? The natural conclusion would be the coupling to two-magnon excitations. These statesgive us an even higher energy manifold than single magnon excitations that can also be exploited to obtain squeezing.

To study the anisotropy as a perturbation at the level of the Heisenberg model, we simply add and subtract terms in our Hamiltonian to recover the XXX model with an extra term $-J_{\perp}(1-\Delta)\sum_j \hat{S}_j^z \hat{S}_{j+1}^z$. This term acts as our perturbation.

While two-magnon states are more complicated to solve and in most cases their solution is not exact [105], their eigenenergies are well defined and are sufficient for our purposes. This is because, while we need to be in the perturbative regime, the perturbation already generates a zero-order term that results in an effective OAT model by itself.

$$\hat{H}_{\mathrm{eff}}^{(1)} = \chi^{(1)} \hat{S}_z^2, \tag{7.2}$$

with $\chi^{(1)} = J_{\perp}(1-\Delta)/(M-1)$. As we excite all the two-magnon states, we need to fulfil the energy gap condition for the smallest of them or we risk getting out of the perturbative regime. As the smallest energy gap depends on the inverse of the system size, this effect will vanish when $M \to \infty$.

Contribution from second-order processes can be largely ignored as they are much smaller in principle and provides squeezing around the same axis. It can be found that they provide terms $\propto \hat{S}_z^2$ and $\propto \hat{S}_z^4$, but the specific coefficients are difficult to derive.

While this method to generate squeezing disappears when $M \to \infty$, any slight difference in contact interactions will have a relevant effect in the system. Moreover, the smaller this difference is, the faster the squeezing process will be. This is a relevant effect that needs to be taken into account for realistic setups and also a strong contender in terms of implementation simplicity.

7.2 Squeezing via Inhomogeneous Magnetic Field in the Mott Insulating Phase

Another way to experimentally engineer the spin orbit coupling term is to produce a spatially varying magnetic field across the lattice, polarised perpendicularly to the spin quantisation axis. This scheme still suffers from the same problem of achieving a commensurate phase with the lattice, but it gives us an insight on how to make our proposed model more robust: magnon excitations also happen if we polarise the magnetic field along the spin quantisation axis as

$$\hat{H}_{\mathrm{B}} = \sum_{j=1}^{M} \beta_j \hat{S}_j^z. \tag{7.3}$$

While this might be a soft conceptual realisation, it makes mathematical derivations much more straightforward.

As the spin excitation term is now diagonal in the Fock state basis, there is no need to use the rotated frame to study the virtual transitions. We can instead directly apply perturbation theory to the Hubbard model with eq. (7.3) to retrieve the first effective Hamiltonian for the Mott insulating phase condition, with $J \ll U_{\sigma,\sigma'}, |\beta_j - \beta_{j+1}|/2 \ll U_{\sigma,\sigma'}; \forall j, \sigma, \sigma'$. We refer to $U_{\sigma,\sigma'}$ as the magnitudes of the contact interactions depending on the internal states of the bosons. After that, we obtain the Heisenberg XXZ model with a perturbation in the form of the inhomogeneous magnetic field.

$$\hat{H} = \hat{H}_{\mathrm{XXZ}} + \hat{H}_{\mathrm{B}}. \tag{7.4}$$

To remove the contribution from the two magnon excitations that comes from the anisotropic contact interactions, we choose $\Delta = 1$ so that our Hamiltonian becomes

$$\hat{H} = \hat{H}_{\mathrm{XXX}} + \hat{H}_{\mathrm{B}}. \tag{7.5}$$

As we discussed, single magnon states can be defined along any axis and in turn this results in an easier derivation of the effective OAT model with respect to the Heisenberg model.

$$\hat{H}_{\mathrm{eff}}^{(2)} = \chi \hat{S}_z^2 + v \hat{S}_z, \tag{7.6}$$

where $\chi = \sum_q |f_q|^2/E_q$ with f_q being the fidelity to the single magnon states with the perturbation and $v = \sum_j \beta_j/M$.

If we excite a single magnon of quasi-momenta q, the perturbative condition will be $|\beta_j| \ll E_q; \forall j$. In general, we might be exciting to more single magnon states, so the energy gap can become smaller. However, this also depends on the exact shape of the inhomogeneous magnetic field, as it might have negligible fidelity with magnon excitations of lower q.

This guarantees the existence of squeezing for any sufficiently small inhomogeneous magnetic field. For instance, we can even use a random magnetic field and obtain squeezing if the magnitude of the field is, at worst, $\ll E_{q=1}$. The setup we propose is both very resilient and sufficiently easy to construct. We thus conclude the inhomogeneous magnetic field is a strong candidate to obtain scalable spin squeezing in the lab.

7.3 Effect of hole doping

In this chapter, we have derived effective models under two scenarios, inhomogeneous magnetic field or anisotropy in contact interactions for the Bose–Hubbard model. Both of them yield an effective OAT model with or without a linear term, respectively. However, both results rely on the half-filling condition to fix particles in place. The corresponding t–J model in the presence of holes

$$\hat{H}_{t-J} = -t \sum_{\langle j,i \rangle} \hat{P}_0^\dagger \left(\hat{a}_j^\dagger \hat{a}_i + \hat{b}_j^\dagger \hat{b}_i \right) \hat{P}_0 + \hat{H}_{\mathrm{XXZ}} + \hat{H}_{\mathrm{B}}, \tag{7.7}$$

where $t \in \{0, J\}$ and $\hat{P}_0$ projects into the single occupied states, is difficult to study analytically. We can nevertheless find limiting cases that are easier to analyse to obtain an estimation of the squeezing level we will obtain. In this section we explore such a case where position and number of holes are fixed over time. We will see how they make the dynamics separable into partial chains. The opposite limiting case is when holes move infinitely fast across the lattice and the system acts as if fully filled.

As discussed in previous chapters, when holes are present in the system in the Mott insulating phase, the system maps into a t–J model, where tunnelling processes are still possible among single occupied states. While the tunnelling rate is the same as before applying perturbation theory, this rate will be larger than the magnitude of the spin exchange term by virtue of the approximation itself. In other words, since $J \ll U_{\sigma,\sigma'}$, we obtain $J \gg J_\perp$.If we express the evolution of a coherent state in units of $J_\perp$, the tunnelling processes will be very quick in comparison. We can picture particles moving across neighbour vacancies, while the spin exchange processes will occur as if no holes where present in the system, up to a filling factor correction. Of course, this does not mean particles move across the lattice without friction like in the superfluid regime. Particles will still block each other from tunnelling to their respective sites as $U_{\sigma,\sigma'} \gg J$, but when a particle finds a hole next to its position, it will immediately travel to the next site. This approximation makes sense in the limit where $U_{\sigma,\sigma'}/J \to \infty$.

The opposite limiting case, which is reached due to the perturbation condition, is the case where holes are fixed in certain locations across the lattice in time. This is a relevant limit of the system, even if idealised, which gives us insight into the dynamics of the t–J model.

Let us then focus on this particular limiting case of fixed holes. If we look at the Heisenberg model described in previous chapters, we will notice the correlations are nearest neighbour only. If a hole is present in the system, it will simply cancel the effect of any term that interacts with it, isolating the sub-systems bounded by these holes from any other part of the system. We will refer to this sub-systems as partial chains, as illustrated in figs. 7.1 and 7.2. We found these partial chains evolve independently from one another, as the Dicke states or the one and two magnon excitations can all be defined independently for each chain, as explained in section 3.3.

The second moments of the spin operators can introduce problems to this realisation, as they are needed to calculate the co-variances present in the spin squeezing parameter ξ^2 and might account for correlations among partial chains. Nevertheless, the co-variances recover this independent behaviour, so the study of the squeezing parameter can be done within this framework.

Let us now focus on the possible effective models for each partial chain. If the model is generated through anisotropic contact interactions, we obtain a pure OAT model (7.2).The probability distributions of the partial chain represented on the Bloch sphere will mostly overlap in time, with small discrepancies due to the spin length of each partial chain and the coefficient χ of each partial chain, which also depends on its length, as illustrated in fig. 7.1.

However, when the model appears as a result of an inhomogeneous magnetic field, a linear term $v\hat{S}_z$ is present in the partial chain Hamiltonian, as described in eq. (7.6). This implies the mean spin direction will rotate along the equator of the Bloch sphere at a rate $\propto \cos 2\pi/v$. As v changes on each partial chain, the partial chain mean spin directions will rotate at different rates with respect to each other. This is detrimental for squeezing as it inevitably lowers $\langle \hat{S}_n \rangle$ unless they overlap. Another effect of the magnetic field is that the coefficient χ of each sub-system might be different depending on both the partial chain length and the magnetic field itself. In any case, the largest contribution to the loss of squeezing is the misalignment of the mean spin directions, as we demonstrate in fig. 7.2.

In any case, this gives us a semi-analytical model, as each partial chain evolution is analytical but adding them up can be non-trivial.

7.4 Movement of holes

In the previous section we mentioned the limiting cases of the model when tunnelling is allowed in the presence of holes: frozen holes during dynamics and infinite effective tunnelling. In this section, we explore numerical results of the corresponding t–J models, for which we tune the effective tunnelling

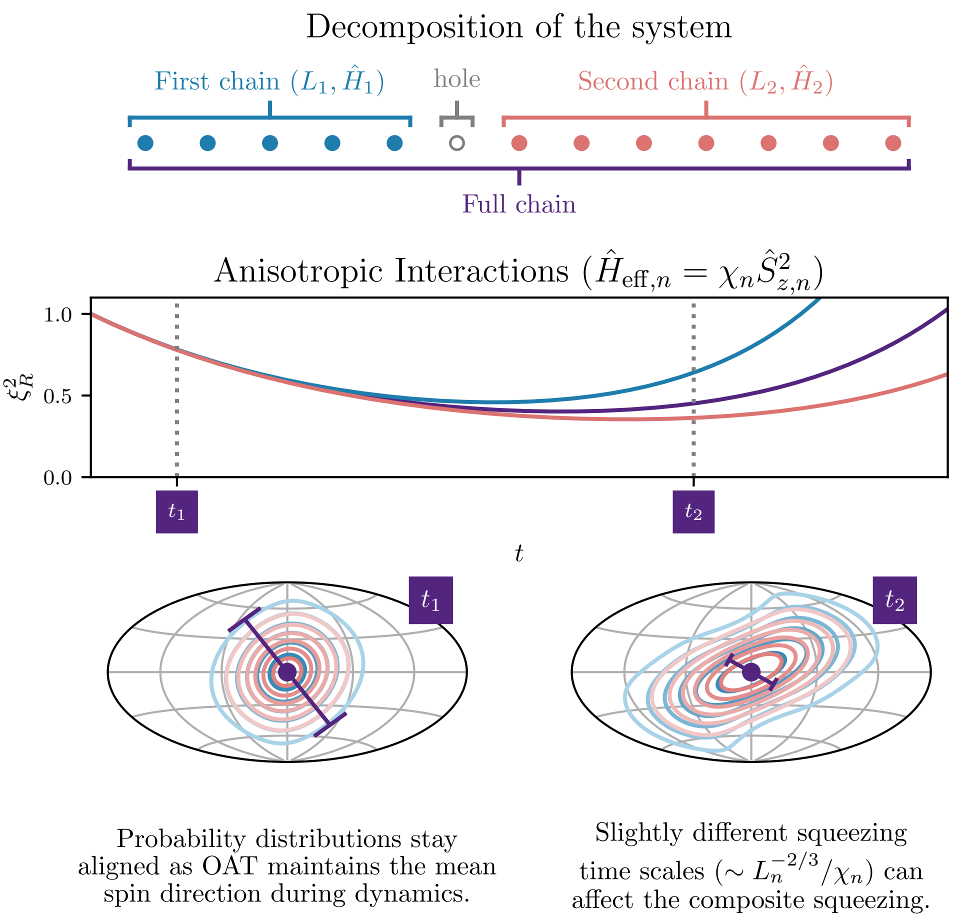

Figure 7.1: Spin squeezing dynamics induced by anisotropy of the contact interactions in the presence of a hole in the system. When the hole is fixed at a given site, we can decompose the system as two independent spin chains. Results for independent chains as well as for the full chain are indicated by different colors, as in the upper diagram. The purple point in the Bloch spheres indicate the mean spin direction of the full chain. The purple brackets that accompany the point indicate the minimal variance $(\Delta\hat{S}_{\text{min}})^2$ direction and magnitude. We label the partial chains by numbers 1 and 2. $M = 13, N = 12$. $L_1 = N_1 = 5$, $L_2 = N_2 = 7$. $\Delta = 0.98, \beta_j = 0$.

$t/J_\perp$ from zero (fixed holes) to a large value with respect to the energy scale of the system.

Let us imagine we perform an experiment where we have a fixed number of sites M and a number of particles N such that $N \leq M$, but the location of the particles in the lattice is completely random for each realisation. After

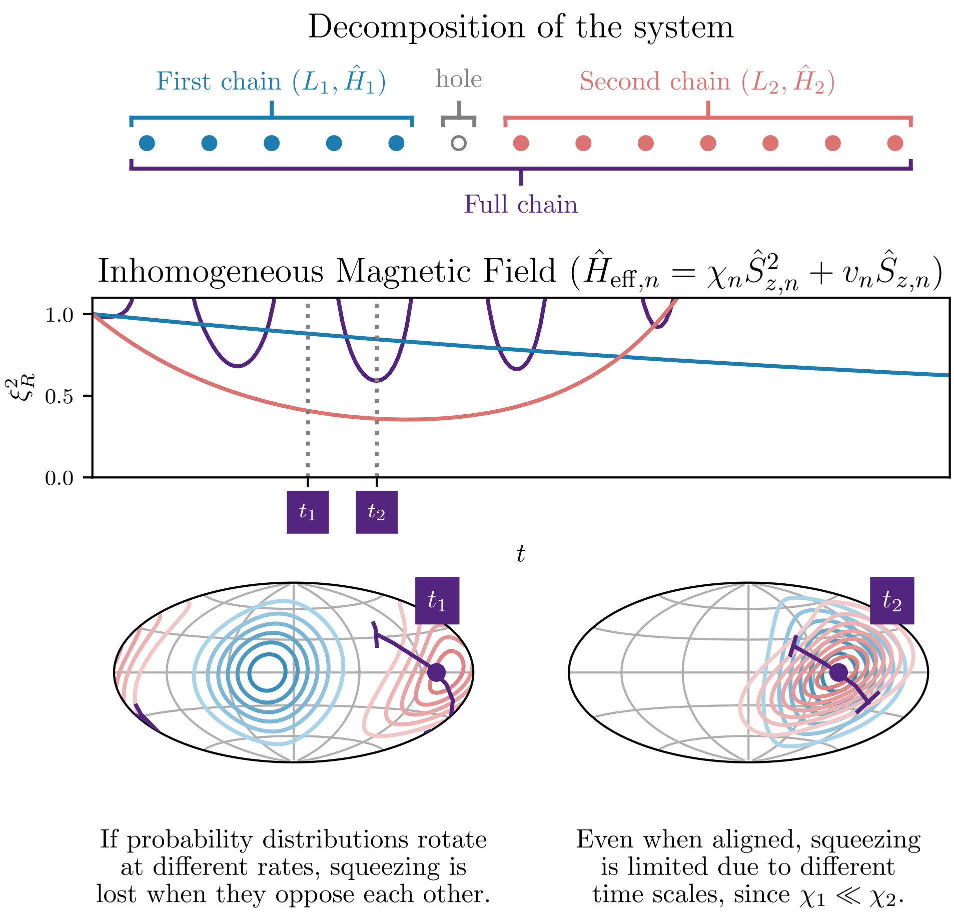

Figure 7.2: Spin squeezing dynamics induced by an inhomogeneous magnetic field in the presence of a hole in the system. When the hole is fixed at a given site, we can decompose the system as two independent spin chains. Results for independent chains as well as for the full chain are indicated by different colors, as in the upper diagram. The purple point in the Bloch spheres indicate the mean spin direction of the full chain. The purple brackets that accompany the point indicate the minimal variance $(\Delta\hat{S}_{\text{min}})^2$ direction and magnitude. We label the partial chains by numbers 1 and 2. $M = 13, N = 12$. $L_1 = N_1 = 5$, $L_2 = N_2 = 7$. $\Delta = 1, \beta_j = E_M^{(M-1)}/50 \cos\left(\frac{\pi}{M}(M-1)(j-1/2)\right)$.

averaging over many of then, we will obtain an initial density matrix like

$$\hat{\rho}(0) = \frac{1}{N_{\mathcal{P}}} \mathcal{P} \left(\bigotimes_{j=1}^{N} |\uparrow_j\rangle\langle\uparrow_j| \bigotimes_{k=M-N}^{M} |0_k\rangle\langle 0_k| \right), \tag{7.8}$$

where $\mathcal{P}$ stands for the sum of all possible permutations of N particles in M

sites and $N_{\mathcal{P}}$ is the total number of said permutations.

In fig. 7.3 we can see how, in the case of the spin squeezing induced by the inhomogeneous magnetic field, the squeezing is quickly suppressed with the reduction of particles in the system of fixed size M. Moreover, the time scale of the squeezing seems to grow with the effective tunnelling. These effects can be traced to the presence of a linear term in the effective Hamiltonian, which makes the coherent evolution of the partial chains difficult, even when correlations between them due to tunnelling appear.

On the contrary, the coherent squeezing for the scenario of anisotropic contact interactions is remarkable even in the case where the effective tunnelling is suppressed. The different configurations add up coherently, since the absence of a linear term in the effective Hamiltonian allows for the alignment of the probability distributions of the partial chains. In the cases where effective tunnelling is allowed, the squeezing level immediately jumps very close to the idealised scenario of infinite tunnelling, even for small values. Also, the squeezing is much more resilient to the reduction of the particle number.

Similar conclusions can be drawn from the results reflected in the publication, where we employ a more involved density matrix related to the on-site filling factor. In that case, time scales seem to adhere better to the proposed estimations, but the conclusions about the drastic change for the magnetic field scenario and the resilience of the anisotropic scenario are the same.

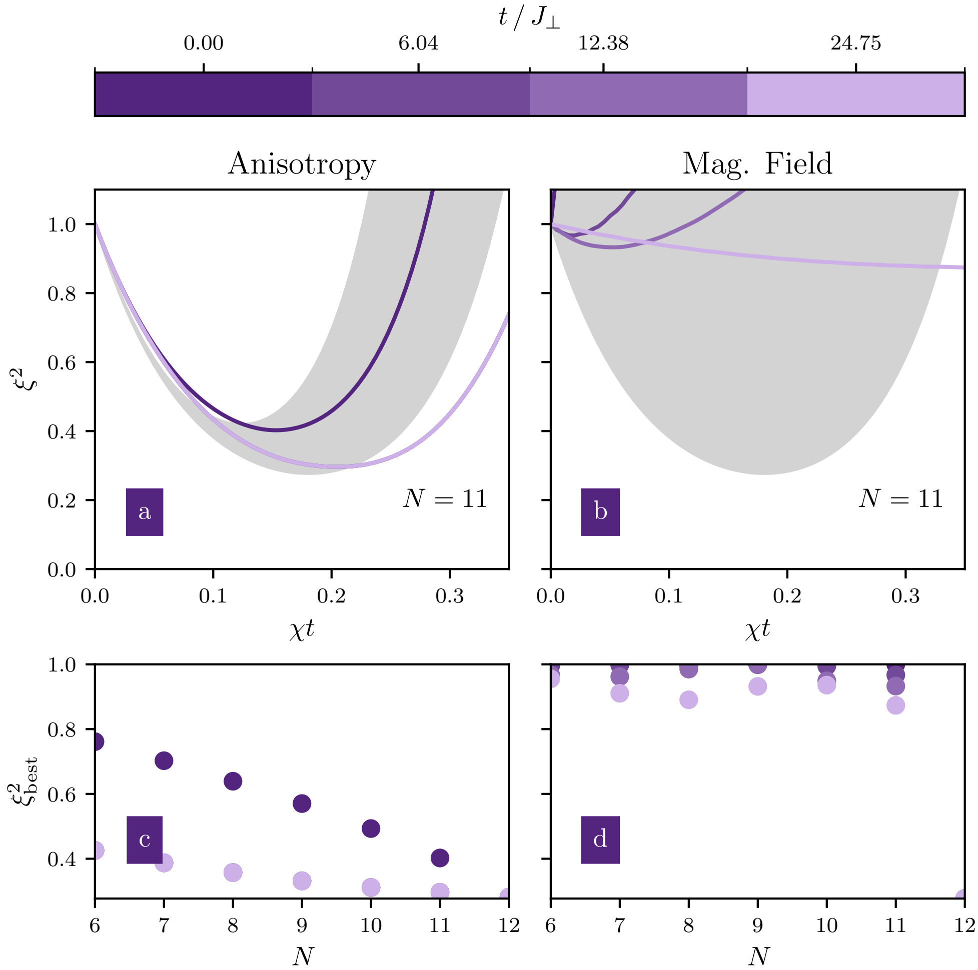

Figure 7.3: Evolution of spin squeezing parameter induced by anisotropy (a) and inhomogeneous magnetic field (b) for different values of the tunnelling rate $t \in \{0, J\}$ and filling factor f. In each instance, χ is estimated from the corresponding effective models when $N = M = 12$. In all cases, the initial state is characterized by the density matrix in eq. (7.8). Grey areas indicate the regions between the semi-analytical upper and lower bounds bounds. The best squeezing ξ^2_{best} with respect to N is shown in (c) and (d) when its generation is governed by anisotropy and inhomogeneous magnetic field, respectively. To tune the effective tunnelling, we fix $J = 1$ but change $2U_{ab}/(1+\Delta) \in \{24.4J, 50J, 100J\}$, with $J_\perp = J^2/(4U_{ab}), U_{aa} = U_{bb} = 2U_{ab}/(1+\Delta)$. For the anisotropic case $\Delta = 0.98, \beta_j = 0$, while for the magnetic field case $\Delta = 1, \beta_j = E_M^{(M-1)}/50 \cos\left(\frac{\pi}{M}(M-1)(j-1/2)\right)$.

Dostęp do artykułu „Exploring spin squeezing in the Mott insulating regime: Role of anisotropy, inhomogeneity, and hole doping”

znajduje się tutaj: https://doi.org/10.1103/PhysRevB.109.214310

Chapter 8

Entanglement of squeezed states under occupation defects

The schemes we have shown involving the Mott insulating phase where we excite spin wave states via a small perturbation are very effective at reproducing models akin to OAT and TACT. The absence of double occupied states in this mapping prevents particle losses due to collisions. Moreover, the proposed schemes do not involve complicated setups and are sufficiently resilient to small changes in the system parameters. In the previous chapter we also developed a model for the case of holes pinned in different locations of the lattice. We also explored the t–J model in the context of spin squeezing, where we allowed particles to move in the lattice. The study of dynamics in the presence of holes is relevant since, in an experiment, we might have little control on the number of particles that survive the preparation stage. An aspect of the spin squeezing parameter which we have yet to explore is its utility as an entanglement witness. We may then question how holes affect correlations and entanglement in the context of spin squeezing. In this work we propose a two-site Bell correlator to certify entanglement, which can be conveniently expressed in terms of the normalized mean spin and the spin squeezing parameter. The correlator accounts for occupation defects and is well bounded by limiting cases obtained through a toy model. The occupation defects under study appear either at the state preparation stage or the measurement stage.

The results shown in this chapter are the result of our own research and the pre-print of the research article is available as:

T. H. Yanes, Y. Bamaara, A. Sinatra, and E. Witkowska, *Bounds on detection of Bell correlations with entangled ultra-cold atoms in optical lattices under occupation defects*, (Sept. 4, 2024) `http://arxiv.org/abs/2409.02873` (visited on 09/08/2024), pre-published.

8.1 Two-body Bell Correlator

While we could use standard definitions of the spin squeezing parameter to detect negative pairwise correlations [9] or rely on a set of generalized spin squeezing inequalities [72], we instead opt for a data-driven approach to construct Bell correlators based on local measurements [37]. Bell inequality violation represents the most robust scheme for entanglement certification, avoiding assumptions on physical nature and degrees of freedom to be measured or calibration of measurement.

We consider the M sites of our lattice as separate subsystems where at least two observables α are measured, each having d possible outcomes. A Bell experiment checks if correlations can be provided through a local hidden variable theory, meaning the obtained results depend on local correlations from the past. To check this, we may choose an arbitrary observable for each of the M subsystems $\alpha = \{\alpha_j\}_{j=1}^{M}$ to calculate probabilities of the measurement outcomes $r = \{r^{(j)}\}_{j=1}^{M}$. The expected pair probability distribution is given by

$$P_M^{(\mathrm{LV})}(r|\alpha) = \int d\lambda\, q(\lambda) \prod_{j=1}^{M} P^{(j)}(r^{(j)}|\alpha_j, \lambda). \tag{8.1}$$

Instead of working with eq. (8.1), we equivalently consider one- and two-body correlations summed over the permutations of the subsystems as

$$M_\alpha = \sum_{j=1}^{M} \left\langle r_\alpha^{(j)} \right\rangle, \tag{8.2}$$

$$C_{\alpha\beta} = \sum_{i,j\neq i} \left\langle r_\alpha^{(i)} r_\beta^{(j)} \right\rangle, \tag{8.3}$$

$$\tilde{C}_{\alpha\beta} = C_{\alpha\beta} - M_\alpha M_\beta. \tag{8.4}$$

We can use these correlations to build up a vector $\vec{M}$ and matrix $\tilde{C}$ to represent the non-locality condition as a convex optimization problem. Then, given a positive-semi-definite matrix $A \succeq 0$ and a vector $\vec{h}$, we find

$$L(A, h) = \mathrm{tr}(A\tilde{C}) + \vec{h} \cdot \vec{M} + E_{\max} \geq 0, \tag{8.5}$$

where $E_{\max}$ is the classical limit, as long as $\vec{M}, \tilde{C}$ are compatible with a local hidden variable theory. If we introduce data corresponding to a spin-squeezed state in the proposed convex optimization problem, we may obtain [37]

$$L = \tilde{C}_{00} + \tilde{C}_{11} - \tilde{C}_{01} - \tilde{C}_{10} - M_0 - M_1 + M \geq 0, \tag{8.6}$$

While this inequality was originally proposed for systems with two possible measurement outcomes, we numerically found the convex optimization that yields eq. (8.6) from eq. (8.5) is also satisfied with our proposed three possible measurement outcomes $r_j \in \{-1/2, 0, +1/2\}$.

To recover the collective character of the spin squeezing parameter in the Bell correlators, we choose all local measurements to be along the same directions, retrieving coherent measurement expressions. Our two chosen measurement settings $\alpha \in \{0, 1\}$ are

$$\hat{S}_j^{0,1} = \cos\theta \hat{S}_j^n \pm \sin\theta \hat{S}_j^{\min}, \tag{8.7}$$

where n is the mean spin direction and min is the minimal variance direction of the state. While some local measurements survive this choice of settings, they can be effectively replaced with basic information about the initial state of the system, as we show later. Moreover, we implicitly assume that any local measurement outcome outside the eigensubspace of eigenvalues $r^{(j)} = \pm 1/2$ is treated as if the site was empty.

We can introduce eq. (8.7) into eq. (8.6) and optimize over the change of variable $x = \cos\theta$, as the inequality takes the form of a simple quadratic polynomial. Through this approach we derive a general two-site Bell correlator which only depends on first and second moment results of the form

$$L_{\text{opt}}^{(1)} = M - \frac{\mathcal{M}_n^2}{4(\mathcal{M}_{\min}^2 - \mathcal{C}_{\min,\min})} - 4(\mathcal{M}_{\min}^2 - \mathcal{C}_{\min,\min}), \tag{8.8}$$

where we considered the averages along the mean spin and squeezing directions,

$$\mathcal{M}_n = \sum_{j=1}^{M} \langle \hat{S}_j^n \rangle, \tag{8.9}$$

$$\mathcal{M}_{\min} = \sum_{j=1}^{M} \langle \hat{S}_j^{\min} \rangle, \tag{8.10}$$

as well as the two-site correlations along the squeezing direction

$$\mathcal{C}_{\min,\min} = \sum_{i,j\neq i}^{M} \langle \hat{S}_i^{\min} \hat{S}_j^{\min} \rangle. \tag{8.11}$$

We can rewrite this definition with collective expectation values by introducing the average number of unit-filled site $\bar{M} \equiv \sum_i \text{Tr}(\rho_i)$, which is a time-independent on-site measurement. This is because we do not consider the generation of occupation defects during dynamics, meaning the Hamiltonian maintains the different occupation sectors separated. In such case, we obtain

$$L_{\text{opt}}^{(1)} = M - \frac{\langle \hat{S}_n \rangle^2}{\bar{M} - 4(\Delta \hat{S}_{\min})^2} - (\bar{M} - 4(\Delta \hat{S}_{\min})^2), \tag{8.12}$$

where $|\langle \hat{S}_n \rangle| \leq |\bar{M} - 4(\Delta \hat{S}_{\min})^2|$; otherwise we have $L_{\text{opt}}^{(1)} = M - 2|\langle \hat{S}_n \rangle|$.

The result can be expressed in terms of the spin squeezing parameter ξ^2 and the normalized mean spin direction $v = 2\langle \hat{S}_n \rangle / N$ as

$$L^{(1)}_{\text{opt}} = M - \frac{N}{4} \frac{N v^2}{\bar{M} - N\xi^2 v^2} - (\bar{M} - N\xi^2 v^2). \tag{8.13}$$

8.2 Occupation defects and toy model

This data-driven approach to derive our target Bell correlator becomes relevant when we include measurement conditions in our experiment. In particular, we explore the effects of occupation defects on the system. To demonstrate the usefulness of the proposal, we assume two possible scenarios which provide two different sources of occupation defects: particle losses at the preparation stage and double occupations at the measurement stage. In the former scenario, state preparation is imperfect and we loose particles with a given probability before the start of the dynamics. In the latter scenario, preparation and dynamics are as expected but we loose single occupancy per site at the measurement stage.

To have a reference of the entanglement limit in these different scenarios, we develop a toy model that assumes complete decoupling between the internal degrees of freedom (spin) and the external ones (spatial distribution). While this is a broad simplification, we observe the toy model closely benchmarking the correlation limit of our models under occupation defects. This treatment requires an adaptation of the Bell correlator to each of the scenarios with the toy model, based on the particular constrains on entanglement they impose.

For instance, the particle losses scenario yields the toy model two-site Bell correlator

$$\frac{L^{(\text{V})}}{M} = 1 - \frac{p(N-1)}{N-p} \frac{\langle \hat{S}_n \rangle^2_{\text{SS}}}{N\left[N - 4(\Delta \hat{S}_{\min})^2_{\text{SS}}\right]} - \frac{p(N-p)}{N-1}\left[1 - \frac{4(\Delta \hat{S}_{\min})^2_{\text{SS}}}{N}\right], \tag{8.14}$$

where SS signifies expectation values of a purely squeezed state of N particles, p is the probability of finding a given site at unit-filling, and $N = pM$. Equation (8.14) can be obtained from eq. (8.12) by introducing

$$\begin{aligned} N =& pM, \\ \bar{M} =& pM = N \\ \langle \hat{S}_n \rangle =& \langle \hat{S}_n \rangle_{SS}, \\ (\Delta \hat{S}_m)^2 =& \frac{N-p}{N-1}\left[(\Delta \hat{S}_m)^2_{SS} - \frac{N}{4}\right] + \frac{N}{4}. \end{aligned}$$

Equation (8.14) holds when $N \leq M$, that is $p \leq 1$. The asymptotic behaviour in the large particle limit, $N \to \infty$, sets a fixed limit on the Bell correlations with respect to the probability p. Values above the critical probability p_c are unable to provide non-local correlations. In this case, $\lim_{N\to\infty} p_c = 5/4$.

Instead, the measurement defects scenario yields the following result

$$\frac{L^{(\mathrm{VI})}}{M} = 1 - \frac{\langle \hat{S}_n \rangle^2_{\mathrm{SS}}}{N\left[N - 4(\Delta \hat{S}_{\min})^2_{\mathrm{SS}}\right]} - p^2\left[1 - \frac{4(\Delta \hat{S}_{\min})^2_{\mathrm{SS}}}{N}\right], \tag{8.15}$$

where $N = M$. Equation (8.15) can be obtained from eq. (8.12) by introducing

$$\begin{aligned} N =& M, \\ \bar{M} =& pM \\ \langle \hat{S}_n \rangle =& p \langle \hat{S}_n \rangle_{SS}, \\ (\Delta \hat{S}_m)^2 =& \sum_{i,j} \langle \hat{s}_{im} \hat{s}_{jm} \rangle + \langle \hat{S}_m \rangle^2 = \sum_{i\neq j} \langle \hat{s}_{im} \hat{s}_{jm} \rangle_{SS} + \frac{\bar{M}}{4} + \langle \hat{S}_m \rangle^2 \\ =& p^2 \left[(\Delta \hat{S}_m)^2_{SS} - \frac{M}{4}\right] + p\frac{M}{4}, \end{aligned}$$

In this case, $\lim_{N\to\infty} p_c = \sqrt{3}/2$.

8.3 Realistic implementations

We exemplify the particle losses scenario in the Mott insulating phase through two different sources of squeezing given an average filling factor. As seen in chapter 7, we can generate OAT dynamics through a weak anisotropy of the contact interactions such that the effective Hamiltonian of a partial chain n isolated by empty sites is given by

$$\hat{H}^{(0)}_{\mathrm{eff},n} = -\chi^{(0)}_n \hat{S}^2_{z,n}. \tag{8.16}$$

Alternatively, if we implement a weak inhomogeneous magnetic field, we may obtain the effective Hamiltonian

$$\hat{H}_{\mathrm{eff},n} = \chi_n \hat{S}^2_{z,n} + v_n \hat{S}_{z,n}. \tag{8.17}$$

We demonstrate numerically that the presence of a linear term in the effective Hamiltonian, usually negligible in the unit-filling regime, greatly affects the generation of non-local correlations, as we showed previously with spin squeezing in chapter 7.

We also compare the obtained two-site correlator with an M-site correlator capable of detecting GHZ states [77] to benchmark its usefulness. While the M-site correlator is sensitive to non-local correlations up to $p > p_c = 1/\sqrt{2}$ in the large particle number limit, it requires larger time scales ($\chi t = \pi/2$) and experimentally challenging correlation measurements involving all sites of the lattice. On the contrary, the two-site correlator shows optimal detection at the best squeezing time scale ($\chi t \ll \pi/2$) and the correlation measurements are only two-body collective measurements.

Dostęp do artykułu „Bounds on detection of Bell correlations with entangled ultra-cold atoms in optical lattices under occupation defects”

znajduje się tutaj: https://doi.org/10.1103/PhysRevA.111.023312

Chapter 9

Conclusions

Spin squeezing provides highly entangled states that retain Gaussian probability distributions. These states are useful for metrological and technical applications like atomic clocks, quantum sensing or quantum computing. This work has provided new methods to obtain spin-squeezed states in relatively simple setups in one-dimensional optical lattices. With the Schieffer-Wolff transformation as our main analytical tool in specific perturbative regimes, we obtained precise and well defined effective models. While an intuitive picture on the build up of correlations can be seen in the coupling to a correlated external field or among pairs of particles, perturbation theory provides a different view: brief transitions to eigenstates with different types of correlations ultimately provides more entanglement than a strong coupling, which could even lower the total spin of the state. The proposed Hamiltonians are achievable in state-of-the-art experiments of ultra-cold atoms in the optical lattice, but they can potentially be implemented in other setups.

The chapters of this work explained different implementation proposals to obtain relevant effective models and predictions, with a natural progression in complexity and refinement of the techniques developed through the work. In chapters 1 to 4 we introduced the topics of spin squeezing and the tools we employ to study its dynamical generation in the optical lattice. In chapter 5 we augmented the known simulation of the OAT model by the two-component Bose-Hubbard model in the superfluid phase with a term that arises from dipolar interactions to obtain an anisotropic TACT model. We also proved how its spin squeezing generation strongly resembles TACT until the anisotropy parameter $\eta \ll 1$. In chapter 6 we obtained qualitatively different effective models depending on the boundary conditions for the Fermi-Hubbard model in the Mott insulating phase with the introduction of spin-orbit coupling. In both cases we are able to engineer one- and two-axis twisting models by either adding a second spin-orbit coupling term or accurately tuning the coupling phase. In chapter 7 we again used the single-magnon excitations results from the previous works to derive a one-axis twisting model by including a weak inhomogeneous magnetic field in the two-component Bose-Hubbard model. We also found the perturbation regime for the contact interactions anisotropy parameter, where one-axis twisting is also generated through two-magnon excitations. While these systems share the same effective model at half-filling, they showed striking differences in the presence of holes. The existence of an incoherent linear term in the effective model of the subsystems can destroy entanglement generation. In chapter 8 we further explored the effect of occupation defects in the Bose-Hubbard model by analyzing Bell correlators tailored for defects at two stages: preparation and measurement. For the preparation stage scenario we again studied the systems from chapter 7 when the initial state is defined through an ensemble of different number of particles. The presence of a linear term in the partial chains of the system proved highly detrimental for generating non-local correlations. For the measurement stage scenario we studied the effect of temperature on the measurements of the one-axis twisting model generated through contact interactions anisotropy in the superfluid regime. As the lattice is raised until the Mott insulating phase for measurement of the state, temperature affects the average single occupancy of the superfluid phase. We obtained a critical value of the temperature above which non-local correlations are undetected. Critical values of the single particle per site probability for both scenarios were found bellow unit-filling, implying experiments testing Bell correlations with imperfect stage preparation or measurements are feasible.

In each of the proposed cases, limitations and advantages are well understood and described. This catalogue of spin-squeezing generating Hamiltonians provides a nuanced perspective on entanglement generation in optical lattices.Future research directions point towards extension to large spin, higher dimensions, or the understanding of more complex effective models.

Bibliography

[1] M. Dziurawiec, T. Hernández Yanes, M. Płodzień, M. Gajda, M. Lewenstein, and E. Witkowska, “Accelerating Many-Body Entanglement Generation by Dipolar Interactions in the Bose-Hubbard Model”, Physical Review A **107**, 013311 (2023).

[2] T. Hernández Yanes, M. Płodzień, M. Mackoit Sinkevičienė, G. Žlabys, G. Juzeliūnas, and E. Witkowska, “One- and Two-Axis Squeezing via Laser Coupling in an Atomic Fermi-Hubbard Model”, Physical Review Letters **129**, 090403 (2022).

[3] T. Hernández Yanes, G. Žlabys, M. Płodzień, D. Burba, M. M. Sinkevičienė, E. Witkowska, and G. Juzeliūnas, “Spin Squeezing in Open Heisenberg Spin Chains”, Physical Review B **108**, 104301 (2023).

[4] T. Hernández Yanes, A. Niezgoda, and E. Witkowska, “Exploring spin squeezing in the Mott insulating regime: Role of anisotropy, inhomogeneity, and hole doping”, Physical Review B **109**, 214310 (2024).

[5] T. H. Yanes, Y. Bamaara, A. Sinatra, and E. Witkowska, *Bounds on detection of Bell correlations with entangled ultra-cold atoms in optical lattices under occupation defects*, (Sept. 4, 2024) `http://arxiv.org/abs/2409.02873` (visited on 09/08/2024), pre-published.

[6] M. Kitagawa and M. Ueda, “Squeezed Spin States”, Physical Review A **47**, 5138 (1993).

[7] D. J. Wineland, J. J. Bollinger, W. M. Itano, F. L. Moore, and D. J. Heinzen, “Spin squeezing and reduced quantum noise in spectroscopy”, Physical Review A **46**, R6797 (1992).

[8] D. J. Wineland, J. J. Bollinger, W. M. Itano, and D. J. Heinzen, “Squeezed atomic states and projection noise in spectroscopy”, Physical Review A **50**, 67 (1994).

[9] D. Ulam-Orgikh and M. Kitagawa, “Spin Squeezing and Decoherence Limit in Ramsey Spectroscopy”, Physical Review A **64**, 052106 (2001).

[10] J. K. Stockton, J. M. Geremia, A. C. Doherty, and H. Mabuchi, “Characterizing the entanglement of symmetric many-particle spin-1/2 systems”, Physical Review A **67**, 022112 (2003).

[11] C. Simon and J. Kempe, "Robustness of multiparty entanglement", Physical Review A **65**, 052327 (2002).

[12] Y. Li, Y. Castin, and A. Sinatra, "Optimum Spin Squeezing in Bose-Einstein Condensates with Particle Losses", Physical Review Letters **100**, 210401 (2008).

[13] X. Yin, X. Wang, J. Ma, and X. Wang, "Spin squeezing and concurrence", Journal of Physics B: Atomic, Molecular and Optical Physics **44**, 015501 (2010).

[14] J. Ma and X. Wang, "Fisher information and spin squeezing in the Lipkin-Meshkov-Glick model", Physical Review A **80**, 012318 (2009).

[15] L. Song, X. Wang, D. Yan, and Z. Zong, "Spin squeezing properties in the quantum kicked top model", Journal of Physics B: Atomic, Molecular and Optical Physics **39**, 559 (2006).

[16] L. Song, D. Yan, J. Ma, and X. Wang, "Spin squeezing as an indicator of quantum chaos in the Dicke model", Physical Review E **79**, 046220 (2009).

[17] J. Ye and P. Zoller, "Essay: Quantum Sensing with Atomic, Molecular, and Optical Platforms for Fundamental Physics", Physical Review Letters **132**, 190001 (2024).

[18] A. Kuzmich, L. Mandel, and N. P. Bigelow, "Generation of Spin Squeezing via Continuous Quantum Nondemolition Measurement", Physical Review Letters **85**, 1594 (2000).

[19] L. K. Thomsen, S. Mancini, and H. M. Wiseman, "Spin Squeezing via Quantum Feedback", Physical Review A **65**, 061801 (2002).

[20] G. Tóth and M. W. Mitchell, "Generation of macroscopic singlet states in atomic ensembles", New Journal of Physics **12**, 053007 (2010).

[21] R. Kaubruegger, P. Silvi, C. Kokail, R. van, A. M. Rey, J. Ye, A. M. Kaufman, and P. Zoller, "Variational Spin-Squeezing Algorithms on Programmable Quantum Sensors", Physical Review Letters **123**, 260505 (2019).

[22] J. Hald, J. L. Sørensen, C. Schori, and E. S. Polzik, "Spin Squeezed Atoms: A Macroscopic Entangled Ensemble Created by Light", Physical Review Letters **83**, 1319 (1999).

[23] A. Dantan and M. Pinard, "Quantum-state transfer between fields and atoms in electromagnetically induced transparency", Physical Review A **69**, 043810 (2004).

[24] I. D. Leroux, M. H. Schleier-Smith, and V. Vuletić, "Implementation of Cavity Squeezing of a Collective Atomic Spin", Physical Review Letters **104**, 073602 (2010).

[25] M. F. Riedel, P. Böhi, Y. Li, T. W. Hänsch, A. Sinatra, and P. Treutlein, "Atom-chip-based generation of entanglement for quantum metrology", Nature **464**, 1170 (2010).

[26] G. Vitagliano, I. Apellaniz, I. L. Egusquiza, and G. Tóth, "Spin Squeezing and Entanglement for an Arbitrary Spin", Physical Review A **89**, 032307 (2014).

[27] V. Giovannetti, S. Lloyd, and L. Maccone, "Quantum-Enhanced Measurements: Beating the Standard Quantum Limit", Science **306**, 1330 (2004).

[28] M. Lewenstein, A. Sanpera, and V. Ahufinger, *Ultracold Atoms in Optical Lattices: Simulating Quantum Many-Body Systems* (OUP Oxford, Mar. 8, 2012), 494 pp.

[29] I. Buluta and F. Nori, "Quantum Simulators", Science **326**, 108 (2009).

[30] J. M. Robinson, M. Miklos, Y. M. Tso, C. J. Kennedy, T. Bothwell, D. Kedar, J. K. Thompson, and J. Ye, "Direct comparison of two spin-squeezed optical clock ensembles at the 10-17 level", Nature Physics **20**, 208 (2024).

[31] E. S. Polzik and J. Ye, "Entanglement and spin squeezing in a network of distant optical lattice clocks", Physical Review A **93**, 021404 (2016).

[32] T. Bilitewski, L. De Marco, J.-R. Li, K. Matsuda, W. G. Tobias, G. Valtolina, J. Ye, and A. M. Rey, "Dynamical Generation of Spin Squeezing in Ultracold Dipolar Molecules", Physical Review Letters **126**, 113401 (2021).

[33] M. A. Perlin, C. Qu, and A. M. Rey, "Spin Squeezing with Short-Range Spin-Exchange Interactions", Physical Review Letters **125**, 223401 (2020).

[34] Y. Trifa and T. Roscilde, "Scalable Spin Squeezing in Two-Dimensional Arrays of Dipolar Large-S Spins", Physical Review Letters **133**, 083601 (2024).

[35] B. Zhu, A. M. Rey, and J. Schachenmayer, "A generalized phase space approach for solving quantum spin dynamics", New Journal of Physics **21**, 082001 (2019).

[36] A. Patscheider, B. Zhu, L. Chomaz, D. Petter, S. Baier, A.-M. Rey, F. Ferlaino, and M. J. Mark, "Controlling dipolar exchange interactions in a dense three-dimensional array of large-spin fermions", Physical Review Research **2**, 023050 (2020).

[37] G. Müller-Rigat, A. Aloy, M. Lewenstein, and I. Frérot, "Inferring Nonlinear Many-Body Bell Inequalities From Average Two-Body Correlations: Systematic Approach for Arbitrary Spin-j Ensembles", PRX Quantum **2**, 030329 (2021).

[38] G. Müller-Rigat, M. Lewenstein, and I. Frérot, "Probing Quantum Entanglement from Magnetic-Sublevels Populations: Beyond Spin Squeezing Inequalities", Quantum **6**, 887 (2022).

[39] R. J. Glauber, "Coherent and Incoherent States of the Radiation Field", Physical Review **131**, 2766 (1963).

[40] R. J. Glauber, "Photon Correlations", Physical Review Letters **10**, 84 (1963).

[41] E. C. G. Sudarshan, "Equivalence of Semiclassical and Quantum Mechanical Descriptions of Statistical Light Beams", Physical Review Letters **10**, 277 (1963).

[42] A. M. Perelomov, "Coherent states for arbitrary Lie group", Communications in Mathematical Physics **26**, 222 (1972).

[43] R. Gilmore, "Geometry of symmetrized states", Annals of Physics **74**, 391 (1972).

[44] J. R. Klauder, "The action option and a Feynman quantization of spinor fields in terms of ordinary c-numbers", Annals of Physics **11**, 123 (1960).

[45] E. H. Lieb, "The classical limit of quantum spin systems", Communications in Mathematical Physics **31**, 327 (1973).

[46] A. O. Caldeira and A. J. Leggett, "Influence of damping on quantum interference: An exactly soluble model", Physical Review A **31**, 1059 (1985).

[47] W. H. Zurek, "Decoherence and the Transition from Quantum to Classical", Physics Today **44**, 36 (1991).

[48] F. STROCCHI, "Complex Coordinates and Quantum Mechanics", Reviews of Modern Physics **38**, 36 (1966).

[49] W.-M. Zhang, D. H. Feng, and J.-M. Yuan, "Integrability and nonintegrability of quantum systems. II. Dynamics in quantum phase space", Physical Review A **42**, 7125 (1990).

[50] W.-M. Zhang, D. H. Feng, and R. Gilmore, "Coherent States: Theory and Some Applications", Reviews of Modern Physics **62**, 867 (1990).

[51] J. Klauder and B. Skagerstam, *Coherent states* (WORLD SCIENTIFIC, 1985).

[52] C.-F. Kam, W.-M. Zhang, and D.-H. Feng, *Coherent States: New Insights into Quantum Mechanics with Applications*, Vol. 1011, Lecture Notes in Physics (Springer International Publishing, Cham, 2023).

[53] F. A. Berezin, "Covariant and contracovariant symbols of operators", Mathematics of the USSR-Izvestiya **6**, 1117 (1972).

[54] J. Aasi et al., "Enhanced Sensitivity of the LIGO Gravitational Wave Detector by Using Squeezed States of Light", Nature Photonics **7**, 613 (2013).

[55] Virgo Collaboration et al., "Increasing the Astrophysical Reach of the Advanced Virgo Detector via the Application of Squeezed Vacuum States of Light", Physical Review Letters **123**, 231108 (2019).

[56] M. Tse et al., "Quantum-Enhanced Advanced LIGO Detectors in the Era of Gravitational-Wave Astronomy", Physical Review Letters **123**, 231107 (2019).

[57] H. P. Yuen, "Two-photon coherent states of the radiation field", Physical Review A **13**, 2226 (1976).

[58] J. M. Radcliffe, "Some properties of coherent spin states", Journal of Physics A: General Physics **4**, 313 (1971).

[59] F. T. Arecchi, E. Courtens, R. Gilmore, and H. Thomas, "Atomic Coherent States in Quantum Optics", Physical Review A **6**, 2211 (1972).

[60] C. Qu and A. M. Rey, "Spin squeezing and many-body dipolar dynamics in optical lattice clocks", Physical Review A **100**, 041602 (2019).

[61] Y. Baamara, A. Sinatra, and M. Gessner, "Squeezing of Nonlinear Spin Observables by One Axis Twisting in the Presence of Decoherence: An Analytical Study", Comptes Rendus. Physique **23**, 1 (2022).

[62] J. Ma, X. Wang, C. P. Sun, and F. Nori, "Quantum Spin Squeezing", Physics Reports **509**, 89 (2011).

[63] Y. Li, "Spin Squeezing in Bose-Einstein Condensates", PhD thesis (Ecole Normale Supérieure de Paris - ENS Paris, July 6, 2010).

[64] X. Wang and B. C. Sanders, "Spin Squeezing and Pairwise Entanglement for Symmetric Multiqubit States", Physical Review A **68**, 012101 (2003).

[65] A. S. Sørensen and K. Mølmer, "Entanglement and Extreme Spin Squeezing", Physical Review Letters **86**, 4431 (2001).

[66] A. Sørensen, L.-M. Duan, J. I. Cirac, and P. Zoller, "Many-Particle Entanglement with Bose–Einstein Condensates", Nature **409**, 63 (2001).

[67] G. Tóth, C. Knapp, O. Gühne, and H. J. Briegel, "Spin Squeezing and Entanglement", Physical Review A **79**, 042334 (2009).

[68] G. Tóth, "Entanglement Detection in Optical Lattices of Bosonic Atoms with Collective Measurements", Physical Review A **69**, 052327 (2004).

[69] O. Gühne, "Characterizing Entanglement via Uncertainty Relations", Physical Review Letters **92**, 117903 (2004).

[70] J. K. Korbicz, J. I. Cirac, and M. Lewenstein, “Spin Squeezing Inequalities and Entanglement of N Qubit States”, Physical Review Letters **95**, 120502 (2005).

[71] J. K. Korbicz, O. Gühne, M. Lewenstein, H. Häffner, C. F. Roos, and R. Blatt, “Generalized Spin-Squeezing Inequalities in N-Qubit Systems: Theory and Experiment”, Physical Review A **74**, 052319 (2006).

[72] G. Tóth, C. Knapp, O. Gühne, and H. J. Briegel, “Optimal Spin Squeezing Inequalities Detect Bound Entanglement in Spin Models”, Physical Review Letters **99**, 250405 (2007).

[73] M. Kitagawa and Y. Yamamoto, “Number-Phase Minimum-Uncertainty State with Reduced Number Uncertainty in a Kerr Nonlinear Interferometer”, Physical Review A **34**, 3974 (1986).

[74] A. Sinatra, J.-C. Dornstetter, and Y. Castin, “Spin Squeezing in Bose–Einstein Condensates: Limits Imposed by Decoherence and Non-Zero Temperature”, Frontiers of Physics **7**, 86 (2012).

[75] F. Trimborn, D. Witthaut, and H. J. Korsch, “Beyond Mean-Field Dynamics of Small Bose-Hubbard Systems Based on the Number-Conserving Phase-Space Approach”, Physical Review A **79**, 013608 (2009).

[76] D. Kajtoch and E. Witkowska, “Quantum Dynamics Generated by the Two-Axis Countertwisting Hamiltonian”, Physical Review A **92**, 013623 (2015).

[77] M. Płodzień, M. Lewenstein, E. Witkowska, and J. Chwedeńczuk, “One-Axis Twisting as a Method of Generating Many-Body Bell Correlations”, Physical Review Letters **129**, 250402 (2022).

[78] G. J. Milburn, J. Corney, E. M. Wright, and D. F. Walls, “Quantum Dynamics of an Atomic Bose-Einstein Condensate in a Double-Well Potential”, Physical Review A **55**, 4318 (1997).

[79] A. S. Sørensen and K. Mølmer, “Entangling Atoms in Bad Cavities”, Physical Review A **66**, 022314 (2002).

[80] P. He, M. A. Perlin, S. R. Muleady, R. J. Lewis-Swan, R. B. Hutson, J. Ye, and A. M. Rey, “Engineering spin squeezing in a 3D optical lattice with interacting spin-orbit-coupled fermions”, Physical Review Research **1**, 033075 (2019).

[81] L. I. R. Gil, R. Mukherjee, E. M. Bridge, M. P. A. Jones, and T. Pohl, “Spin Squeezing in a Rydberg Lattice Clock”, Physical Review Letters **112**, 103601 (2014).

[82] W. J. Eckner, N. Darkwah Oppong, A. Cao, A. W. Young, W. R. Milner, J. M. Robinson, J. Ye, and A. M. Kaufman, “Realizing spin squeezing with Rydberg interactions in an optical clock”, Nature **621**, 734 (2023).

[83] W. Muessel, H. Strobel, D. Linnemann, T. Zibold, B. Juliá-Díaz, and M. K. Oberthaler, "Twist-and-Turn Spin Squeezing in Bose-Einstein Condensates", Physical Review A **92**, 023603 (2015).

[84] G. Sorelli, M. Gessner, A. Smerzi, and L. Pezzè, "Fast and Optimal Generation of Entanglement in Bosonic Josephson Junctions", Physical Review A **99**, 022329 (2019).

[85] A. G. Rojo, "Optimally Squeezed Spin States", Physical Review A **68**, 013807 (2003).

[86] C. K. Law, H. T. Ng, and P. T. Leung, "Coherent Control of Spin Squeezing", Physical Review A **63**, 055601 (2001).

[87] M. Gessner, A. Smerzi, and L. Pezzè, "Metrological Nonlinear Squeezing Parameter", Physical Review Letters **122**, 090503 (2019).

[88] D. M. Greenberger, M. A. Horne, and A. Zeilinger, in *Bell's Theorem, Quantum Theory and Conceptions of the Universe*, edited by M. Kafatos (Springer Netherlands, Dordrecht, 1989), pp. 69–72.

[89] A. André and M. D. Lukin, "Atom Correlations and Spin Squeezing near the Heisenberg Limit: Finite-size Effect and Decoherence", Physical Review A **65**, 053819 (2002).

[90] A. André, L.-M. Duan, and M. D. Lukin, "Coherent Atom Interactions Mediated by Dark-State Polaritons", Physical Review Letters **88**, 243602 (2002).

[91] C. Miller, A. N. Carroll, J. Lin, H. Hirzler, H. Gao, H. Zhou, M. D. Lukin, and J. Ye, *Two-Axis Twisting Using Floquet-engineered XYZ Spin Models with Polar Molecules*, (Apr. 30, 2024) `http://arxiv.org/abs/2404.18913` (visited on 06/23/2024).

[92] C. Luo, H. Zhang, A. Chu, C. Maruko, A. M. Rey, and J. K. Thompson, *Hamiltonian Engineering of collective XYZ spin models in an optical cavity*, (July 2, 2024) `http://arxiv.org/abs/2402.19429` (visited on 08/25/2024), pre-published.

[93] O. Dutta, M. Gajda, P. Hauke, M. Lewenstein, D.-S. Lühmann, B. A. Malomed, T. Sowiński, and J. Zakrzewski, "Non-Standard Hubbard Models in Optical Lattices: A Review", Reports on Progress in Physics **78**, 066001 (2015).

[94] T. Chanda, L. Barbiero, M. Lewenstein, M. J. Mark, and J. Zakrzewski, *Recent Progress on Quantum Simulations of Non-Standard Bose-Hubbard Models*, (May 13, 2024) `http://arxiv.org/abs/2405.07775` (visited on 06/17/2024).

[95] N. W. Ashcroft and N. D. Mermin, *Solid State Physics* (Holt, Rinehart and Winston, 1976).

[96] R. Walters, G. Cotugno, T. H. Johnson, S. R. Clark, and D. Jaksch, "Ab Initio Derivation of Hubbard Models for Cold Atoms in Optical Lattices", Physical Review A **87**, 043613 (2013).

[97] V. Fock, "Konfigurationsraum und zweite Quantelung", Zeitschrift für Physik **75**, 622 (1932).

[98] E. Altman, W. Hofstetter, E. Demler, and M. D. Lukin, "Phase diagram of two-component bosons on an optical lattice", New Journal of Physics **5**, 113 (2003).

[99] V. Colussi, F. Caleffi, C. Menotti, and A. Recati, "Quantum Gutzwiller approach for the two-component Bose-Hubbard model", SciPost Physics **12**, 111 (2022).

[100] M. Płodzień, M. Kościelski, E. Witkowska, and A. Sinatra, "Producing and Storing Spin-Squeezed States and Greenberger-Horne-Zeilinger States in a One-Dimensional Optical Lattice", Physical Review A **102**, 013328 (2020).

[101] W. Heisenberg, "Mehrkörperproblem und Resonanz in der Quantenmechanik", Zeitschrift für Physik **38**, 411 (1926).

[102] P. A. M. Dirac and R. H. Fowler, "On the Theory of Quantum Mechanics", Proceedings of the Royal Society of London. Series A, Containing Papers of a Mathematical and Physical Character **112**, 661 (1926).

[103] H. Bethe, "Zur Theorie der Metalle", Zeitschrift für Physik **71**, 205 (1931).

[104] H. Bethe, in *Selected Works of Hans A Bethe*, Vol. Volume 18, World Scientific Series in 20th Century Physics Volume 18 (WORLD SCIENTIFIC, July 1997), pp. 155–183.

[105] M. Karbach and G. Muller, *Introduction to the Bethe Ansatz I*, (Sept. 10, 1998) `http://arxiv.org/abs/cond-mat/9809162` (visited on 06/03/2024).

[106] E. H. Lieb and W. Liniger, "Exact Analysis of an Interacting Bose Gas. I. The General Solution and the Ground State", Physical Review **130**, 1605 (1963).

[107] R. H. Dicke, "Coherence in Spontaneous Radiation Processes", Physical Review **93**, 99 (1954).

[108] H. Puszkarski, "Eigenvalue Problem of a Finite Monoatomic Linear Chain with Asymmetrical Boundary Conditions; Surface States", Surface Science **34**, 125 (1973).

[109] B. D. a. F. L. Claude Cohen-Tannoudji, *Cohen-Tannoudji, Diu and Laloë - Quantum Mechanics (Vol. I, II and III, 2nd Ed.)* (Dec. 16, 2019).

[110] A. L. Fetter and J. D. Walecka, *Quantum Theory of Many-particle Systems* (Dover Publications, 2003).

[111] I. Lindgren, “The Rayleigh-Schrodinger perturbation and the linked-diagram theorem for a multi-configurational model space”, Journal of Physics B: Atomic and Molecular Physics **7**, 2441 (1974).

[112] S. Bravyi, D. P. DiVincenzo, and D. Loss, “Schrieffer–Wolff Transformation for Quantum Many-Body Systems”, Annals of Physics **326**, 2793 (2011).

[113] J. A. Oteo, “The Baker-Campbell-Hausdorff formula and nested commutator identities”, Journal of Mathematical Physics **32**, 419 (1991).

[114] G. Bornet, G. Emperauger, C. Chen, B. Ye, M. Block, M. Bintz, J. A. Boyd, D. Barredo, T. Comparin, F. Mezzacapo, T. Roscilde, T. Lahaye, N. Y. Yao, and A. Browaeys, “Scalable Spin Squeezing in a Dipolar Rydberg Atom Array”, Nature **621**, 728 (2023).

[115] C. Trefzger, C. Menotti, B. Capogrosso-Sansone, and M. Lewenstein, “Ultracold dipolar gases in optical lattices”, Journal of Physics B: Atomic, Molecular and Optical Physics **44**, 193001 (2011).

[116] F. Heidrich-Meisner, S. R. Manmana, M. Rigol, A. Muramatsu, A. E. Feiguin, and E. Dagotto, “Quantum Distillation: Dynamical Generation of Low-Entropy States of Strongly Correlated Fermions in an Optical Lattice”, Physical Review A **80**, 041603 (2009).

[117] J. Spałek, “Effect of Pair Hopping and Magnitude of Intra-Atomic Interaction on Exchange-Mediated Superconductivity”, Physical Review B **37**, 533 (1988).